Dynamics of Barred Galaxies

J A Sellwood[1,2] and A Wilkinson[3]

[1]Space Telescope Science Institute, 3700 San Martin Drive, Baltimore, MD 21218, USA
[2]Department of Physics and Astronomy, Rutgers University, PO Box 849, Piscataway, NJ 08855-0849, USA
[3]Department of Astronomy, The University, Manchester M13 9PL, England

Abstract

Some 30% of disc galaxies have a pronounced central bar feature in the disc plane and many more have weaker features of a similar kind. Kinematic data indicate that the bar constitutes a major non-axisymmetric component of the mass distribution and that the bar pattern tumbles rapidly about the axis normal to the disc plane. The observed motions are consistent with material within the bar streaming along highly elongated orbits aligned with the rotating major axis. A barred galaxy may also contain a spheroidal bulge at its centre, spirals in the outer disc and, less commonly, other features such as a ring or lens. Mild asymmetries in both the light and kinematics are quite common.

We review the main problems presented by these complicated dynamical systems and summarize the effort so far made towards their solution, emphasizing results which appear secure. Bars are probably formed through a global dynamical instability of a rotationally supported galactic disc. Studies of the orbital structure seem to indicate that most stars in the bar follow regular orbits but that a small fraction may be stochastic. Theoretical work on the three-dimensional structure of bars is in its infancy, but first results suggest that bars should be thicker in the third dimension than the disc from which they formed. Gas flow patterns within bars seem to be reasonably well understood, as are the conditions under which straight offset dust lanes are formed. However, no observation so far supports the widely held idea that the spiral arms are the driven response to the bar, while evidence accumulates that the spiral patterns are distinct dynamical features having a different pattern speed. Both the gaseous and stellar distributions are expected to evolve on a time-scale of many bar rotation periods.

Table of Contents

1. Introduction

Galaxies are beautiful objects, and the graceful symmetry of many barred galaxies is particularly striking. One of the best examples close enough for us to examine in detail is NGC 1365 in the Fornax cluster (Figure 1). Such objects are doubly pleasing to the astro-physicist because they also present a number of very challenging dynamical problems.

Barred galaxies are a heterogeneous class of objects, as can be seen from the selection assembled in Figure 2. The bar component ranges from a minor non-axisymmetric perturbation to a major feature in the light distribution. Other properties, such as the size of the bar relative to the host galaxy, the degree of overall symmetry, the existence of rings and the numbers (and position relative to the bar) of spiral arms in the outer disc, the gas and dust content, *etc.*, vary considerably from galaxy to galaxy.

Bars can be found in all types of disc galaxies, from the earliest to the latest stages of the Hubble sequence.[3] Because there is a continuum of apparent bar strengths from very weak oval distortions to major features, it becomes more a matter of taste to decide what strength of bar in a galaxy is sufficient to merit a barred classification. Figure 3 shows the fraction of each spiral type judged to contain bars, compiled from *A Revised Shapley Ames Catalogue* (Sandage and Tammann 1981, hereafter RSA), *The Second Reference Catalogue* (de Vaucouleurs *et al.* 1976, hereafter RC2) and the *Uppsala General Catalogue* (Nilson 1973, hereafter UGC). Apart from the very latest types, there is rough agreement over the fractions containing strong bars (shaded); when combined over all stages, the SB family constitutes between 25% and 35% of all disc galaxies. However, there is considerably less agreement over intermediate cases, the SAB family: the morphological classifications assigned in the RC2 indicate a combined fraction for the SAB family as high as 26.4% – substantially higher than in either of the other two catalogues. Notwithstanding these variations, it is clear that barred galaxies constitute a major fraction of all disc galaxies.

A small number of galaxies which appear unbarred at visual wavelengths have been found to be barred when observed in the near infra-red. The three clearest cases are NGC 1566 (Hackwell and Schweizer 1983), NGC 1068 (Scoville *et al.* 1988, Thronson *et al.* 1989) and NGC 309 (Block and Wainscoat 1991); much shorter or weaker bar-like features have shown up in many others (§2.4). Many more such cases could yet be discovered, as IR cameras are in their infancy; if so, the fraction of barred galaxies could turn out to be much higher than indicated by Figure 3.

Elliptical galaxies are sometimes described as stellar bars, which is apt for certain purposes. However, we exclude such galaxies from this review because, unlike barred galaxies, they appear to be single component systems with no surrounding disc or distinct central bulge. Moreover, the stellar distribution is not thought to be as flattened, or to rotate as fast as bars in disc systems. De Zeeuw and Franx (1991) have surveyed the literature on the dynamics of these objects.

We are still far from a complete understanding of the dynamical structure of barred galaxies. We would really like to know the three-dimensional density distribution of each galaxy in order

---

[3] Galaxies are classified by their morphological appearance in a system based upon that devised by Hubble (1926): the relative luminosity of the central bulge and openness of the spirals are used to define a sequence (S0, Sa, Sb, Sc, Sd) for both barred and unbarred galaxies. Early type galaxies (S0, Sa) have bright bulges and weak, tightly wrapped spirals; late types (Sc, Sd) have little or no bulge and open, ragged spirals.

Figure 1.   NGC 1365, a magnificent barred spiral in Fornax. The galaxy has a very bright amorphous central bulge, a strong bar joined to a nearly symmetrical pair of spiral arms. Pronounced brown dust lanes can be seen in the spiral arms and on the leading edge of the bar (assuming the arms to be trailing). Sites of star formation are tinged in pink while the youngest stars are blue and old stars are yellow. As in most galaxies, the spiral arms are superposed on a much lower surface brightness disc, which is too faint to be distinguishable from the sky in this photograph. (Photograph courtesy of David Malin, Anglo-Australian Observatory.)
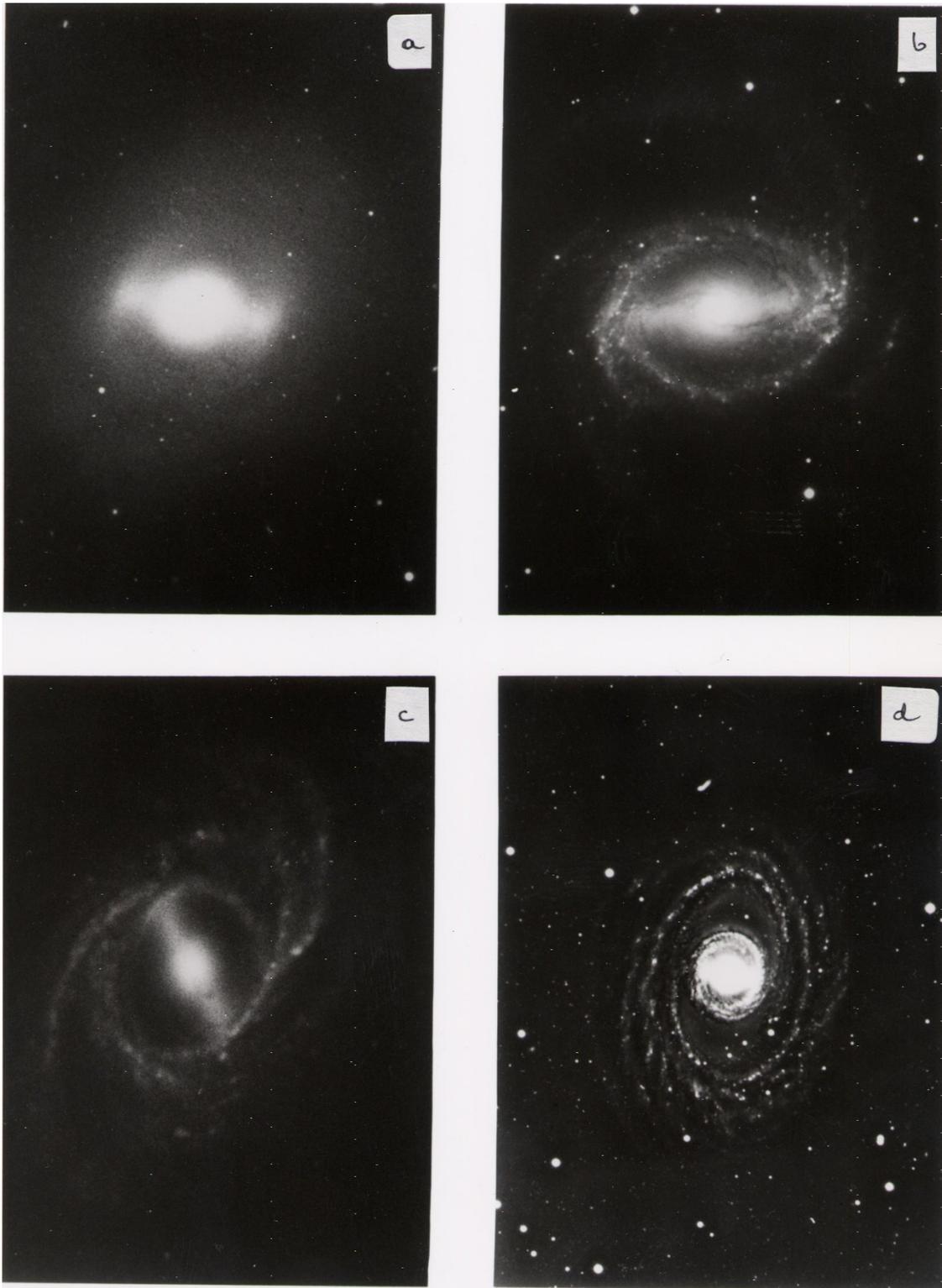
Figure 2. Eight further examples chosen to illustrate the variety of galaxies classified as barred. They are (a) NGC 936, (b) NGC 1433, (c) NGC 2523, (d) NGC 1398, (e) NGC 2217, (f) NGC 5236 (M83), (g) NGC 5383, (h) NGC 1313. Seven photographs are courtesy of Allan Sandage and the Carnegie Institution. The eighth, NGC 1398 (d) which was supplied by David Malin and has been processed to bring out small-scale structure.
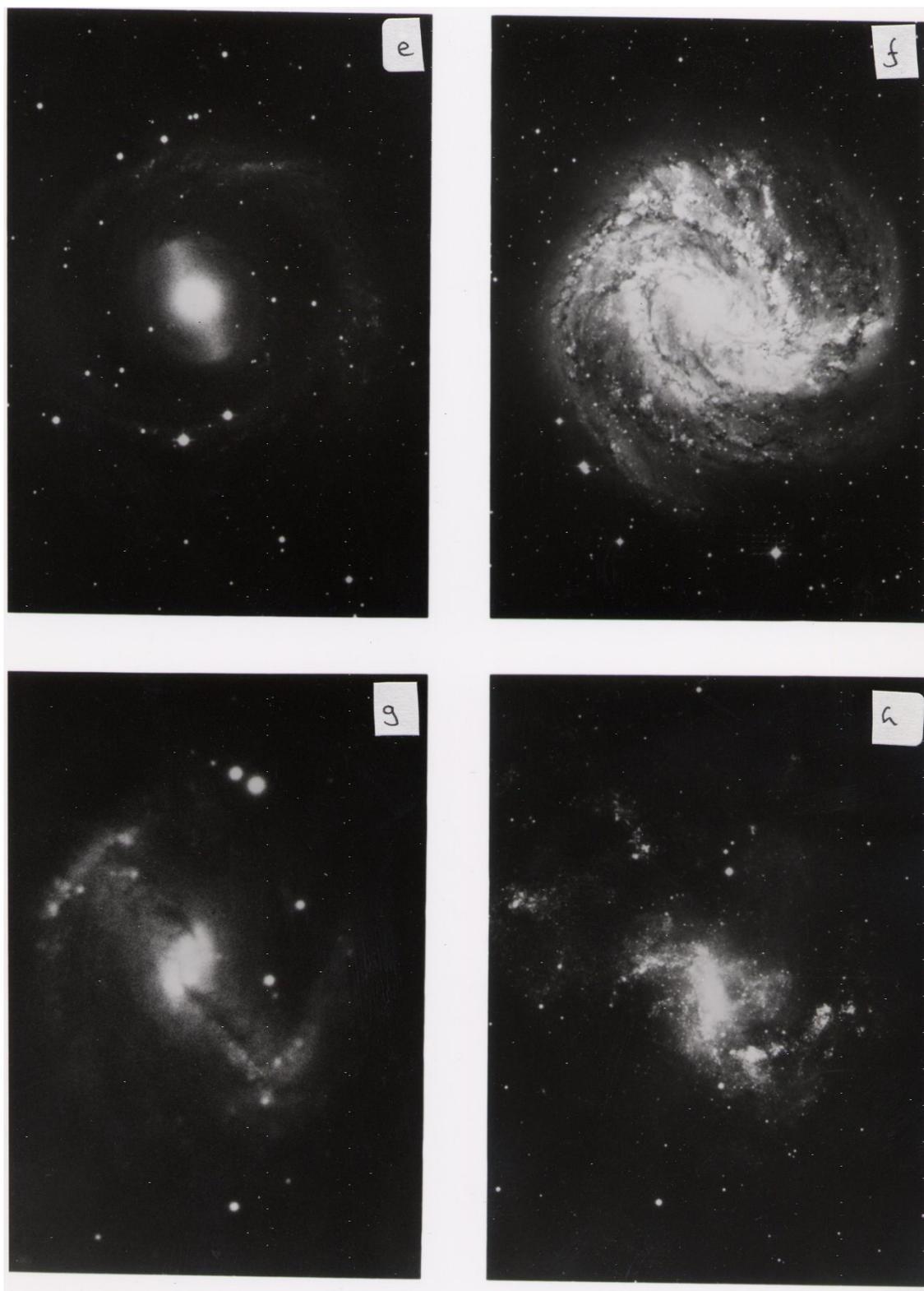
Figure 2. (Continued)
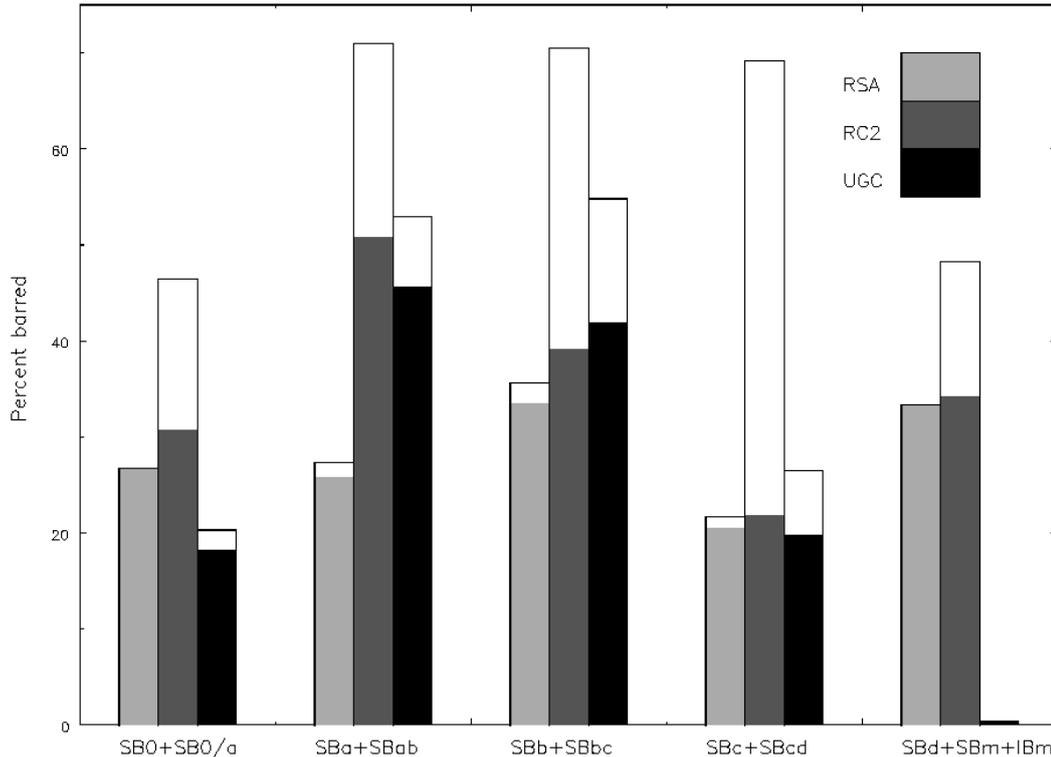
Figure 3. The fractions of barred (SB, shaded) and intermediate (SAB, unshaded) types at different stages along the Hubble sequence of spiral galaxies identified in three independent morphological classifications. The statistics from the RSA are based upon 987 objects (only the first classification was used here). The RC2 sample contains 1339 objects, after excluding peculiar, uncertain and "spindle" types, edge-on objects (those with axis ratios > 3) and those with diameters less than 1 arcmin – unless large-scale plate material was available. The UGC sample contains 4169 galaxies when selection criteria similar to those for the RC2 were applied. The statistics are insensitive to the selection criteria, provided they remain within sensible ranges.

to be able to calculate the gravitational potential. This information, combined with the rotation rate of the bar, would enable us to calculate the motion of stars and gas. We could claim we understood the dynamical equilibrium if we were able to propose a self-consistent model in which the various orbits were populated so as to reconstruct the observed mass distribution. We should then ask whether the equilibrium model would be dynamically stable, or how it would evolve, how the object was formed in the first place, *etc.* Here we will be able to do no more than scratch the surface of the majority of these problems.

There are many excuses for our ignorance:

 i The distance of these objects, combined with a surface brightness which declines to below that of the night sky, makes it very hard to make measurements of the quality required.
 ii We see these objects only in projection. As we believe they are disc-like, we might naïvely hope that there is a plane of symmetry, but because barred galaxies are intrinsically non-circular, determination of the inclination angle is more difficult than in their unbarred counterparts.
iii Worse still, it is unlikely that a single plane of symmetry exists in many galaxies. Those seen edge-on frequently exhibit warps mainly in the outer parts, yet this is precisely where the problem of point (2) is best avoided.

iv We have very little knowledge of the thickness along the line of sight; it is reasonable to believe that the thickness of discs seen edge-on is typical, but some edge-on systems have box-shaped bulges – we have no way of telling whether these are strongly barred galaxies, or whether the box shape is uncorrelated with the morphology in the plane.

v The line-of-sight velocity component, which is all we can measure, also gives us no more than the average integrated through the object, or to the point at which it becomes opaque (itself a controversial question; *e.g.* Disney *et al.* 1989, Valentijn 1990, Huizinga and van Albada 1992, *etc.*).

vi Our "snapshot" view of each galaxy prevents our making direct measurements of the rotation rate (or pattern speed) of the bar; the angular speed of the non-axisymmetric features inferred from the observed motions of gas and stars are highly uncertain.

vii Many features, *e.g.* dust lanes and rings, result from dissipative processes in the gaseous component. Unfortunately, we lack a good theoretical description for the large-scale behaviour of gas, which is stirred and damped on scales of a few parsecs, while we wish to model gaseous features traceable over many kiloparsecs.

viii We are uncertain of the extent to which the internal dynamics are affected by dark matter. At large radii, the orbital motion in barred galaxies resembles the nearly circular rotation pattern typical of a normal spiral galaxy and, as emphasized by Bosma (1992), the mass again appears to have a different distribution from the light. There is some evidence that the luminous matter dominates the dynamics of the inner parts of unbarred galaxies (*e.g.* Casertano and van Albada, 1990) and we shall proceed by assuming that this is the case in the bar region. This, perhaps rash, assumption is buttressed by the kinematic evidence (§§2.5 & 6) that the more prominent bars are associated with large departures from simple circular motion in the disc plane, indicating that the bar contains a significant fraction of the mass in the inner galaxy.

ix The weakest excuse is that our mathematical ability is so limited that we are unable to solve the equations which should describe the structure of such objects, except in a few highly idealized cases. Our understanding of the dynamics has therefore to be laboriously pieced together using numerical techniques, which themselves have limitations.

It is customary to break the light of a barred galaxy into a number of different components, or building blocks: a disc, a bulge, a bar and, sometimes, a lens and/or rings (*e.g.* Kormendy 1979). Most of these components are evident from Figures 1 & 2, only the lens requires description: if present, it is a comparatively bright, oval part of the inner disc surrounding the bar. It is distinguished by a moderately sharp edge, which causes a locally steep gradient in the photometric profile. Although the working hypothesis of separate components seems justified by the fact that the individual features are readily distinguished by the eye, it is much more difficult to separate the components quantitatively (§2.1). The idea of morphologically distinct components has been taken much further, however, and each component is frequently assumed to be a separate dynamical entity. This fundamental assumption is rarely discussed or even stated. Because it is obviously much easier to understand the dynamics of each apparent component separately, we also treat them as dynamically independent for the first part of the review, and examine the validity of this assumption only towards the end.

Most of the mass in the inner bright regions of a galaxy is in stars; the gas mass is rarely sufficient to affect the gravitational potential and we have already indicated that we assume dark matter begins to dominate only in the faint outer parts. We therefore consider the dynamics

of the inner galaxy to be that of a purely stellar system in which any gas present acts as tracer material (§6).

Galaxies are thought to be of intermediate dynamical age; a typical star might have completed some 50 orbits around the centre. This is neither so old that the galaxy must be in settled equilibrium (the existence of spiral structure and on-going star formation show this is not the case) nor so young that its morphological features just reflect initial transients. It is most appropriate, therefore, to consider the slow evolution of a nearly equilibrium model. Accordingly we discuss equilibrium models before we go on to consider how they might have arisen and will evolve. We conclude by considering interactions between the different components.

2. Observed properties of bars

We begin by summarizing the observational information relating to the dynamical structure of the stellar bar, and leave data on gas to §6 and on rings to §7, where we discuss these other phenomena.

Unfortunately we cannot make direct measurements of even the most basic properties, and are forced to make indirect inferences from the observables. Our requirements fall into three general areas:

  i The distribution of mass, in order to determine the gravitational potential. This has to be deduced from measurements of (a) the light distributions and (b) the velocity field.
 ii The bar rotation velocity, or pattern speed, which can be inferred only with considerable uncertainty from the velocity field or, still less directly, through modelling the gas flow pattern.
iii The full three-dimensional velocity dispersion which, jointly with orbital streaming, determines the stellar dynamical equilibrium. This can be constructed from the projected velocity dispersion data only with the aid of a mass model.

2.1. Components of the light distribution

Deprojection of the light distribution of barred galaxies is more difficult than for nearly axisymmetric galaxies since it is far from clear that any isophote should be intrinsically round. The inclination is generally inferred by assuming that the outer faint isophotes are projected circles, but it should be borne in mind that even far out the shape could be intrinsically elliptical, especially if an outer ring is present (§7), or the plane is warped.

The major axis of the bar is always less than the diameter of the host galaxy. In general, bars in late-type systems are shorter relative to the total galaxy size ($D_{\mathrm{bar}}/D_{25} = 0.2$ to 0.3) than those in early-type galaxies ($D_{\mathrm{bar}}/D_{25} = 0.3$ to 0.6), where D_{25} is the diameter at which the surface brightness of the galaxy falls below 25 mag arcsec^{-2} (*e.g.* Athanassoula and Martinet 1980, Elmegreen and Elmegreen 1985, Duval and Monnet 1985).

There also appears to be a correlation between the length of the bar and the size of the bulge. Athanassoula and Martinet (1980) suggest that the deprojected length of the bar scales as ~ 2.34 times the bulge diameter, while Baumgart and Peterson (1986) estimate 2.6 ± 0.7.

2.2. Fraction of total luminosity in the bar

Estimates of the luminosity fraction in the bar depend not only on the radius to which the total light is measured but also on how the decomposition is performed. Luminosity fractions

are usually quoted as a fraction of either the light out to the end of the bar, or integrated out to some faint isophotal level, *e.g.* D_{25}.

Decompositions were originally performed by attempting to fit the components with idealized models: prolate bars, exponential discs, *etc.* (*e.g.* Crane 1975, Okamura 1978, Duval and Athanassoula 1983, Duval and Monnet 1985). Blackman (1983) used breaks, or changes of slope, in the photometric profile to define the boundaries between the different components. Others have tried Fourier analysis of the light distribution (*e.g.* Elmegreen and Elmegreen 1985, Buta 1986b, 1987, Ohta *et al.* 1990, Athanassoula and Wozniak 1992), which imposes no prejudice as to the form of the components and gives direct measurements of the strengths of the different non-axisymmetric features, once the inclination is determined. Probably the most successful decomposition technique for a barred galaxy was proposed by Kent and Glaudell (1989) who devised an iterative method to separate an oblate bulge model from the bar.

It is not surprising therefore that the estimates for the same object vary widely from author to author. For example, for the SBc galaxy NGC 7479 they range from the unrealistically low value of 8% by the modelling technique (Duval and Monnet 1985) to a more likely 40% by direct estimation of the light within an approximate isophote at the edge of the bar (Blackman 1983) and 38% by Fourier decomposition (Elmegreen and Elmegreen 1985). Ohta *et al.* (1990) give values in the range ~ 25 to $\sim 50\%$ in the "bar region" to ~ 10 to $\sim 30\%$ out to D_{25} for their sample of early-type galaxies.

2.3. The light distribution within the bar

Generally, the shapes, strengths and lengths of bars seem to vary systematically from early to late-type systems.

2.3.1. Early-type galaxies.   Many bars in galaxies of types SB0 and SBa have a pronounced rectangular shape seen in projection (Ohta *et al.* 1990, Athanassoula *et al.* 1990) with axial ratios between 0.3 to 0.1. The surface brightness decreases slowly along the bar major axis, in some cases as a shallow exponential but in others it is almost constant until close to the end of the bar (*e.g.* Elmegreen and Elmegreen 1985, Kent and Glaudell 1989). There is no difference between the leading and trailing sides (Ohta *et al.*).

The surface brightness contrast between bars and the axisymmetric component can range from 2.5 to 5.5 (Ohta *et al.*). Bars are considerably brighter on the major axis, and usually fainter on the minor axis, than the inwardly extrapolated disc profile. Azimuthally averaged, however, the radial profiles are no more varied than those of ordinary spirals; Wozniak and Pierce (1991) fit an exponential to the disc profile outside the bar but ring features, which are much more common in barred galaxies, can make this a poor approximation (*e.g.* Buta 1986b).

2.3.2. Late-type galaxies.   The light distribution in late-type galaxies is generally less smooth owing to greater dust obscuration and more intense knots of young stars. The difficulties created by both these problems are lessened by making the observations at wavelengths as far into the infra-red as possible (*e.g.* Adamson *et al.* 1987).

Bars in galaxies of types SBbc to SBm are generally more elliptical (*e.g.* Duval and Monnet 1985), shorter and weaker than their earlier counterparts. They also begin to show quite pronounced asymmetries, *e.g.* one end may appear squarer than the other (see §8).

The surface brightness distribution of weak bars in late-type systems is much more centrally peaked and falls off exponentially along the bar, sometimes even more steeply than the disk

(Elmegreen and Elmegreen 1985, Baumgart and Peterson 1986). Across the bar, the light profile is close to Gaussian (*e.g.* Blackman 1983).

2.3.3. Light distribution normal to the galactic plane. Although we cannot see them, we expect bars to be as common in edge-on systems as in all disc galaxies. It has therefore been argued that since we do not see a large fraction of unusually thick discs, bars must be as thin as the rest of the disc. A range of values has been suggested for the bar thickness: Kormendy (1982) suggests typical axis ratios of 1:2:10 and extremes of perhaps 1:3:15 or $1:\frac{3}{2}:4$ (*e.g.* Burstein 1979, Tsikoudi 1980), 1:x:10 (Wakamatsu and Hamabe 1984).

However, this argument could be fallacious. The bulges at the centres of a significant fraction of nearly edge-on galaxies do not have a simple spheroidal or ellipsoidal shape, but are squared-off, boxy or even indented peanut-shaped (*e.g.* Sandage 1961 plate 7, Jarvis 1986, Shaw 1987, de Souza and dos Anjos 1987). It has been suggested (Combes and Sanders 1981, Raha *et al.* 1991) that such bulges may be the signature of a bar seen edge-on, and if so bars are much thicker than discs. We discuss this point further in §10.2.

Bottema (1990) has measured the velocity dispersion profile of a bar which we see nearly face on. He finds that the dispersion, which is dominated by the vertical component, remains approximately constant at ~ 55 km s^{-1} from just outside the bulge to the end of the bar. As the light profile declines strongly along this late-type bar, we might expect the surface mass density to do so also. Data of this kind should be examined more closely to see whether they imply a flaring bar.

2.4. Tri-axial bulges and/or nuclear bars

The position angle of the major axes of isophotes in the inner regions of many barred galaxies twists away from the bar major axis near the centre. The twist angles are substantial and may, when deprojected, be consistent with a central elongation perpendicular to the bar. Such features have been seen mainly in the optical (*e.g.* de Vaucouleurs 1974, Sandage and Brucato 1979, Buta 1986b, Jarvis *et al.* 1988) but also in the infrared (Baumgart and Peterson 1986, Pierce 1986, Shaw *et al.* 1992), in molecular gas (Ball *et al.* 1985, Canzian *et al.* 1988, Ishizuki *et al.* 1990, Kenney 1991) and even radio continuum (Hummel *et al.* 1987a & b).

It has frequently been suggested that such features indicate a tri-axial, rather than an axially symmetric, bulge (*e.g.* de Vaucouleurs 1974, Kormendy 1979, 1982, Gerhard and Vietri 1986, and many others). Others have claimed it indicates a small nuclear bar, in both barred and unbarred galaxies. As there are theoretical reasons to expect twisted isophotes near the bar centre (see §§4.5.1 & 6.4) it is of some importance to determine whether the inner feature is perpendicular to the bar major axis when deprojected to face-on. While this difficult question is not yet settled, there is evidence that the features are frequently almost perpendicular, but Gerhard and Louis (1988) argue that this cannot be so in all cases.

2.5. Kinematic properties of bars

Material in galaxies lacking a bar, or other strong non-axisymmetric feature, seems to follow nearly circular orbits, and the velocity field is simply that of rotational motion seen in projection. Barred galaxies, on the other hand, are more complicated for two reasons: firstly, the velocities, especially in the barred region, manifest strong non-circular streaming motions, and secondly, the viewing geometry is much more difficult to determine. Both the inclination angle

to the plane of the sky and the position angle of the projection axis – the line of nodes – are more difficult to determine when the light distribution is intrinsically non-axisymmetric and the motions depart systematically from circular.

Many early observations consisted of a slit spectrum at a single position angle along the bar or projected major axis. Such data yields very incomplete information; several slit positions, or ideally a full two-dimensional map, are required to determine the velocity field.

2.5.1. Velocity fields.   Kormendy (1983) presented the first clear evidence for non-circular *stellar* streaming motions in a barred galaxy. The non-circular motions in the SB0 galaxy NGC 936 (Figure 2) are about 20% of the circular streaming velocity and are consistent with orbits being elongated along the bar, with the circulation in the forward sense along the bar major axis (assuming the weak spiral arms trail). More recent data for the same galaxy (Kent 1987, Kent and Glaudell 1989) have confirmed this interpretation.

Other examples are: NGC 6684 which shows deviations of 100 km/sec from circular motion (Bettoni *et al.* 1988), NGC 1543, 1574, 4477 for which velocities on the minor axis of ~ 100 km s^{-1} have been detected (Jarvis *et al.* 1988) and NGC 4596 (Kent 1990). Only galaxies for which the bar is inclined to both the projected major and minor axes show non-circular motions clearly (Pence and Blackman 1984b, Long 1992).

Bettoni and Galletta (1988) argued that the picture is more complicated than simple streaming in the same sense as the direction of bar rotation because the apparent streaming velocity does not always rise monotonically when measured along the bar major axis and may even dip back to near zero at a point about one third of the distance from the centre to the end of the bar. They suggested that this behaviour might possibly be due to retrograde stellar streaming within the bar. However, Sparke showed that it can quite naturally be explained as being due to the finite width of the slit, and a possible very small misalignment with the bar major axis, allowing light from stars streaming along the bar to influence the measurement. Her argument is reported by Bettoni (1989).

These measurements establish that the bar distorts the axisymmetric potential of the disc sufficiently strongly to force the stars to stream on highly elliptical orbits inside the bar. Additional evidence which helps to determine the strength of the non-axisymmetric potential comes from observations of the gas kinematics, though these usually need to be interpreted using a model (see §6).

2.5.2. Azimuthally averaged velocity profiles.   Since the potential of a barred galaxy is strongly non-axisymmetric, it is even more difficult than for a nearly axisymmetric galaxy to determine the distribution of mass. Although an approximation to a "rotation curve" found by crudely averaging tangential streaming velocities can be significantly in error (Long 1992), this practice is widespread.

The error is unlikely to affect the comment (Elmegreen and Elmegreen 1985) that many early-type galaxies have bars which extend beyond the rising part of the rotation curve, while late-type bars end before the rotation curve flattens off. However, the positions of resonances within the bar (see §4.2) deduced from an axially symmetrized rotation curve and an estimate of the bar pattern speed, are highly uncertain. Not only could the axisymmetric rotation curve be wrong, but a resonance predicted by linear theory for a weak perturbation could be absent in a strong bar. Orbit integrations are the only reliable way to identify resonances in a strong bar (§4.5).

2.6. Bar angular velocity or pattern speed

The rate of rotation of the bar is one of the most important parameters determining its dynamical structure, but unfortunately it is very difficult to measure directly. Tremaine and Weinberg (1984b) have shown how the continuity equation could in principle be used to determine this quantity from observables alone. The method requires high signal-to-noise long-slit spectra and a photometric light profile both taken along cuts offset from the nucleus and parallel to the major axis. In practice, the pattern speed inferred is sensitive to centering and alignment errors, warps, and the presence of any non-bisymmetric perturbation and is therefore uncertain.

Using this technique, Kent (1987) estimated $\Omega_p \sin i = 5.4 \pm 1.9$ km s^{-1}arcsec^{-1}($\sim 104 \pm 37$ km s^{-1}kpc^{-1}) for NGC 936. Combining his value with Kormendy's rotation curve, Kent's measurement suggests that co-rotation lies within the bar, although a radius just beyond the end of the bar is within the error.[4]

Application of this method to galaxies other than SB0s is even more problematic, because of the presence of dust patches and bright knots. Tremaine and Weinberg tried to apply it to the HI observations of NGC 5383 (Sancisi *et al.* 1979) but were unable to obtain a conclusive result. The method failed because of noise, an extended HI envelope and because any single easily observed species probably does not obey the equation of continuity (*e.g.* atomic to molecular transitions, star formation, stellar mass loss, *etc.*).

The very limited success of this method is disappointing; nevertheless, Kent's measurement does at least furnish independent evidence that the bar in NGC 936 rotates rapidly. We are therefore forced to rely upon less direct alternative techniques. The most reliable method, described in §6, attempts to match the observed gas flow pattern to a set of hydrodynamical models in which the bar pattern speed is varied. Some authors also attempt to associate individual morphological and kinematic features with resonances for the pattern; we note examples in §§6.7 & 7.

2.7. Velocity dispersions

Velocity dispersion profiles have also been determined for some galaxies, though frequently only along the bright bar major axis. The central values of the velocity dispersion are found to be similar to that of the lens (§7) – typically about 150 to 200 km s^{-1} (*e.g.* Kormendy 1982 for the SB0 galaxies NGC 936 and NGC 3945). The ratio of the maximum rotation velocity to the central velocity dispersion, $V_{\mathrm{max}}/\sigma_0$, gives a measure of the relative importance of streaming and random motion. Values are typically between 0.4 and 0.5, implying that there are significant contributions from both streaming motions along the bar and random motions. More generally, the bar velocity dispersion profiles can vary from flat to sharply falling with increasing radius (*e.g.* Jarvis *et al.* 1988).

3. Stellar dynamics of galaxies

In this section we summarize the basic equations of stellar dynamics and some of the techniques used to solve them. The following two sections discuss the structure of steady bars in two and

---

[4] Notwithstanding his measurement, Kent and Glaudell (1989) preferred a pattern speed 64 ± 15 km s^{-1}kpc^{-1} in their dynamical study of this galaxy (§4.7.3), in order to place co-rotation just outside the end of the bar.

three dimensions respectively. An excellent introductory text has been provided by Binney and Tremaine (1987).

3.1. Relaxation time

Since the density of stars throughout the main body of a galaxy is very low, the orbit of an individual star is governed by the large-scale gravitational field of the galaxy and is not appreciably affected by the attraction of the relatively few nearby stars. The gravitational impulses received by a star as it moves through a random distribution of scattering stars nevertheless accumulate over time. The *relaxation time* is the time taken for these cumulative random deflections to change the velocity components along the orbit of a typical star by an amount equal to the stellar velocity dispersion. Chandrasekhar's (1941) formula yields a value of $\sim 10^{13}$ years, or ~ 1000 times the age of the universe, for star-star encounters in the neighbourhood of the Sun. Since the relaxation time varies inversely as the stellar density, considerably shorter timescales apply in the centres of galaxies, where the star density is higher by several orders of magnitude.

Chandrasekhar's formula has not required revision, but the impressively long relaxation time it predicts is believed to be an overestimate. We now know that the distribution of mass in disc galaxies is not always as smooth as he assumed – gas is accumulated into giant molecular cloud complexes, ranging in mass up to 10^5 M$_\odot$ or even 10^6 M$_\odot$, and some bound star clusters are known to contain almost as much mass in stars. Although these objects are much more diffuse than point masses, clumps in this mass range shorten the relaxation time considerably. It is even further reduced by the tendency for the gravitational attraction of massive objects to raise the stellar density near themselves. The accumulated material, known as a polarization cloud, can easily exceed the mass of the perturber when the stellar motions are highly ordered – as in a rotationally supported disc (Julian and Toomre 1966). Nevertheless, the relaxation time in the objects we consider here is never shorter than the orbital period, and is usually considerably longer.

3.2. Dynamical equations

The long relaxation time implies that the distribution of stars in a galaxy approximates a collisionless fluid and therefore obeys dynamical equations similar to those governing a Vlasov plasma. The closest parallel is with a single species plasma (*e.g.* Davidson *et al.* 1991).

To describe such a fluid mathematically, we introduce a distribution function, F, which is the density of particles in an element of phase space – a multi-dimensional space with (generally) three spatial dimensions and three velocity dimensions. The definition of $F(\boldsymbol{x}, \boldsymbol{v}, t)$ is the mass within a volume element of phase space, divided by the volume of that element, and we would like to take this to the limit of infinitesimal volume. As the number of stars in a galaxy is finite, however, F can be defined only for volume elements large enough to contain many stars. Since this can be very inconvenient mathematically, we generally imagine that the number of stars is greatly (infinitely) increased, while their individual masses are correspondingly reduced, so that F can be meaningfully defined for infinitesimal volume elements. (Because encounters are negligible, the masses of individual stars do not enter into the equations.)

The motion of a fluid element in this phase space is governed by the collisionless Boltzmann (or Vlasov) equation

$$\frac{\partial F}{\partial t} + \boldsymbol{v} \cdot \nabla F - \nabla \Phi \cdot \frac{\partial F}{\partial \boldsymbol{v}} = 0. \tag{1}$$

Since the left hand side is the convective derivative in this space, equation (2) simply states that the phase space density is conserved at a point which moves with the flow.

The quantity Φ in (2) is the smooth gravitational potential of the galaxy, which is related to the volume density, ρ, through Poisson's equation

$$\nabla^2\Phi(\boldsymbol{x},t) = 4\pi G\rho(\boldsymbol{x},t), \tag{2}$$

where G is Newton's gravitational constant. The volume density of stars at any point is the integral of the phase space density over all velocities:

$$\rho(\boldsymbol{x},t) = \int_{-\infty}^{\infty} F(\mathbf{x},\mathbf{v},t)d^3\boldsymbol{v}. \tag{3}$$

The right hand side of equation (2) is zero only for a collisionless fluid. Rapid spatial or temporal variations about the mean potential, of whatever origin, can scatter stars in phase space and lead to a non-zero Fokker-Planck term here (*e.g.* Binney and Lacey 1988). We assume, for the purposes of this review, that no such term exists.

The field of galactic dynamics is, to a large extent, concerned with solutions to this coupled set of integro-differential equations. Only a few analytic equilibrium solutions are known in cases where a particularly simple symmetry (*e.g.* spherical, axial, planar, *etc.*) has been assumed. These, and in some cases the stability of the resulting models, are discussed in the monograph by Fridman and Polyachenko (1984).

3.3. Analytic distribution functions

The classical approach to solving these equations for a particular mass distribution is first to identify the integrals; *i.e.* quantities that are conserved by a test particle pursuing any orbit in the potential. In a steady, non-rotating potential, the particle conserves its energy, and if the potential has an axis of symmetry, the component of angular momentum about that axis is conserved. Jeans's theorem tells us that the distribution function for an equilibrium model is a function of the integrals of the motion (*e.g.* Lynden-Bell 1962a).

The identification of integrals with simple physical quantities such as energy or angular momentum is possible only for very simple potentials, and the approach rapidly becomes too hard for realistic, rotating, non-axisymmetric potentials. Vandervoort (1979) and Hietarinta (1987) discuss the possible forms an extra integral could take in a bar-like potential. One possibility had already been exploited by Freeman (1966), who proposed a family of two-dimensional bar models in a rotating potential consisting of two uncoupled harmonic oscillators. His highly idealized models have some interesting properties, but all have retrograde streaming of the stars inside the bar, which conflicts with the observed situation (§2.5).

Vandervoort (1980) developed a set of stellar dynamical analogues to the Maclaurin and Jacobi sequences of gaseous polytropes. These are uniformly rotating, non-axisymmetric, isotropic bodies for which the distribution function is a function of one integral only. These models are not centrally concentrated enough for elliptical galaxies; but this may not be such a drawback for strong bars, in which the density is less centrally concentrated.

The most promising recent bar-like models for which some headway has been, and still is being, made are the so called Stäckel models, which emerged from Hamilton-Jacobi theory (*e.g.* Lynden-Bell 1962b). Stäckel (1890) identified a class of potentials in which the Hamilton-Jacobi equation separates in confocal ellipsoidal coordinates and in which the density is stratified on

concentric tri-axial ellipsoids. Their main advantage for theoretical work is that they have the most general form known to be always integrable (see §3.4). This implies that *once the distribution function is known*, all the observable properties of the model, such as the streaming velocities and velocity dispersion fields are predictable. The principal disadvantage for our subject is that almost all such models so far discussed are non-rotating.

These models have been extensively explored by Eddington (1915), Kuz'min (1956), Lynden-Bell (1962b) and de Zeeuw (1985) and his co-workers as models for galaxies. The central dense part can have a surprisingly wide variety of shapes (de Zeeuw *et al.* 1986), ranging from simple ellipsoids to more rectangular bodies with squared-off ends.

Unfortunately, the distribution functions required to construct self-consistent models are not so easy to obtain. Statler (1987) obtained a variety of approximate solutions using Schwarzschild's method (§3.5) for several three-dimensional ellipsoidal models.[5] Hunter *et al.* (1990) derived exact expressions for the distribution function for arbitrarily flattened prolate models populated by thin tube orbits. Their solutions can be tailored to allow maximal or minimal streaming around the symmetry axis. Hunter and de Zeeuw (1992) have given solutions for the tri-axial case; again they found a wide range of solutions, but were able to show that self-consistent models require some members from all four of the main orbit families.

One integrable bar model noted by Vandervoort (1979) as a curiosity was later shown to be the first known rotating Stäckel model (Contopoulos and Vandervoort 1992). The centrifugal term is exactly balanced by a term in this highly contrived potential, which has the unphysical features of two singularities at the co-ordinate foci and negative mass density at large distances. The orbital structure of the model, studied in depth by Contopoulos and Vandervoort, is quite different from that found in more realistic bar models.

Very little is known about the stability of Stäckel models, though Merritt and his collaborators have initiated a programme to explore this issue. Merritt and Stiavelli (1990) found that lop-sided instabilities developed in *all* oblate models with predominantly shell orbits. Prolate models, on the other hand, were unstable to buckling modes only when highly elongated (Merritt and Hernquist 1991). This numerical approach complements stability analyses which are possible only for extremely simple models (*e.g.* Vandervoort 1991).

3.4. Near-integrable systems

The basic assumption underlying the approach just outlined is that bars are integrable systems, *i.e.* that all stars possess the number of integrals equal to the number of spatial dimensions. This now seems most unlikely, as we show in §§4 & 5; galactic bars furnish an excellent practical example of the kind of near-integrable Hamiltonian system first studied by Hénon and Heiles (1964), also in an astronomical context. The study of near-integrable systems opens up the modern topic of non-linear dynamics. Unfortunately, even a highly simplified introduction would represent too large a digression for this review and we refer the reader to a standard text (*e.g.* Lichtenberg & Lieberman 1983).

The identification of bars as non-integrable systems not only raises the theoretical problem of why they are not integrable, but also a number of practical questions. The most important are: what is the fraction of chaotic orbits within the bar? how much does their density distribution contribute to the bar potential? and what are the long-term consequences of their

---

[5]   Teuben (1987) provides solutions for the two-dimensional analogue, the elliptic disc.

presence? These questions remain largely unanswered, and it should be clear that they represent a formidable obstacle to progress in our understanding of bar dynamics.

The field has therefore resorted to the less elegant numerical methods described in the next two subsections in order to make further progress.

3.5. Linear programming

Schwarzschild (1979) achieved a major breakthrough when he successfully constructed the first numerical models of a self-consistent, non-rotating, tri-axial stellar ellipsoid, without requiring any knowledge of the nature, or even the number, of integrals supported by the potential.

He began by computing a large number of orbits in a potential arising from an *assumed* tri-axial ellipsoidal density distribution and noted the time-averaged density along each orbit in a lattice of cells spanning the volume of the model. He then used linear programming techniques to find the non-negative weights to assign to each orbit in order that the total density in each cell added up to that in his initially assumed model. As he was able to find more than one solution, Schwarzschild added a "cost function" to seek solutions with maximal streaming, for example. However, the method yields only an approximate equilibrium model, even when a fine lattice of cells is used, and gives no indication of its stability.

Newton and Binney (1984) proposed a variation to this strategy based upon Lucy's iterative deconvolution technique. Its main advantages are that it is easy to program, fast and the resulting distribution function is smoother than that yielded by linear programming. Other iterative algorithms are based upon non-negative least-squares (Pfenniger 1984b) and maximum entropy (Richstone 1987).

3.6. N-body techniques

Because of the intractability of the full-blown self-consistency problem, many workers in the field have turned to N-body simulations. Not only does a quasi-steady N-body model represent a self-consistent equilibrium, but it also demonstrates that the model is not catastrophically unstable. Such models have yielded many important results, and have contributed inestimably to our understanding of barred galaxies. We present these results at appropriate points in this review, and confine ourselves here to alerting the reader to some of the essential limitations of the N-body techniques.

Simple restrictions of computer time (and to a lesser extent memory) limit the numbers of particles that can be used in the simulations. Inevitably, therefore, the potential in simulations is less smooth than in the system being modelled. Statistical fluctuations in the particle density, on all scales from the inter-particle separation up to the size of the system, are larger than they ought to be by the square-root of the ratio of the numbers of particles; in some of the most efficient high quality simulations, which employ perhaps a few times 10^5 particles, the noise level remains about one thousand times higher than in a galaxy of stars.[6]

The various techniques available to combat this problem have been reviewed by Sellwood (1987) but only one, the "quiet start" method, removes fluctuations on the largest scales. The technique involves choosing the initial coordinates of particles in some symmetric configuration and filtering out the components of the potential which arise from the imposed symmetry

---

[6] Density fluctuations of this magnitude may be present in the discs of gas-rich galaxies, however.

(Sellwood 1983). Unfortunately, the symmetric configurations themselves are unstable and disintegrate quite rapidly; the respite from noise is therefore only temporary.

The main effect of these irrepressible fluctuations is to scatter particles away from the paths they would have pursued in a noise free potential. The integrals which should be invariant along the orbit of each particle are no longer preserved. There have been comparatively few studies of orbit quality in simulations, but enough to raise substantial worries (*e.g.* van Albada 1986, Hernquist and Barnes 1990). The simulations are thought to be useful for longer than the scattering time of a typical orbit because the individual scattering events, when averaged over the whole population of particles, accumulate only statistically. However, the long-term stability and any possible secular effects cannot be studied by these techniques.

For obvious reasons of computational economy, the particles in a large majority of bar-unstable disc simulations have been confined to a plane. A few early attempts to include full three-dimensional motion (Hockney and Brownrigg 1974, Hohl 1978, Sellwood 1980) revealed behaviour which differed only slightly from models having equivalent resolution in two-dimensions, but the grids used in all these calculations were so coarse that the out-of-plane motions were virtually unresolved. [The results obtained by Combes and Sanders (1981) did reveal an important difference, which was not understood at the time.] As extra resolution in two-dimensions seemed essential (Sellwood 1981), full three-dimensional simulations for this problem were considered unnecessary for several years. However, recent three-dimensional models have rediscovered Combes and Sanders' old result and show that the two-dimensional models miss some of the essential physics (§§5.1 & 10.1).

4. Two-dimensional bar models

We begin our detailed discussion of the dynamics of bars by making the great simplifying approximation that the motion of stars normal to the galactic symmetry plane can be ignored. The usual justification for this is summarized in §4.1, though it is now clear that this approximation is inadequate for bars; the dynamical structure of a three-dimensional bar is more than just a simple addition of independent vertical oscillations to orbits in the plane. Nevertheless, as many properties of orbits in three-dimensional bars can be recognized as generalizations from two-dimensions, a preliminary discussion of the simpler, but by no means straightforward, two-dimensional case remains an appropriate starting point.

As we have no analytic models for rapidly rotating bars, even in two-dimensions, we might hope to construct an approximate one using Schwarzschild's method (§3.5). Despite the vast literature on two-dimensional bars, this programme has been carried through in only one case (Pfenniger 1984b); most papers confine themselves to a discussion of orbits in arbitrarily selected bar-like potentials having simple functional forms. Clearly, it is necessary to learn which of the many possible orbit families could contribute to a self-consistent model and to understand how they are affected by changes in the potential: a good grounding in both these aspects is an essential pre-requisite for a search for a fully self-consistent model. It is also sensible to explore many types of model in the hope of finding some that might be more nearly integrable (§3.4). However, in two-dimensions at least, the field is now sufficiently mature that such arguments are wearing thin.

4.1. Thin disc approximation

There are three principal requirements which must be fulfilled before three-dimensional motion can be neglected as an unnecessary complication. First, the scale of the non-axisymmetric

structures, spirals, bars, *etc.*, should be large compared with the thickness of the disc. Second, the oscillations of stars in the direction normal to the plane must not couple to motion in the plane. Third, there can be no instabilities which would cause the plane to warp or corrugate.

These three conditions are widely believed to be fulfilled for nearly *axisymmetric* discs. The first is doubtful only in the case of flocculent spiral patterns. The second seems valid because the frequency of z-motion is higher than that of any perturbing forces which might arise from disturbances in the plane, and therefore the motion normal to the plane should be adiabatically invariant (see §5.1). Finally, the principal instability which could give rise to corrugations of the plane, the fire-hose instability, is known to be suppressed by a modest degree of pressure normal to the plane, and "galaxy discs seem to be well clear of this stability boundary" (Toomre 1966). However, the second and third requirements are violated for strong bars (Combes and Sanders 1981, Pfenniger 1984a, Raha *et al.* 1991) and introduce the further aspects to the dynamics we discuss in §5.

4.2. Linear theory

With the exception of the Stäckel models, orbits in all strong bar-like potentials must be calculated numerically. The bewildering variety of orbit types found in most numerical studies of a strong bar-like potential is difficult for the newcomer to assimilate. Moreover, the *characteristic diagrams* and *surfaces of section* drawn in many papers, require considerable explanation before the wealth of information they contain can be comprehended. Before plunging into numerically calculated orbits, therefore, we first explore linear theory for a weakly perturbed case. Although a very crude approximation for bars, the results give useful insight to those from more realistic strongly barred models. We also introduce characteristic curves for orbits of arbitrary eccentricity in the simplest possible case of an *axisymmetric* potential.

The equations of motion of a test particle (*e.g.* a star or planet) in the symmetry plane $(r, \theta, z = 0)$ of a potential, Φ, are

$$
\begin{aligned}
\ddot{r} - r\dot{\theta}^2 &= -\frac{\partial \Phi}{\partial r}, \\
\dot{J} &= -\frac{\partial \Phi}{\partial \theta},
\end{aligned}
\tag{4}
$$

where a dot denotes a time derivative and $J \, (= r^2 \dot{\theta})$, is the specific angular momentum of a star. It is useful to divide the potential into an unperturbed part, which is axisymmetric, and a non-axisymmetric perturbation: $\Phi = \Phi_0 + \phi$.

In an axisymmetric potential ($\phi \equiv 0$), J is conserved and we define a home radius, r_c, at which a star would pursue a circular orbit:

$$
\frac{\partial \Phi_0}{\partial r} = r_c \Omega_c^2 = \frac{J^2}{r_c^3},
\tag{5}
$$

where Ω_c is the angular frequency of circular motion at r_c. A star possessing more energy than the minimum required for circular motion for a given J, oscillates about its home radius. As the period of the radial oscillation is generally incommensurable with the orbital period, the orbit does not form a closed figure in an inertial frame, except for a few special cases such as harmonic or Keplerian potentials. Successive apo-galactica of the rosette-like orbit are between π and 2π radians apart in all realistic galactic potentials.

4.2.1. Lindblad epicycles.   When the star's orbit is far from circular, the radial motion is anharmonic and asymmetric about its home radius. For nearly circular orbits, on the other hand, the star's motion approximates an harmonic epicycle about a guiding centre which orbits at Ω_c, as first exploited by Lindblad (1927) in a galactic context.

To see this, we describe the motion in terms of displacements, (ξ, η), from uniform circular motion; ξ in the outward radial and η in the forward tangential, directions. Assuming the displacements (ξ, η) to remain small, the equations of motion (5) can be approximated as (Hill 1878)

$$\ddot{\xi} + 2r_c\Omega_c\frac{d\Omega_c}{dr}\xi - 2\Omega_c\dot{\eta} = -\frac{\partial\phi}{\partial r}$$
$$\ddot{\eta} + 2\Omega_c\dot{\xi} = -\frac{1}{r_c}\frac{\partial\phi}{\partial\theta}, \tag{6}$$

where the potential derivatives on the right hand sides are to be evaluated along the circular orbit.

Setting the perturbing potential $\phi = 0$ for the moment, the solutions to the homogeneous equations are:

$$\xi = ae^{i(\kappa t + \psi_0)} \qquad \text{and} \qquad \eta = ia\frac{2\Omega_c}{\kappa}e^{i(\kappa t + \psi_0)}, \tag{7}$$

where a is the maximum radial excursion of the particle and the Lindblad epicyclic frequency is

$$\kappa = \left[4\Omega_c^2 + r\frac{d\Omega_c^2}{dr}\right]^{1/2}. \tag{8}$$

These equations describe an elliptic epicycle about the guiding centre. Since $2\Omega_c > \kappa$ in all realistic potentials, the major axis of the ellipse lies along the direction of rotation.

In linear theory, we can treat the individual Fourier components of the potential perturbation separately. When a sinusoidal perturbation rotates at a uniform rate Ω_p, we can write it as $\phi(r, \theta, t) = P(r)e^{im(\theta - \Omega_p t)}$, where m is the azimuthal wavenumber of the perturbation: $m = 2$ is the fundamental wave for a bar or bi-symmetric spiral. The function P describes the radial variation of amplitude and phase of the perturbation; for a spiral it is necessarily complex, but it can be purely real at all radii for a bar. (As usual with complex notation, the physical quantity corresponds to the real part.)

With this form for ϕ, equations (7) become

$$\ddot{\xi} + r_c\frac{d\Omega_c^2}{dr}\xi - 2\Omega_c\dot{\eta} = -\frac{\partial P}{\partial r}e^{im[\theta + (\Omega_c - \Omega_p)t]}$$
$$\ddot{\eta} + 2\Omega_c\dot{\xi} = -\frac{im}{r_c}Pe^{im[\theta + (\Omega_c - \Omega_p)t]}. \tag{9}$$

It is convenient to write the angular frequency at which the guiding centre overtakes the perturbation as $\omega = m(\Omega_c - \Omega_p)$. The particular solution is

$$\xi = \frac{-1}{\kappa^2 - \omega^2}\left[\frac{2m\Omega_c}{r_c\omega}P + \frac{\partial P}{\partial r}\right]e^{i(m\theta + \omega t)}, \tag{10a}$$

and

$$\eta = \frac{-i}{\kappa^2 - \omega^2}\left[\frac{2\Omega_c}{\omega}\frac{\partial P}{\partial r} + \frac{4\Omega_c^2 - \kappa^2 + \omega^2}{\omega^2}\frac{m}{r_c}P\right]e^{i(m\theta + \omega t)}, \tag{11b}$$
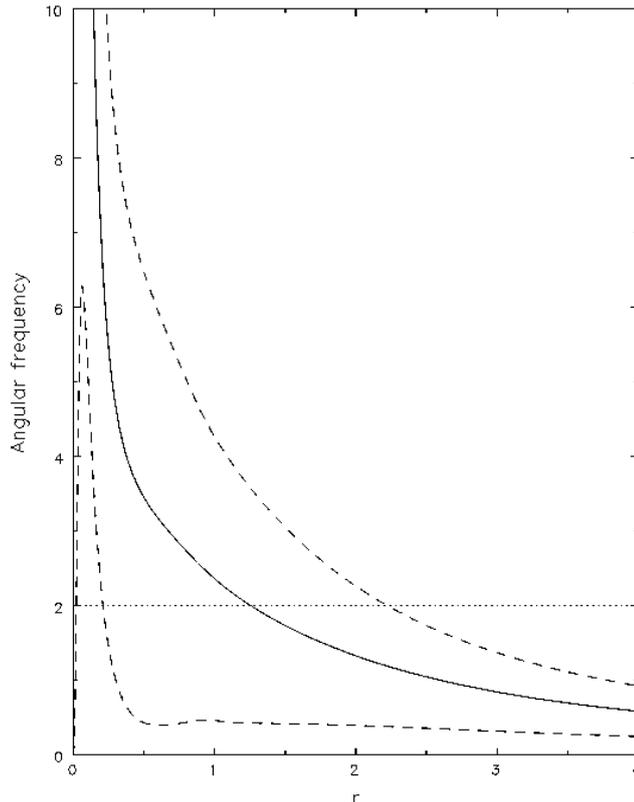
**Figure 4.** The angular frequency of circular motion, Ω_c (full drawn curve) and $\Omega_c \pm \kappa/2$ (dashed curves) for our *axisymmetric* mass model. The horizontal dotted line shows the angular frequency of the frame adopted in §4.2.4; the intersections of this line with the dashed curves mark points where very nearly circular orbits would form closed bi-symmetric figures in this frame.

which describes only the distorted path of the guiding centre. The full solution, which includes epicycles about the new distorted path, is obtained by adding the complementary function [the solution (8) to the homogeneous equations].

A resonant condition occurs wherever the denominators in equations (11) pass through zero. This occurs at co-rotation, where $\omega = 0$, and at the Lindblad resonances, where $\omega = \pm\kappa$. The resonant denominators also imply that, for a fixed amplitude P, the displacements increase without limit as the resonance is approached; our linearized analysis must therefore break down near these radii.

Figure 4 shows the angular frequencies Ω_c and $\Omega_c \pm \kappa/m$, with $m = 2$ as appropriate for a bar, plotted as functions of radius in a reasonably realistic galaxy model. (The axisymmetric mass distribution used is described in §4.3.1.) Resonances for nearly circular orbits occur wherever the horizontal line at the bar pattern speed Ω_p intersects one of these curves. The pattern speed chosen for this illustration has one outer Lindblad resonance (OLR) and two inner Lindblad resonances (ILRs) in this mass model. Clearly there would be no ILRs if Ω_p exceeded the maximum value of $\Omega_c - \kappa/2$; moreover, this peak would be much lower if the galactic potential had a more extensive harmonic core. ILRs need not be present in every barred galaxy, therefore.

4.2.2. Orbit orientations. Equations (11) give the displacements of the guiding centre when subjected to a mild, uniformly rotating, sinusoidal potential perturbation. The guiding centre

moves (at a non-uniform rate) around a centred ellipse which is elongated either parallel or perpendicular to the potential minimum (Sanders and Huntley 1976).

In order to examine the sense of alignment more easily, we neglect the radial derivative, $\partial P/\partial r$, on the grounds that the perturbed potential is likely to vary only slowly with radius. Dropping the exponential factor, the radial displacement of the guiding centre is therefore approximately

$$\xi \simeq -\frac{2m\Omega_c}{r_c\omega(\kappa^2 - \omega^2)}P. \tag{11}$$

If we choose the line $\theta = 0$ for the bar major axis, P is real and negative and ξ has the same sign as ω between the Lindblad resonances, but takes the opposite sign when $|\omega| > \kappa$, *i.e.* further from co-rotation than the Lindblad resonances. Thus the orientation of the orbit changes across every one of the principal resonances. Between the ILR (or the centre, if none is present) and co-rotation, the orbit is aligned with the bar, but it is anti-aligned beyond co-rotation. The orientation reverts to parallel alignment beyond the OLR.

The orbit therefore responds as a harmonic oscillator of natural frequency κ driven at frequency ω, with a negative forcing frequency being interpreted as its absolute value but π out of phase. The switch of alignment across the Lindblad resonances occurs for the familiar reason that any driven harmonic oscillator is in phase with the forcing term when the driving frequency, ω, is below its natural frequency, κ, but is exactly π out of phase when the forcing frequency exceeds the natural frequency.

Even though equations (11) were derived assuming infinitesimal perturbations, most studies in a variety of reasonable potentials have found that the more nearly circular periodic orbits are aligned with the bar inside co-rotation, and that stable perpendicularly oriented orbits are often found inside the ILR.[7]

4.2.3. Action-angle variables.   The epicyclic viewpoint remains valid for arbitrarily eccentric orbits in an axisymmetric potential, but the motion can no longer be described by equations (7). Kalnajs (1965, 1971) was the first to use action-angle coordinates, (J_r, J_a, w_r, w_a), to describe galactic orbits of arbitrary eccentricity. In an axisymmetric potential, the radial velocity of a star of energy (per unit mass) E and specific angular momentum J is

$$\dot{r} = \left\{2\big[E - \Phi(r)\big] - \frac{J^2}{r^2}\right\}^{1/2}. \tag{12}$$

The period of its radial oscillation is

$$\oint \dot{r}^{-1}dr = \tau_r = \frac{2\pi}{\Omega_r}, \tag{13}$$

and the frequency Ω_r thus defined is constant for that star. We define the angle w_r to be the phase of this oscillation; thus $\dot{w}_r = \Omega_r$. The action conjugate to this angle, known as the *radial action,* is the area of the oscillation in phase space (divided by 2π in the normalization used in this field), *i.e.*

$$J_r = \frac{1}{2\pi}\oint \dot{r}\,dr. \tag{14}$$

---

[7] Contopoulos and Mertzanides (1977) found an example where a steep radial gradient in the perturbation, which we neglected in equation (12), caused a local reversal of these normal orbit orientations.
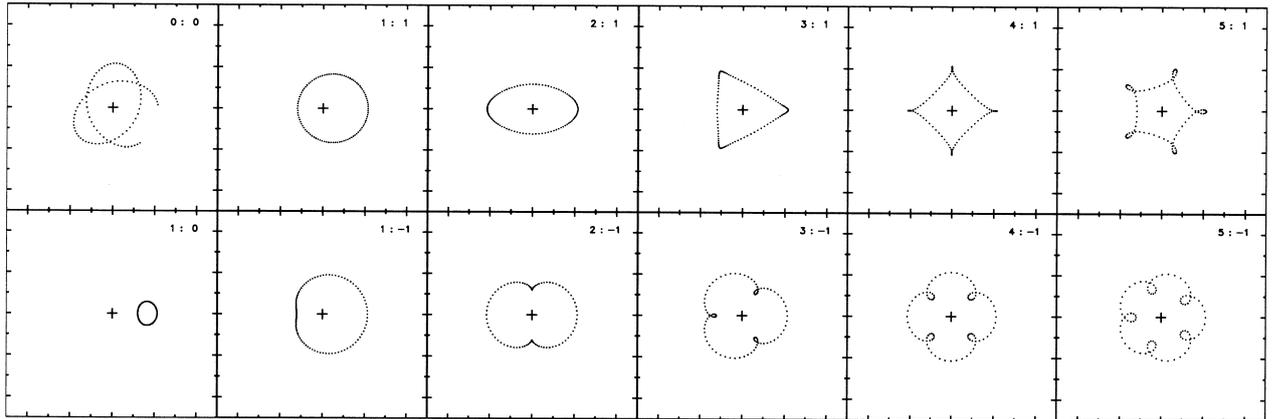
Figure 5. A single orbit drawn in frames rotating at many different rates. The view marked 0:0 is from an inertial frame ($\Omega_{\text{frame}} = 0$) and all the other views are seen when Ω_{frame} is given by equation (17) with the values of $m{:}l$ marked in each. The 1:0 frame shows the Lindblad epicycle. In all frames with l negative, the star orbits less rapidly than the frame, whereas the reverse is true when l is positive. The only frame which rotates counter to the star's orbit is that marked 1:1. The 100 dots in each panel are separated by equal time intervals for that frame.

The radial action has the dimensions of angular momentum and is a measure of the amplitude of a star's radial oscillation.

Because a star conserves its angular momentum during this radial oscillation, it does not progress around the galactic centre at a uniform angular rate (except for circular orbits), but we introduce an angle w_{a} that does. If $\Delta\theta$ is the change in a star's azimuth during one radial period, we define this angle to change at the uniform rate

$$\dot{w}_{\text{a}} \equiv \Omega_{\text{a}} = \frac{\Delta\theta}{\tau_{\text{r}}}. \tag{15}$$

Thus Ω_{a} is the orbital frequency of the guiding centre and w_{a} its phase angle. The action J_{a} conjugate to w_{a} is simply J, the specific angular momentum.

For less eccentric orbits, the motion tends towards the epicyclic description of §4.2.1, and these new coordinates behave as:

$$\begin{aligned} J_{\text{r}} &\to \tfrac{1}{2}\kappa a^2 & J_{\text{a}} &\equiv J \\ \Omega_{\text{r}} &\to \kappa & \Omega_{\text{a}} &\to \Omega_{\text{c}} \end{aligned}. \tag{16}$$

For eccentric orbits in most reasonable potentials, Ω_{a} and Ω_{r} are respectively less than Ω_{c} and κ evaluated at the guiding centre.

4.2.4. Orbits in rotating frames. Because bars (and perhaps spirals) are believed to be steadily rotating features, it is sensible to study orbits in a frame which rotates with the non-axisymmetric pattern. A number of their properties in perturbed potentials can be understood more readily by first considering orbits in an axisymmetric potential viewed from rotating axes.

Although the orbit of a general star in an axisymmetric potential does not close when viewed from an inertial frame, it will appear to close to an observer in a coordinate system which rotates at certain frequencies. The angular rotation rate of the frame in which the orbit will appear to close must be

$$\Omega_{\text{frame}} = \Omega_{\text{a}} - \frac{l}{m}\Omega_{\text{r}}, \tag{17}$$
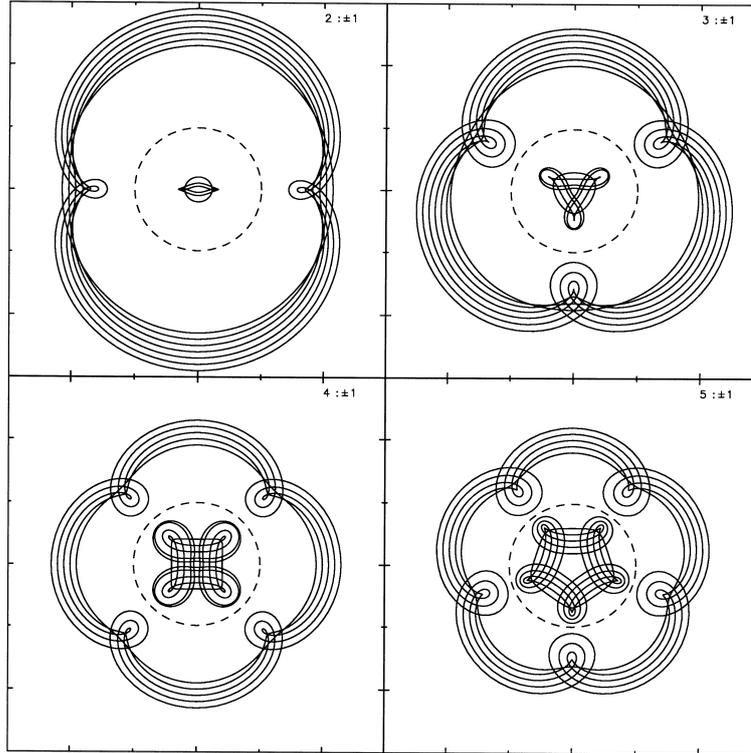
Figure 6. Many orbits which all close in the same rotating frame. Most orbits are highly eccentric, but as the order of the symmetry rises, the more nearly circular orbits lie progressively closer to the co-rotation circle (dashed).

for integer l and m. Figure 5 shows the *same* orbit drawn in several rotating frames, with the values of l and m marked for each. The figure closes after the orbit has made m radial oscillations and $|l|$ turns about the centre of the potential.

Since the frequencies vary from orbit to orbit, most orbits will not close in one arbitrary rotating frame. However, as both Ω_a and Ω_r vary with both the specific energy, E, and angular momentum, J, (18) can be satisfied for more than a few isolated orbits, for a single Ω_{frame}. In fact, there will be an infinite number of 1-D sequences in the two-dimensional (E, J) space along which the orbits appear to close.

To illustrate this important concept, Figure 6 shows many different orbits which close in the *same* rotating frame. (These orbits were found numerically in the axisymmetric mass model described in §4.3.1.) We have grouped these selected orbits by shape, and it should be clear that each group represents a continuous sequence of orbits which close in this frame. Obviously in this axisymmetric potential, the orientation of the shapes is arbitrary; we have simply chosen to draw them so that the axis of reflection symmetry is in the y direction.

Figure 7 shows *characteristic curves* for sequences of orbits in this potential which all close in the same frame. The radial extrema of closed orbits are plotted as a function of the quantity $E_J = E - J\Omega_{\text{frame}}$ (with Ω_{frame} held constant), which is known as Jacobi's integral (see §4.3.2), and we plot these as negative values for stars with $J < 0$. The heavily drawn line shows circular orbits, which trivially close in any frame, and the dashed *zero velocity curve* (or ZVC) marks the radii at which a particle would appear momentarily at rest in this frame. These two curves touch at their maximum values of E_J near the ordinate $r = 1.25$, at which a star on a circular
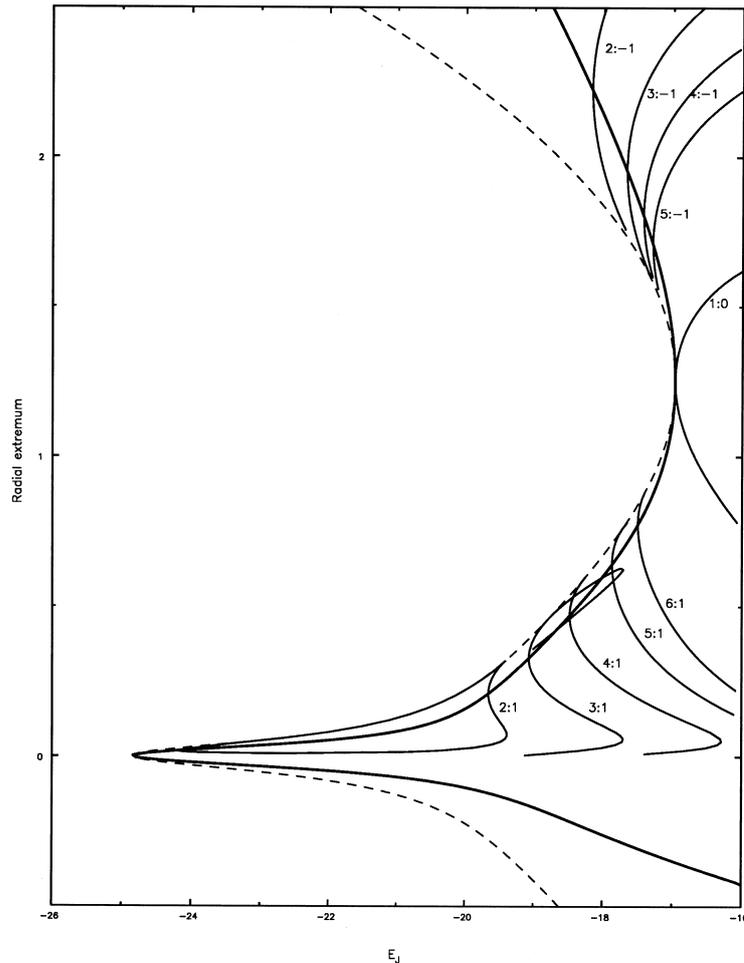
Figure 7. Characteristic curves showing the loci of the radial extrema of families of orbits which all close in one rotating frame; negative values are used for orbits which rotate in a sense counter to the frame. The thick line marks the circular orbits as a function of the Jacobi integral, and the dashed curve marks the ZVC which no orbit can cross. Each characteristic curve is marked with the m:l value for which the orbits close.

orbit appears at rest – *i.e.* it co-rotates with the frame.

All other lines on this Figure show parts of several characteristic curves. Each is marked with the ratio of radial to orbital periods before the orbit closes in the rotating frame. We have selected only orbits for which $l = \pm 1$ or 0 and low values of m and the majority of sequences are incomplete – only in the case of the 3:1 family have we drawn the sequence as far as almost radial orbits. The 1:0 family are simply the extension of Lindblad epicycles (§4.2.1) to more eccentric orbits.

Each m:± 1 sequence crosses the circular orbits at a point known as a *bifurcation*. In an axisymmetric potential, each bifurcation occurs where $\Omega_{\mathrm{frame}} = \Omega_{\mathrm{c}}(r) - \frac{l}{m}\kappa(r)$ for the infinitesimally eccentric orbits discussed above. (The 3:1 sequence crosses the circular orbit line at three points inside co-rotation; the bifurcation occurs only at the point where the orbits are nearly circular.) There is one bifurcation outside co-rotation ($l = -1$) and one inside ($l = 1$) for all sequences except for the 2:1 orbits. In this exceptional case, the two sequences starting from the two 2:1 bifurcations are connected and form a closed loop around the circular orbits, called
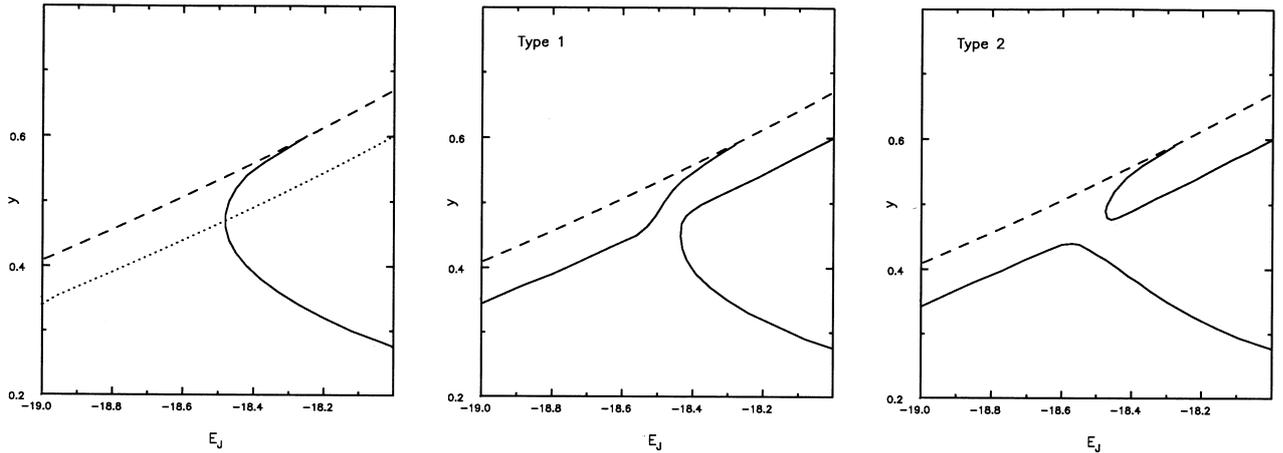
Figure 8.   A schematic representation of the two principal types of resonance gaps. The dashed curve in each panel is the ZVC; the left hand panels show the bifurcation with no potential perturbation, and the other illustrate the two different types of gap that a perturbation can create. These diagrams are drawn for the situation inside co-rotation.

a bubble by Contopoulos (1983a). The 1:1 bifurcations occur outside the diagram; the $l = 1$ lies at large E_J for retrograde orbits and the $l = -1$ at large r.

The two branches of each sequence, on either side of the bifurcation, are not independent, since each traces one of the two extremal radii for the same orbit. Each sequence also touches the ZVC, where the orbit develops cusps. More eccentric orbits loop back on themselves for part of the time (Figure 6), but we have drawn this continuation only for the 3:1 family in order not to clutter the diagram with too many crossing lines.

Similar sequences of higher m (still with $|l| = 1$) can be found closer to co-rotation and are ever more densely packed as they approach this point. More sequences occur for higher values of $|l|$, and correspond to orbits which close after l rotations. For small m, they are found either far outside co-rotation or are retrograde (if they exist at all), but the higher m sequences could also be drawn within the boundaries of Figure 7 – in fact sequences for all $m:l$ would densely fill the plane, except for the region excluded by the ZVC.

4.2.5. Effect of a weak non-axisymmetric perturbation.   If we again add a weak perturbing potential co-rotating with this frame (*i.e.* so $\Omega_{\text{frame}} = \Omega_{\text{p}}$), all these closed non-circular orbits resonate with the perturbation. We should therefore expect them to be substantially altered in a perturbed system.

We have already calculated the effect on the circular orbits in §4.2.2. An infinitesimal, pure m-fold, symmetric potential perturbation introduces Lindblad resonances at the $m:\pm1$ bifurcations. No closed orbits can exist at the resonant point, because a particle there would experience a monotonic acceleration until it is driven off resonance. Linear theory cannot tell us any more, but exact calculations show that the four branches at a bifurcation separate into two, non-crossing pairs; the resonance imposes a gap, both in the circular orbits and in the $m:1$ sequence. The stronger the potential perturbation, the wider the gap becomes.

We can see which pairs must join from the direction in which the perturbation moves the circular orbits in the characteristic diagram (Figure 7), a small part of which is shown enlarged in the first panel of Figure 8. It is customary in these diagrams to plot the intercept of the

distorted orbit on the *minor* axis of the potential perturbation; thus the circular orbits are displaced in the direction given by the sign of $-\xi$ in (11a).

When $\partial P/\partial r$ is negligible, ξ has the same sign as $2m\Omega_c/[r_c\omega(\kappa^2-\omega^2)]$, since P is negative. In this case, the circular orbit branch on the co-rotation side of the Lindblad resonance bends away from the ZVC, while that on the other side of the resonance bends towards the ZVC, which is called a gap of type 1. On the other hand, should the perturbation amplitude decrease rapidly with increasing radius, the term containing $\partial P/\partial r$ could outweigh the other in (11a); under these circumstances, the bends occur in the opposite sense creating a gap of type 2. Both types of gap are shown schematically in Figure 8.[8]

Linear theory predicts gaps only at the Lindblad ($m{:}{\pm}1$) resonances. Finite perturbations, however, give rise to many more gaps for two distinct reasons. Firstly, in most reasonable bar-like potentials, the perturbation is not a pure $m=2$ sinusoid, but also contains other Fourier components. We should therefore expect gaps at every $m{:}{\pm}1$ resonance for which the Fourier component m is non-zero; these will be at even values of m whenever the perturbation has exact two-fold rotational symmetry. However, gaps continue to occur at all even m bifurcations when the perturbation has a pure $\cos(2\theta)$ form (Contopoulos 1983a). This is because the finite radial extent of the distorted path of the guiding centre breaks the precise m-fold symmetry of the potential explored by the star. The first such additional resonances for non-linear orbits, the $2m{:}{\pm}1$ resonances, are known as ultra- or hyper-harmonic resonances, and occur at $4{:}{\pm}1$ for a bar.

No gaps develop at the odd $m{:}{\pm}1$ bifurcations for a purely symmetric potential perturbation. Some authors rather confusingly continue to refer to a resonance gap as a bifurcation; the phrase *pitchfork bifurcation* is useful to emphasize a bifurcation without a gap.

4.3. Strong bars

The daunting task of summarizing the major results on the dynamical structure of two-dimensional stellar bars is made still harder by the number of rival conventions adopted by the various groups. The most obvious is the number of different naming conventions for the orbit families in current use, but even such simple things as the bar orientation in diagrams has not been standardized: *e.g.* its major axis lies up the page in some papers and across the page in others and a recent author has decided it looks nicer at 45°! While a careful reader can always infer the orientation, it is frequently left unstated. Other inconsistencies abound in the important characteristic diagrams (§4.4).

A large number of different mass models has been investigated. This has the dual advantages that we can "separate what is generic from what is accidental" (Contopoulos and Grosbøl 1989) and can begin to understand how the properties of the orbits change as parameters are varied. However, this strategy makes it impossible for a reviewer to select sample diagrams from the literature to illustrate all aspects of a single model. The relation between the three principal diagrams, showing shapes of periodic orbits, characteristic curves and surfaces of section, and the reason for constructing all three, is much easier to comprehend if an illustrative example of each can be shown for the same model.

---

[8] This is not precisely the convention used by Contopoulos and Grosbøl (1989), who define 4 types of gap.

4.3.1. Mass model.   We have therefore anchored this part of our review around a single mass model which we introduce to illustrate the main results from the literature. The model we have selected is constructed from building blocks in the usual artificial manner. However, it is among the simplest which display many of the properties frequently discussed and its orbital structure is qualitatively similar to the more realistic N-body and photometric models discussed in §§4.9.2 & 4.9.3, for which the gravitational potential is known only numerically. We also make no attempt to ascertain whether the orbital structure of our model is favourable for complete self-consistency.

Our model, which most closely resembles those used by Sanders and his collaborators, has the following three mass components:

B A uniformly tumbling Ferrers (1877) ellipsoid to model the bar. This is an inhomogeneous prolate spheroid of mass M_B having a density profile

$$\rho_B(m) = \begin{cases} \frac{105}{32\pi ac^2} M_B (1-\mu^2)^2 & \mu < 1 \\ 0, & \mu \geq 1 \end{cases} \tag{18}$$

where

$$\mu^2 = \frac{x^2}{a^2} + \frac{y^2 + z^2}{c^2}, \tag{19}$$

and $a > c$. The major axis of the ellipsoid, a, is therefore aligned with the x-axis [following the convention in Binney and Tremaine (1987)] and the bar and coordinate system rotate about the z-axis. De Vaucouleurs and Freeman (1972) give the potential of this mass distribution in the following convenient form: let $\epsilon^2 = a^2 - c^2$ and define ψ by

$$\begin{aligned} y^2 \tan^2 \psi + x^2 \sin^2 \psi = \epsilon^2 \qquad & \mu > 1 \\ \cos \psi = c/a \qquad & \mu \leq 1 \end{aligned} \tag{20}$$

and

$$w_{lk}(\psi) = 2 \int_0^\psi \tan^{2l-1} \theta \sin^{2k-1} \theta d\theta.$$

These integrals are all straightforward. The potential can now be written as

$$\begin{aligned} \Phi_B(x,y) = \frac{105 G M_B}{32\epsilon} \Big[& \frac{1}{3} w_{10} - \frac{1}{\epsilon^2}(x^2 w_{11} + y^2 w_{20}) \\ & + \frac{1}{\epsilon^4}(x^4 w_{12} + 2x^2 y^2 w_{21} + y^4 w_{30}) \\ & - \frac{1}{3\epsilon^6}(x^6 w_{13} + 3x^4 y^2 w_{22} + 3x^2 y^4 w_{31} + y^6 w_{40}) \Big]. \end{aligned} \tag{21}$$

S A small dense spherically symmetric component to model the bulge/spheroid which has the density profile of a Plummer sphere

$$\rho_S(r) = \frac{3M_S}{4\pi s^3} \left(1 + \frac{r^2}{s^2}\right)^{-\frac{5}{2}}, \tag{22}$$

where M_S is the mass of the spheroid and s is a length scale. (Of course, r is here a spherical radius.)
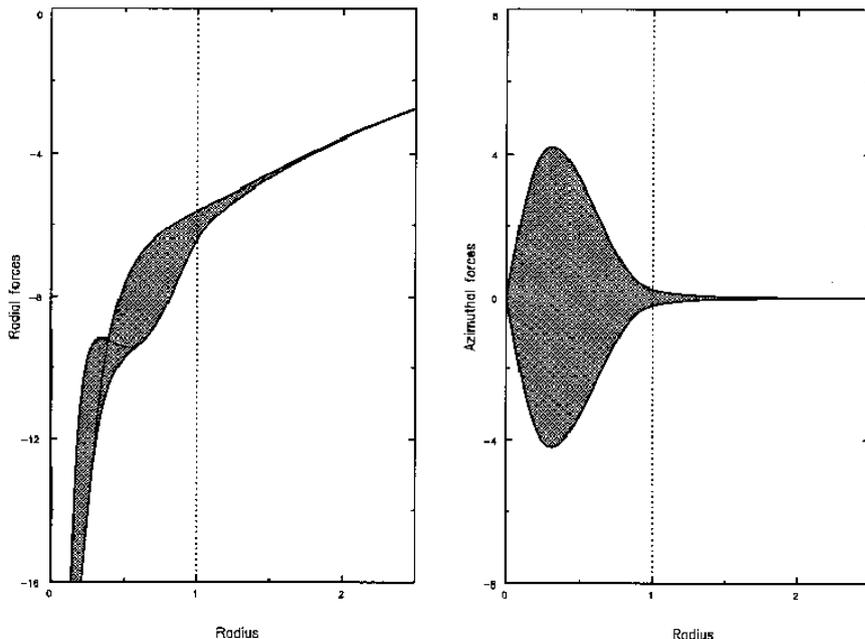
Figure 9. The two force components at various azimuthal angles in our barred model as functions of radius. The boundaries to the shaded areas indicate the largest and smallest values attained around at circle at that radius. Within radius 1 (the semi-major axis of the bar) the forces vary strongly with azimuth, but their range decays rapidly outside the bar.

H An extensive spherically symmetric component to model the halo which has the same form as equation (23), but a much lower central density, larger total mass, M_{H}, and longer length scale, h.

Although all three components are 3-dimensional, we require the potential in the plane $z = 0$ only – its variation out of the plane is of no importance in this section. We therefore do not need to distinguish a separate disc component: component H can be thought of as representing both the disc and halo.

The advantages of choosing a Ferrers ellipsoid to represent the bar are that the potential and its derivatives can be written in closed form and that the potential is continuous up to its third derivative (because only the second derivative of the density is discontinuous at the boundary). The disadvantage is that being elliptical with a constant eccentricity at all radii, the mass distribution does not resemble that of real bars (see §2.3). We have adopted this model here because it is easy to program and widely used, and because it exhibits almost all the generic properties we wish to illustrate.

We set the gravitational constant $G = 1$ and adopt the bar major axis as our unit of length ($a = 1$); in this unit $s = 0.05$ and $h = 1.5$. The masses of the three components are $M_{\mathrm{B}} = 1.1852$, $M_{\mathrm{S}} = 0.3$ and $M_{\mathrm{H}} = 25$. The axis ratio of the ellipsoid we choose to be $a/c = 3$ and we set its angular rotation rate $\Omega_{\mathrm{p}} = 2$ in these units. [The axisymmetric mass model used in §4.2 was very similar, differing only in that the Ferrers ellipsoid was spherical ($a/c = 1$) and had a mass of precisely 1 unit.]

Figure 9 shows the azimuthal variations in both the radial and tangential forces in our model. The gravitational forces therefore vary quite strongly with azimuth within the bar, but quickly approach axial symmetry beyond it.
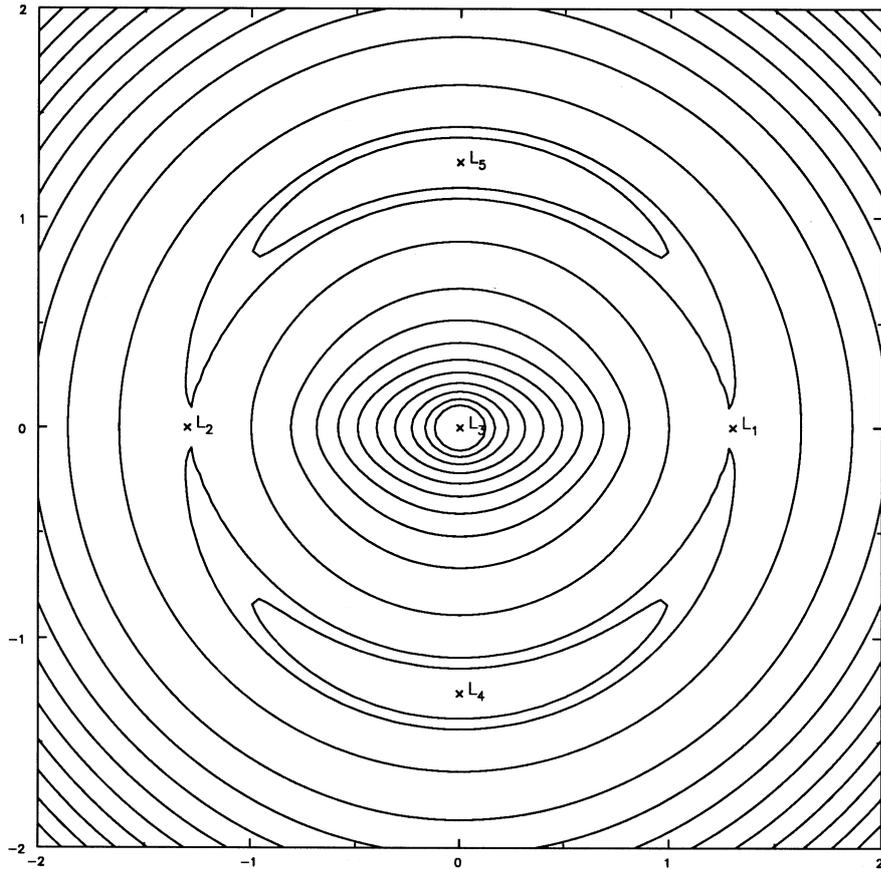
Figure 10.   Contours of the effective potential in our barred model and the locations of the five Lagrange points. The L_3 point at the centre is a minimum, the points marked L_4 and L_5 are equal absolute maxima and those marked L_1 and L_2 are saddle points. Well beyond this ring of Lagrange points, the effective potential slopes away parabolically to infinity. The bar major axis is across the page.

4.3.2. Rotating non-axisymmetric potentials.   The gravitational potential of a uniformly rotating, non-axisymmetric density distribution, is steady when viewed from axes which co-rotate with the perturbation. We define an *effective potential* in a frame rotating at the angular rate $\Omega_{\rm p}$:

$$\Phi_{\rm eff} = \Phi - \tfrac{1}{2}\Omega_{\rm p}^2 r^2, \tag{23}$$

where r is the distance from the rotation centre. The equation of motion in the rotating frame of reference may then be written

$$\ddot{\boldsymbol{r}} = -\nabla\Phi_{\rm eff} - 2(\Omega_{\rm p} \times \dot{\boldsymbol{r}}). \tag{24}$$

Though the second (Coriolis) term complicates the dynamics, the gradient of the effective potential at least determines the acceleration of a particle momentarily at rest in this frame.

Figure 10 shows contours of the effective potential in our model. The topology has been aptly likened by Prendergast (1983) to that of a volcano; there is a deep minimum at the centre which forms the crater, a rim whose height varies slightly and steep walls sloping away to infinity. There are five *Lagrange points* altogether at which the gradient of $\Phi_{\rm eff}$ is zero: a

minimum at the centre (L$_3$) and the other four lie at symmetry points on the crater rim: there are two global maxima on the bar minor axis (L$_4$ and L$_5$), and two saddle points on the major axis (L$_1$ and L$_2$). A stationary particle located at any one of these points would remain at rest in this rotating frame, or would co-rotate with the bar. The equilibrium at the saddle points, L$_1$ and L$_2$, is always unstable, that at the bar centre, L$_3$, is always stable, but the stability of the minor axis Lagrange points, L$_4$ and L$_5$, depends upon the details of the mass distribution (*e.g.* Binney and Tremaine 1987);[9] they are stable in many reasonable models, including that we have chosen.

Neither the specific energy, E, nor the angular momentum, J, of a particle is separately conserved in a rotating non-axisymmetric potential, but Jacobi's integral ($E_J = E - \Omega_p J$, introduced in §4.2.4) is conserved. It may also be expressed in terms of the effective potential:

$$E_J = \tfrac{1}{2}|\dot{\boldsymbol{r}}|^2 + \Phi_{\text{eff}}, \tag{25}$$

and is therefore the energy with respect to rotating axes. As a consequence, it is often loosely referred to as the energy.

This form for E_J renders the concept of the effective potential doubly useful, since it determines whether a particle of a given energy (E_J) is confined to particular regions of the space. A particle for which $E_J < \Phi_{\text{eff}}$ at the Lagrange points L$_1$ or L$_2$ is confined to remain either inside co-rotation or outside it. Only those particles having $E_J > \Phi_{\text{eff}}$ at the Lagrange points L$_4$ or L$_5$ (the absolute maxima of Φ_{eff}) are free energetically to explore all space. Note however, that a particle having a specific E_J will not necessarily explore the whole region accessible to it; in particular, particles beyond the Lagrange points may not be unbound in reality, even though they appear to be so energetically, because the Coriolis force generally prevents them from escaping to infinity.

4.4. Periodic orbits

A simple periodic orbit is a special orbit which a star would retrace identically on each passage around the galaxy in the rotating frame of the perturbation. More complicated periodic orbits also exist which close after more than one passage around the galaxy. All orbits which close in a steady (rotating) potential are therefore periodic orbits (§4.2.4).

Stars in any barred galaxy are most unlikely to follow periodic orbits, yet the study of periodic orbits is of interest because many non-periodic orbits are *trapped* to oscillate about a parent periodic orbit, in a manner exactly analogous to non-circular orbits following the path of the guiding centre (which is a periodic orbit) in an unperturbed or weakly non-axisymmetric potential (§4.2.1). A periodic orbit therefore gives an approximate indication of the shape of the density distribution of stars trapped about it.

Unlike the infinitesimally perturbed case, however, it is possible to find orbits which are not trapped about any periodic orbit, but explore a much larger region of phase space. This is the distinguishing property of a near-integrable system (§3.4). We may determine whether an orbit is trapped or not through an examination of the *surface of section* (§4.6), introduced by Poincaré (1892).

---

[9] Unfortunately, their application to the logarithmic potential has a minor flaw, pointed out by Pfenniger (1990).

4.4.1. Techniques.   The shooting method is the most widely used to find periodic orbits. One chooses an initial set of coordinates in phase space, $\mathbf{x_0}$, usually on one of the principal axes of the potential, and integrates the orbit until it recrosses the same axis at some point $\mathbf{x_1}$. The orbit integration can be considered as a mapping

$$T(\boldsymbol{x}_0) = \boldsymbol{x}_1, \tag{26}$$

and a periodic orbit is then defined by $T(\boldsymbol{x}_0) = \boldsymbol{x}_0$. The map is, in fact, a Hamiltonian map (*e.g.* Lichtenberg and Lieberman 1983) and periodic orbits are also known as *fixed points* in the map. To find such a point, we calculate the mapped points for other trial orbits in the vicinity of an initial guess $\mathbf{x_0}$, to determine the changes required to $\mathbf{x_0}$ in order to move the end point $\mathbf{x_1}$ towards $\mathbf{x_0}$. The calculation proceeds iteratively and generally converges quickly to a periodic orbit to high precision. An alternative relaxation, or Henyey, method is described by Baker *et al.* (1971), but is less widely used.

Although $\mathbf{x_0}$ has four components (for planar motion) there are only two degrees of freedom for the search, since the Jacobi integral is conserved by the mapping and a change of starting phase along the orbit is trivial. It is customary to search for orbits which cross the minor (*y*-) axis of the bar with $\dot{y} = 0$ by adjusting y_0 and $\dot{x}_0$. All orbits found by this search strategy must be reflection symmetric about the *y*-axis; searches in which $\dot{x}_0$ and $\dot{y}_0$ are varied are required to find asymmetric periodic orbits.

4.4.2. Orbit stability.   A star on any periodic orbit will forever retrace exactly the same path. Floquet's theorem (*e.g.* Mathews and Walker 1970, Binney and Tremaine 1987) tells us that a star whose starting point is very close to that of a periodic orbit, will follow a path which either winds tightly around that of the periodic orbit, or diverges away from it in an exponential fashion, at least while the departure from the periodic orbit remains small. These two types of behaviour imply that the periodic orbit is, respectively, stable or unstable.

In practice, having found a periodic orbit, one then integrates two neighbouring orbits, each having the same value of $E_{\rm J}$ but displaced slightly from $\mathbf{x_0}$ in different directions, to find the end points $\mathbf{x_1}$ where it recrosses the *y*-axis. In the neighbourhood of a periodic orbit, these must be approximately

$$\boldsymbol{x}_1 = T(\boldsymbol{x}_0 + \delta\boldsymbol{x}) \simeq \boldsymbol{x}_0 + \left.\frac{\partial T}{\partial \boldsymbol{x}}\right|_{\boldsymbol{x}_0} \delta\boldsymbol{x}. \tag{27}$$

The 2×2 Jacobian matrix of partial derivatives of T can be estimated numerically from the displacements of the final point, given the initial displacements $\delta\mathbf{x}$. Because Hamiltonian maps are area preserving (*e.g.* Lichtenberg and Lieberman 1983), the determinant of the matrix, and therefore the product of the eigenvalues, is unity. Since the matrix is real there are just two cases: the orbit is stable if the eigenvalues are complex and lie on the unit circle, and it is unstable when the eigenvalues are real and one lies outside the unit circle. The two cases are respectively elliptic or hyperbolic fixed points in mapping parlance.

4.5. Periodic orbit families

Numerous orbit families have been described in the literature. We do not attempt to enumerate them all here, but confine our discussion to those which are relevant to the structure of real bars. Contopoulos and Grosbøl (1989) give a more comprehensive review.

A selection of periodic orbits supported by our model (§4.3.1) is shown in Figure 11. In every panel of this figure, the dashed curve marks the outer boundary of the Ferrers ellipsoid. Stable periodic orbits are full drawn, unstable ones are dotted.

There are a number of different naming conventions for the orbit families. In Figure 11 we use that developed by Contopoulos, which is neither descriptive nor easily memorable, simply because it is the most widely used. Athanassoula *et al.* (1983) attempted an alternative system but, like others, theirs is not easily generalized to three-dimensions, and even those authors have reverted to the Contopoulos system in their more recent papers. The x_1 family (Figure 11a), also referred to as the *main* family, is elongated parallel to the bar within co-rotation. The x_2 family is represented by the two orbits within the bar in Figure 11(b); note that these are elongated perpendicularly to the bar axis. We do not show any x_3 orbits which are about as extensive as the x_2 family, but are much more elongated and always unstable. The retrograde x_4 family (Figure 11c) are very nearly round, but are slightly extended perpendicular to the bar. All four x_i families are 2:1 orbits. Figure 11(d-e) shows both the inner and outer 3:1 and 4:1 resonant families while Figure 11(f) shows the short and long period orbit families which circulate about the Lagrange points.

We show characteristic curves for most of the main periodic orbit families in Figure 12. This diagram, which plots the y (minor axis) intercepts of the orbits in each family plotted as a function of Jacobi's integral, should be compared with that for the axisymmetric potential (Figure 7). Again we differentiate between stable (full drawn) and unstable (dotted) families; *n.b.* all bound orbits in an axisymmetric potential are stable (Figure 7).

There are broad similarities and important differences between Figures 12 and 7. The most obvious difference is that the circular orbit sequence in the axisymmetric potential has been broken by numerous gaps in this strong bar case; these gaps are so large and frequent in some regions that the sequence becomes hard to trace, especially inside co-rotation.

4.5.1. Bi-symmetric families. Starting with retrograde orbits, we see that the x_4 family in Figure 12 closely corresponds to the retrograde circular orbits in Figure 7. Both the characteristic curve and the orbit shape (Figure 11c) indicate that these counter rotating orbits are not much affected by the bar potential, being only slightly elongated perpendicularly to the major axis. These seem to be generic properties of the retrograde orbits in every potential investigated.

The direct 2:1 families are substantially affected by the bar; however, those beyond co-rotation are more easily related to their counterparts in Figure 7. The orbital eccentricity of the bi-symmetric families outside co-rotation rises in the vicinity of the OLR. The orbits of the outer nearly circular family are elongated parallel to the bar (Figure 11a) while the inner family are perpendicular, creating a typical gap of type 1. All this is consistent with the linear theory predictions of §4.2, even though the eccentricity rises well beyond the linear regime.

The correspondence with Figure 7 is less apparent inside co-rotation, because what was the circular orbit sequence has been broken by two yawning gaps. For $E_J < -18$, the nearly circular orbits have become very elongated and the characteristic curve is therefore much further from the ZVC. At the 2:1 resonant gap, the nearly circular sequence joins to the lower branch of the bubble in Figure 7 while the continuation of the circular sequence has broken away and lies much closer to the ZVC to form the x_2 sequence. The third branch, that which lies very close to the ZVC in Figure 7, becomes the highly eccentric and unstable x_3 family. Thus the x_1 family derives from the circular orbits only very near the centre and near $E_J = -20$ while
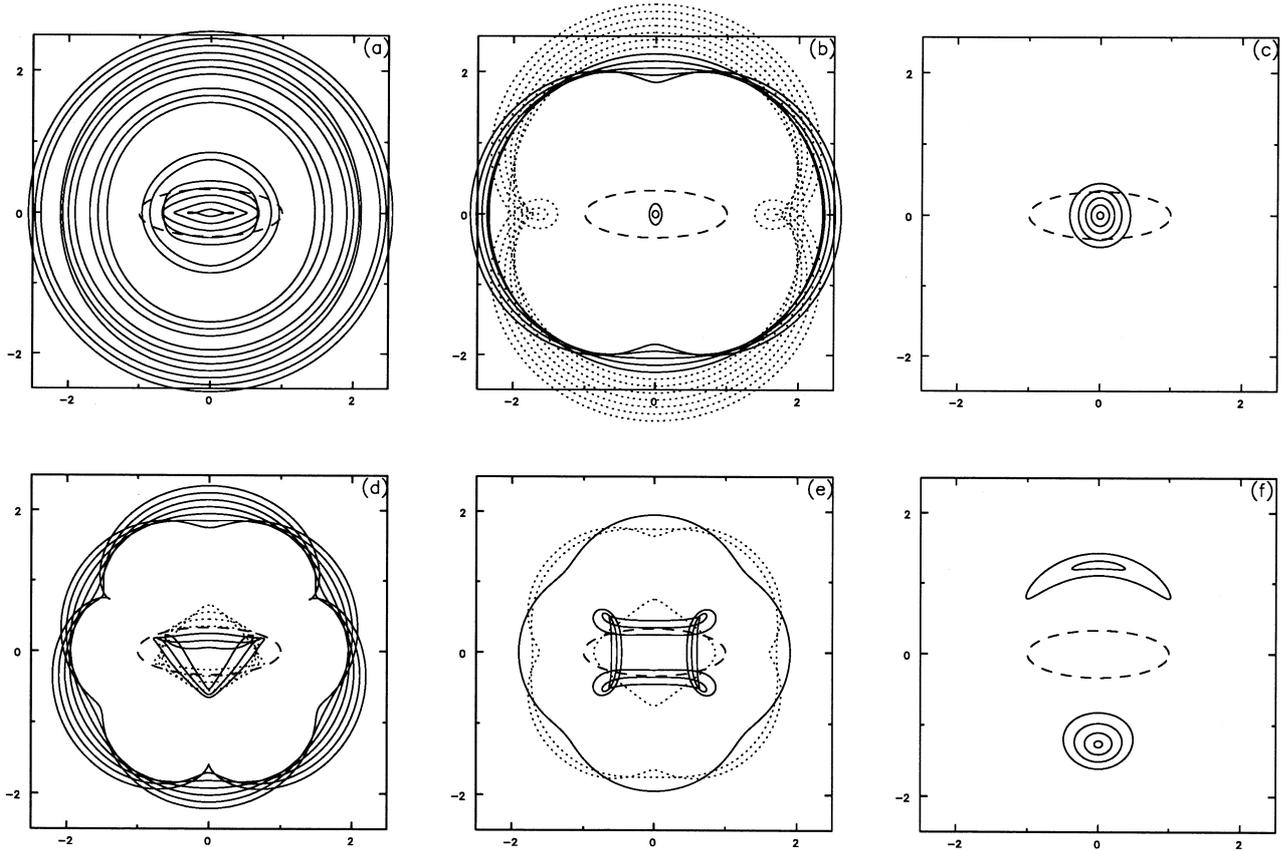
Figure 11. Some periodic orbits in our barred model; those drawn with full lines are stable orbits, unstable orbits are drawn as dotted curves. The boundary of the elliptical bar is marked with a dashed curve. Orbits from the main x_1 family are shown in (a). The small orbits near the bar centre in (b) are x_2 while the others are members of the outer 2:1 families. (c) shows the retrograde family x_4, (d) & (e) show inner and outer 3:1 and 4:1 orbits respectively and (f) shows two kinds of orbits about the Lagrange points; the elongated banana orbits are known as long period orbits (LPO), while the rounder are members of the short period orbit (SPO) family. *n.b.* both SPO and LPO orbits occur around both Lagrange points.

at intermediate energies it derives from the eccentric 2:1 family. Contopoulos (1983a) calls the closed loop formed by the x_2 and x_3 families a floating bubble. The appearance of Figure 12 is typical of a strong bar; the resemblance to Figure 7 is much closer for weaker bars.

The existence of an ILR in the axially symmetrized model is a necessary, but *not sufficient*, condition for the perpendicular x_2 and x_3 families to exist. They are therefore absent when the central density is less high (Teuben and Sanders 1985), or when the pattern speed is higher. However, studies in which the bar strength is varied show that the gaps at the two 2:1 bifurcations in the axisymmetric case widen, and the radial extent of the perpendicular families shrinks, as the bar strengthens. Eventually, the x_2 and x_3 families completely disappear for very strong bars (Contopoulos and Papayannopoulos 1980). Van Albada and Sanders (1983) suggest that the existence and extent of the x_2 family can be used to generalize the concept of an ILR to finite amplitude perturbations.

As also found by Athanassoula *et al.* (1983), the x_1 family in our model does not have loops at higher energies [Figure 11(a)]. However, many other papers (Contopoulos 1978, Papayannopoulos and Petrou 1983, Teuben and Sanders 1985) have reported x_1 orbits with loops,
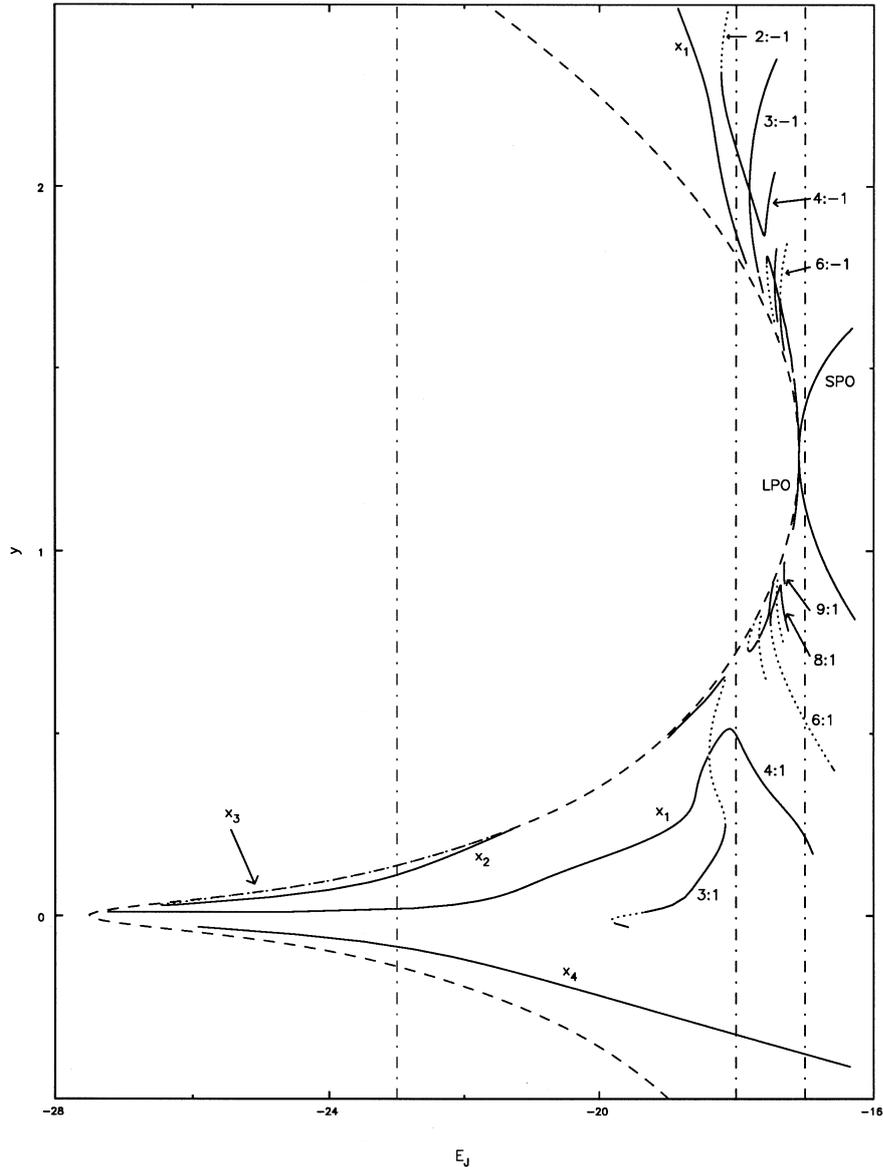
Figure 12. Characteristic curves for orbits in our bar model. The point at which the orbit crosses the bar minor $(y-)$axis is plotted as a function of E_J for each family of periodic orbits. Full-drawn segments of these curves indicate the orbit family is stable, and unstable parts of the sequence are marked as dotted lines. The dashed curve shows the ZVC and the three vertical dot-dashed lines mark the energies at which the surfaces of section are drawn in Figure 13. This diagram should be compared to figure 7.

which are sometimes very large. Athanassoula (1992a) shows that such loops appear when the bar either rotates more slowly, or has a high axial ratio, or when the mass distribution is more centrally concentrated.

4.5.2. Higher order resonance families. Because the potential in our model is bi-symmetric, the m:±1 bifurcations in the axisymmetric case become gaps only for even m. Although it is hardly noticeable in Figure 12, the x_1 family becomes unstable close to the odd bifurcations; a discussion of this phenomenon is given by Contopoulos (1983a).

Extensive 3:1 families exist both inside and outside co-rotation, Figure 11(d). It is very common for the inner 3:1 family to be unstable, but few authors report that the sequence becomes stable again for very high eccentricities. Papayannopoulos and Petrou (1983) found a family of orbits having a similar appearance, but which in their case resulted from a 1:1 bifurcation in a rather slowly rotating bar. Our model rotates too rapidly to exhibit a 1:1 bifurcation; the conditions under which this could be present are discussed by Martinet (1984).

The gap in the characteristic curves at the inner 4:1 resonance is particularly wide even for our ellipsoidal bar; square ended bars in real galaxies can be expected to have still stronger $m = 4$ components to the potential and therefore stronger resonances and yet bigger gaps. Notice that the gap in this case is of type 2, which means that the low energy x_1 family joins the more nearly rectangular orbits of the 4:1 family. As orbits on this branch remain aligned with the bar, while orbits on the other branch are roughly diamond shape and anti-aligned, the gap type at this resonance may be important for self-consistency. The type of gap to be expected is more difficult to predict at these higher order resonances as it depends upon the relative amplitude and radial variation of more than a single Fourier component (Contopoulos 1988). Type 2 gaps seem to be more common (*e.g.* Athanassoula 1992a). Despite the strong resonance, the qualitative appearance of the 4:1 orbits, Figure 11(e), particularly further out, is not greatly affected by the presence of the bar (*cf.* Figure 6c).

As we move closer towards the Lagrange points, the pattern of resonant gaps for even families and pitchfork bifurcations for odd, recurs repeatedly. The additional families are ever more closely confined to the vicinity of co-rotation and of rapidly vanishing importance to a self-consistent bar.

4.5.3. Orbits around the Lagrange points.   The two families of orbits shown in Figure 11(f) are present whenever the Lagrange points L_4 and L_5 are stable; note that both families exist about both Lagrange points. The more energetic short period orbits (SPO) derive simply from Lindblad epicycles (§4.2.1) in the unperturbed potential.

The banana shaped long period orbits (LPO), are the extension of the nearly circular sequence, x_1 which continues through all the bifurcations as the Lagrange point is approached (Papayannopoulos 1979). Once the energy exceeds the effective potential at the major axis Lagrange points L_1 and L_2, a nearly circular orbit crossing the minor axis cannot complete an orbit around the entire galaxy, but will be turned back as it approaches the bar major axis. The LPOs are of exactly the same type as the horseshoe orbits discussed in the field of planetary ring dynamics (*e.g.* Goldreich and Tremaine 1982).

Because they lie at large distances on the minor axis, neither of these families has any relevance to self-consistent bar models, though the LPO family may be important for rings (§7).

4.5.4. Other types of periodic orbit.   All orbits shown in Figure 11 are reflection symmetric about the minor axis, and cross this axis with $\dot{y} = 0$. Yet more families of asymmetric periodic orbits exist, some of which are stable. They are generally ignored in the majority of papers since stars following asymmetric families are not expected to be present in large numbers in symmetric bar models.

Moreover, we have described only simple periodic orbits which return to the same point on the bar minor axis at each crossing. Many more periodic orbits exist for which the star returns to the same point only after more than one orbit around the galaxy. Again these are not

thought to be present in great numbers in any bar model, but the existence of these additional families is very important for the onset of chaos (see §4.7).

4.6. Non-periodic orbits

The orbits of most stars in a bar are not periodic, but when most are trapped to librate about a *parent* periodic orbit, the structure of the bar is largely determined by the shapes of the parent orbits. It is important therefore to determine the extent to which orbits are trapped.

A stable periodic orbit must support a trapped region, but the extent of this region cannot be determined from the stability test (§4.4.2); conversely, an unstable orbit has no orbits trapped about it but could lie in a region where all nearby orbits are trapped about stable periodic orbits. The stability test alone therefore does not tell us the extent of the trapped region and we need the more powerful tool of the surface of section (SOS) to determine whether one trajectory through 4-D phase space oscillates about another. We illustrate this tool with three examples in Figure 13, again drawn for our model. Note that the scales differ substantially between the three panels and that for the two lower energies, we have not drawn what happens outside co-rotation.

To construct these diagrams, we integrate the trajectory of a test particle numerically, and mark the point in the $(y, \dot{y})$ plane each time it crosses the line $x = 0$. The points created by successive crossings of the y-axis are called *consequents*. Only points for which $\dot{x} < 0$ are plotted; thus points with $y > 0$ are created by a star whose orbital motion is in the direct sense in the rotating frame. This is the same Hamiltonian map discussed in §4.4.1.

Each panel in Figure 13 contains consequents calculated for many different orbits all having the same Jacobi constant; the dashed curves mark the boundaries of the region accessible to any orbit of that energy. A number of different types of behaviour can be seen.

4.6.1. Regular orbits.

The single most striking feature in all three panels of Figure 13 is that in some parts of the plane the consequents lie on closed curves, known as *invariant curves*; an orbit which gives rise to an invariant curve is known as a *regular* or *quasi-periodic* orbit. Successive consequents are usually well separated along each curve, but as the orbit is followed for longer and longer, the consequents populate the curve more and more densely. Topologically, the star is confined to a two-dimensional toroidal surface in the 4-D phase space and the closed invariant curve in the surface of section is simply a cross-section of this torus. Invariant curves from different orbits of the same energy can never cross,[10] and characteristically form a nested sequence generally centred on the single point representing the parent periodic orbit (or elliptic fixed point).

It is clear from Figure 13 that the trapped region around some periodic orbits covers a substantial region of accessible phase space. At $E_{\mathrm{J}} = -23$, the regular region on the right is trapped about the family x_2; that near the centre about x_1 and the closed curves on the left are trapped about a retrograde orbit from family x_4.

---

[10] An invariant curve appears to cross itself at an unstable periodic orbit (*e.g.* Hénon and Heiles 1964) but the curves there are the limits of two hyperbolae whose apices just touch at that point.
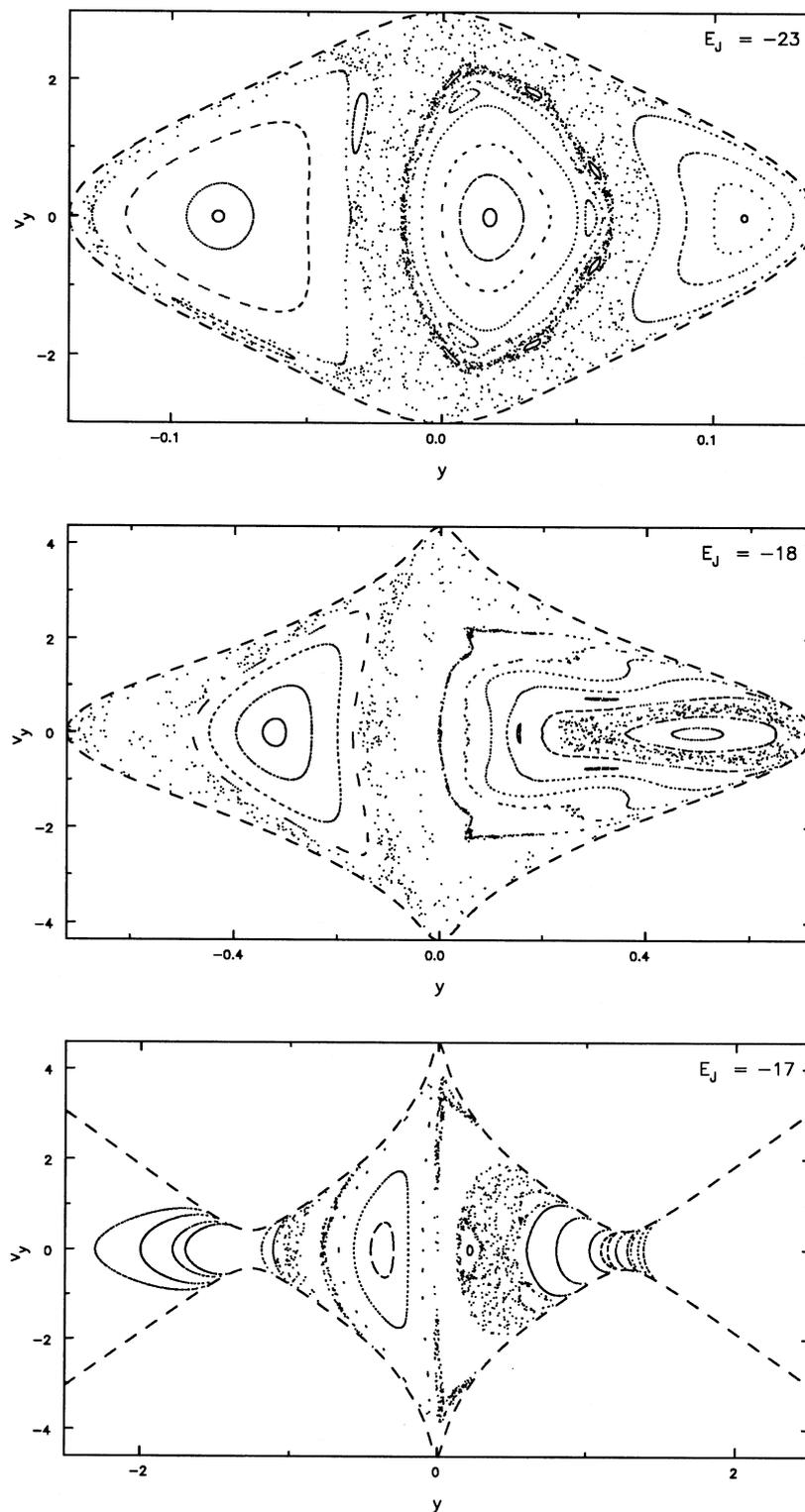
Figure 13. Surfaces of section at three energies in our model; many different orbits of the same energy contribute to each plot. The points mark the $(y, \dot{y})$ values at which an orbit crosses the y-axis with $\dot{x} < 0$ and more such crossings are marked for complex orbits. The dashed curves surround the region to which all particles are confined energetically; at lower energies (top two plots) we show only the region inside co-rotation, but the energy of particles in the lower plot is sufficient for them to cross the Lagrange points.

4.6.2. Irregular orbits. Not every orbit gives rise to an invariant curve, however. Well beyond these three regular regions for $E_J = -23$, is an example of an *irregular* orbit.[11] The consequents from an irregular orbit gradually fill an area of the plane more and more densely with a random scatter of points as the integration is continued. In this case, the area is bounded by the zero velocity curve and the regions occupied by regular orbits. As can clearly be seen for $E_J = -18$ in Figure 13, an irregular orbit may also be confined between two closed invariant curves. This is an example of a *semi-trapped* orbit.

MacKay *et al.* (1984) note that some irregular orbits appear to be confined to a part of the surface of section for a very large number of periods, before suddenly crossing to spend a long time in another part. The boundary, or *cantorus* (Percival 1979), which appears to separate these regions may be likened to an invariant curve that is not "water-tight". We have not found a very clear example of this behaviour in our model.

4.6.3. Other features. In the surface at $E_J = -23$, just outside the fourth invariant curve around x_1, there are two examples of a more complicated invariant curve: one has three distinct loops, the other seven. This type of invariant curve is created by a regular orbit trapped about a periodic orbit which closes only after several crossings of this plane. A further example occurs around the retrograde family, but in that case the orbit closes after two passages and is also asymmetric. We have not drawn the twin of this orbit, its reflection about the y-axis, since it would no longer have been clear that these were a pair of distinct periodic orbits.

The final type of behaviour of note is to be seen surrounding the seven-fold regular orbit. This orbit illustrates a dissolving invariant curve; the consequents surround the chain of islands, and although the orbit is clearly not regular, it does not escape to the stochastic region just outside it for many crossings. This is a characteristic feature in the SOS when the degree of regularity is changing with energy (Hénon and Heiles 1964); at energies just a little lower ($E_J = -24$), phase space is entirely regular, while at slightly higher energies ($E_J = -22$), the trapped region around x_1 is very small.

4.6.4. Higher energies. In the SOS at $E_J = -18$, the regular region on the directly rotating side has recovered somewhat, but it is centred around the 4:1 orbit near $y = 0.5$, which is well outside the bar. (The bar semi-minor axis is $\frac{1}{3}$.) The regular region around the retrograde x_4 family is still strongly evident, but the energy is now too great for the x_2 family to be present.

At $E_J = -17$, the orbits are unconstrained energetically. Phase space near the Lagrange points is still regular, but some invariant curves appear as segments at both positive and negative y because, as it oscillates about the parent periodic orbit, the orbit may cross the minor axis going in either direction on either side of the galaxy. As such orbits spend most of their time on the minor axis well outside the bar they cannot be of any real importance to the maintenance of the bar density.

4.7. Onset of chaos

The reason for the dissolution of invariant curves is one of the principal concerns of non-linear dynamics. Lichtenberg & Lieberman (1983) and Hénon (1983) give accounts of this complex

---

[11] In astronomical papers, these orbits are also variously denoted as *chaotic*, *stochastic* or even *semi-ergodic*, but these terms are not all considered to be fully interchangeable in other fields.

issue, but we have also found the article by Dragt and Finn (1976) and the informal review by Berry (1978) especially helpful.

Unstable periodic orbits provide the key. Although most lie in irregular regions of phase space, not all of them do – examples are in the original Hénon and Heiles experiment and our model discussed here. Unstable periodic orbits can be found in regular regions when the two branches of the invariant curve from that point meet again only at another unstable periodic orbit, forming a *separatrix*. The region around the fixed point suddenly becomes ergodic as soon as two branches from hyperbolic fixed points fail to join smoothly, but cross at some point other than a fixed point. The breakdown of large-scale regularity seems to take place in stages, however, as chains of islands of stability survive for short energy ranges around multiply periodic stable orbits. These chains are often surrounded by dissolving orbits (as in Figure 13) signifying the breakdown of the corresponding separatrix.

The KAM (Kolmogorov, Arnol'd and Moser, *e.g.* Moser 1973) theorem concerns the survival of invariant tori when an integrable system, such as an axisymmetric disc, is subjected to a perturbation, such as a bar. The theorem states that those tori "sufficiently far from resonance" survive, in a deformed state, when a "sufficiently small" perturbation is imposed. It does not predict the strength of the perturbation sufficient to destroy a torus, but it does give a scaling law related to the order of the resonance concerned and the associated frequencies. Thus we should expect, as we have found, that trapped orbits exist in non-axisymmetric potentials. We also observe that the extent of the regular region of phase space generally diminishes as the strength of the bar perturbation rises.

This last observation is particularly true near co-rotation where ever more resonances occur as co-rotation is approached. As the strength of the perturbation rises, more and more of these resonances overlap, which is a condition for the destruction of regularity (Chirikov 1979). Athanassoula (1990) has argued that the square-ended nature of the bar density distribution may also hasten the onset of chaos in this region, because the $m = 4$ component of the potential has greater strength relative to the $m = 2$ than would a more elliptical potential, causing greater overlap of resonances for a fixed bar strength.

Further, Martinet and Udry (1990) note that interactions of higher order resonances in the vicinity of the unstable x_3 family seem to be a particularly effective generator of chaos. They argue that the contraction of this family as the angular speed of the bar is raised may account for the apparent reduction in the chaotic fraction of phase space found in faster bars.

Contopoulos (1983a) noted that an infinite sequence of period-doubling bifurcations in the characteristic diagram is a second factor which gives rise to ergodic behaviour. This seemed to occur over a wide region around co-rotation in his strongly barred case (Contopoulos 1983b).

Liapunov exponents (Liapunov 1907), which give a quantitative measure of the degree of stochasticity in an irregular region, have been calculated in recent studies (*e.g.* Udry and Pfenniger 1988, Contopoulos and Barbanis 1989). They are a set of exponents describing the rate of separation of two nearby orbits in phase space as the motion proceeds; the region is regular if all the exponents vanish, irregular otherwise. They are formally defined for orbits infinitely extended in time, but in astronomical systems the interest lies in the behaviour over a Hubble time.

4.8. Actions

In steady potentials, one quantity is conserved for all orbits: the energy, if the potential is non-rotating, or Jacobi's integral in a non-axisymmetric rotating potential. If this were the only

conserved quantity, the particle would be able to explore all parts of phase space accessible with this energy and the entire surface of section would be filled by one single irregular orbit.

We already noted that regular orbits are, however, confined to a two-dimensional toroidal surface, and therefore respect an additional integral, other than the energy. In an axisymmetric potential, this additional conserved quantity is obviously the angular momentum, but no such simple physical quantity can be identified in non-axisymmetric potentials, whether stationary or rotating.

Binney and Spergel (1982, 1984) give a vivid illustration that regular orbits have just two independent oscillation frequencies and can therefore be described by action-angle variables. Irregular orbits on the other hand, are not quasi-periodic and cannot be described by such variables. Their first application was for a planar non-rotating potential but the technique is not restricted to this simple case.

Since the actions *are* a set of integrals, they would furnish the ideal variables with which to describe regular regions, in as much detail as for integrable systems, such as Stäckel models (§3.3). We could write the dynamical equations in a very simple form (*e.g.* §9.2), express the distribution function in terms of the actions (Jeans theorem), and take advantage of their adiabatic invariance (away from resonances) for the study of slowly evolving models.

Their principal drawback, however, is that we have no analytic expressions for them, though they can be determined numerically from the area bounded by the invariant curve in the appropriate surface of section (*e.g.* Binney *et al.* 1985). Worse, we cannot easily transform back to real space coordinates in order, for example, to compute the shape of an orbit of known actions. This very serious limitation is a major handicap to progress in the entire subject. Ratcliff *et al.* (1984) suggested a general technique based upon Fourier expansion, but ran into a number of operational difficulties. The canonical mapping approach outlined by McGill and Binney (1990) may be more successful.

4.9. Self-consistency

It is widely believed that self-consistent bars are largely supported by stars on orbits trapped or semi-trapped about the x_1 family, which is highly elongated in the direction of the bar. Most other families are too round, or elongated in the opposite sense, to make any useful contribution in a self-consistent model. Somewhat surprisingly, the 4:1 family does not appear to be responsible for the "rectangular" shapes of real bars (§2.3.1).

Contopoulos (1980) was the first to argue that the properties of the x_1 family suggest that self-consistent bars were likely to extend almost as far as co-rotation. Teuben and Sanders (1985) concluded that stars in such rapidly rotating bars are likely to move in a well organized streaming pattern, much as observed (*cf.* §2.5) whereas much less coherent streaming would be expected were the bar to rotate more slowly. Petrou and Papayannopoulos (1986) argued that self-consistent models having much lower pattern speeds might also be possible. However, the majority of authors favour pattern speeds high enough that co-rotation is not far beyond the end of the bar.

We have already noted that the nearly round, anti-aligned shapes of retrograde orbits within the bar implies that they cannot be significantly populated in any self-consistent model of a bar (see also Teuben and Sanders 1985). However, these orbits do play an important negative rôle in self-consistent bars, since the remarkably large regular regions that surround this family in Figure 13 (and in most other studies) mean that it "reserves" a substantial fraction of the phase space volume which the stochastic orbits cannot enter.

Irregular orbits raise a major difficulty for exactly self-consistent models that would survive indefinitely, though for practical purposes this may be too abstract a theoretical requirement. As their name implies, irregular orbits follow chaotic trajectories with no periodicities whatever. The density distribution produced by a population of stars having irregular orbits can never be steady, therefore. It is not clear what this means in practice: bars in galaxies are typically quite young dynamically, perhaps only 50 rotation periods. We might speculate that a significant fraction of irregular orbits may not have begun to explore the full space available to them, or the changes they cause could be sufficiently small and slow that the bar can adjust continuously without being weakened or destroyed. It is far from clear how these ideas can be tested.

4.9.1. Tour de force.   Pfenniger (1984b) presents by far the most extensive attempt to show that some mathematically convenient elliptical bar model could be made self-consistent. Adopting Schwarzschild's approach (§3.5), but with a non-negative least-squares algorithm instead of linear programming, he managed to obtain self-consistent models which, to our knowledge, remain the only solutions in the literature for a rapidly rotating two-dimensional bar.

In constructing his orbit library, Pfenniger considered that the density distribution had converged to a steady state when the largest change in the occupation number of any cell dropped below 0.5% upon doubling the integration time. Most regular orbits converged after a short integration, but when his criterion proved impractical for some irregular orbits, he imposed an arbitrary maximum integration time of about 550 bar rotation periods.

Pfenniger was able to use his approximately self-consistent solutions to calculate velocity and velocity dispersion fields, and found at least four different forms. The simplest flow, for the maximum angular momentum, consisted of directly rotating elongated flowlines within the bar and circular flowlines corresponding to the inner ring. This flow pattern was the one which agreed most closely with observations of early-type galaxies and N-body models. Other more complicated eddying flows were also possible. Some retrograde orbits were always required, involving typically between 10 and 30% of the mass, and populating the lens-like part of his assumed elliptical bar model. Models could be constructed without irregular orbits, but usually about 10% of irregular orbits were required. The dispersion fields showed little anisotropy, with the dispersion decreasing from the central value by a factor of about two by the co-rotation radius.

4.9.2. N-body model.   An entirely different approach was adopted by Sparke and Sellwood (1987), who examined the orbital structure of a bar formed in an N-body simulation. They were able to find many of the usual orbit families in the frozen potential of the model, and determined, from their distribution in the SOS, that the majority of particles making up the bar were either trapped, or semi-trapped about the x_1 family. Their N-body bar had a quite realistically rectangular appearance, yet they found, somewhat surprisingly, that the 4:1 family was of little importance. Instead, the orbits librating about the x_1 family seemed to be responsible for the rectangular shape.

Sparke and Sellwood noted that their two-dimensional bar model was remarkably robust and could adjust essentially immediately to major alterations of the global potential. Unfortunately, their conclusion applies only to models restricted to two-dimensions; once particles are allowed to move normal to the symmetry plane, the bar appears to suffer another type of instability (see §10.1).

4.9.3. Photometric models. There is a recent welcome trend in the literature to adopt mass distributions which bear some resemblance to the light distributions of barred galaxies, which nature has constructed self-consistently. One of the first such attempts was made by Kent and Glaudell (1989) for the well studied SB0 galaxy, NGC 936. This galaxy is one of the most favourable for such a study (Figure 2), being bright and nearby, largely free from star-formation regions and obscuring dust and viewed from an ideal angle. Unfortunately, even for this galaxy, major free parameters remain essentially undetermined by the observational data, the most important being the pattern speed of the bar and the mass-to-light ratio of the stellar populations; the latter is most unlikely to be a universal constant throughout one galaxy. Kent and Glaudell attempted to constrain the mass-to-light ratio from the observed velocity field and experimented with two pattern speeds. Their results were rather weakly in favour of the higher of the two pattern speeds, which places co-rotation a little beyond the end of the bar.

A more recent study of the same galaxy, based on new photometric data, has been undertaken by Wozniak and Athanassoula (1992). Instead of trying to decompose the model into components, they adopt a mass model based directly on the observed light distribution. They concur with Sparke and Sellwood (1987) that the rectangular bar shape is supported by orbits trapped about x_1, and owes little to the 4:1 family.

5. Three-dimensional bar models

The N-body experiments of Combes and Sanders (1981) provided the first indication that an exclusively two-dimensional treatment of barred galaxies is inadequate, although their result was not understood at the time. We now believe that the thin disc approximation cannot be invoked for bars for two distinct reasons: firstly, vertical resonances occur in the bar which couple horizontal to vertical motions and secondly, thin bars are subject to out-of-plane buckling instabilities. (We describe buckling modes together with other forms of bar evolution in §10, after discussing bar formation.) Thus, a simple addition of small vertical oscillations to the orbits discussed in the previous section would give a seriously incomplete description of the three-dimensional dynamics of bars. Work on fully three-dimensional models of rapidly rotating bars is still in its infancy, however.

5.1. Vertical resonances

For a nearly circular orbit in a weakly perturbed potential, we expect resonances between the vertical oscillation and a rotating, m-fold symmetric perturbation wherever $m[\Omega_{\rm c}(r) - \Omega_{\rm p}] = n\kappa_{\rm z}(r)$; here $\kappa_{\rm z}$ is the frequency of oscillation normal to the symmetry plane and n is an integer. The vertical co-rotation ($n = 0$) resonance is of no dynamical importance, but the $n \neq 0$ resonances could couple motion in the plane to vertical excursions (Binney 1981). The $n = \pm 1$ resonances are sometimes known as "vertical Lindblad resonances" and the $n = \pm 2$ resonances give rise to the much discussed "Binney instability strips" which occur only for retrograde orbits in the inner galaxy or far outside co-rotation for direct orbits. (*n.b.* m/n in our notation $= n$ in Binney's.)

It is useful to compare $\kappa_{\rm z}$ to κ. We write Poisson's equation for an *axisymmetric* mass distribution as

$$\frac{1}{r}\frac{\partial}{\partial r}\left(r\frac{\partial \Phi}{\partial r}\right) + \frac{\partial^2 \Phi}{\partial z^2} = 4\pi G\rho. \tag{28}$$

Recognizing that the combination $r\frac{\partial \Phi}{\partial r}$ is the square of the circular velocity, the first term vanishes in the mid-plane of a galaxy having a flat rotation curve. The remainder of the equation then gives us the standard result

$$\kappa_z = \sqrt{4\pi G \rho_0}, \tag{29}$$

where ρ_0 is the density in the mid-plane. To estimate κ, we note that $\kappa^2 \sim 2\Omega_c^2$ (exact for a flat rotation curve), and that $\Omega_c^2 \sim \frac{4\pi}{3}G\bar{\rho}$, where $\bar{\rho}$ is the mean, spherically distributed, density of matter interior to the point in question. Thus the ratio $\kappa_z/\kappa \sim \sqrt{\rho_0/\bar{\rho}}$ which is large wherever the self-gravity of the disc is important (Tremaine 1989).

The inequality $\kappa_z \gg \kappa$ holds for the majority of stars which remain close to the plane and implies that the $n = \pm 1$ resonances lie further from co-rotation than do the horizontal Lindblad resonances, which delimit the spiral pattern. The perturbing potential for spiral waves in a cool disc can therefore be expected to be negligible at the first, and all subsequent, vertical resonances. Thus it is legitimate to ignore vertical resonant coupling when the orbits of stars are nearly circular, the disc is thin and the non-axisymmetric component of the potential weak.

Obviously, expression (30) for κ_z fails in a strong bar. Not only does a strong bar add a large non-axisymmetric term to (29), but stars also move on highly eccentric orbits. Therefore local estimates of the vertical oscillation frequency cease to be meaningful for an orbit and the existence of resonances can be determined only from orbit integrations. Pfenniger (1984a) was the first to show that vertical resonances were important within the bar of a reasonably realistic three-dimensional model.

5.2. Periodic orbits in three-dimensions

Unfortunately, very few studies of three-dimensional periodic orbits have been published for models which bear much resemblance to barred galaxies; the large majority are concerned with slowly rotating, tri-axial ellipsoids. We mention this work insofar as it seems relevant, but space considerations preclude a thorough review of the literature on the orbital structure of slowly rotating ellipsoidal models (see *e.g.* de Zeeuw and Franx 1991).

5.2.1. Orbital stability. As for rotating two-dimensional potentials, Jacobi's integral is conserved for all orbits (§4.3.2) in a potential which is steady in rotating axes. There are therefore four adjustable coordinates for the shooting method (§4.4), which are usually $(y, \dot{y}, z, \dot{z})$, and again we seek solutions such that $T(\boldsymbol{x}_0) = \boldsymbol{x}_0$. (For consistency with the previous section, we use y for the bar minor axis.)

The stability test for a periodic orbit now requires the determination of the eigenvalues of a 4×4 Jacobian matrix of partial derivatives (equation 28). As for two-dimensions, the orbit is stable when all eigenvalues lie on the unit circle. However, there are six physically distinct types of instability which have been discussed for a very similar celestial mechanics problem by Broucke (1969), Hadjidemetriou (1975) and Hénon (1976), and for bars by Pfenniger (1984a) and Contopoulos and Magnenat (1985). The phenomenon of *complex instability*, which appears only in systems with more than two degrees of freedom, has been discussed extensively; in this case, all four eigenvalues are complex and not located on the unit circle. What causes an orbit sequence to become complex unstable is not well understood, but the transition frequently occurs at boundaries of stochastic regions (Magnenat 1982b).

5.2.2. Notation. A very substantial fraction of the work in this area has been carried out by the group at the Geneva Observatory. Notwithstanding the importance of their work, we find the notation they adopt, which is an attempt to generalize from two-dimensions, so cumbersome that we feel unable to use it here. To our knowledge, there are at least four other competing systems in the literature – an indication perhaps of the new and unsettled nature of the field, and a source of confusion to all but the expert. Since no consensus on nomenclature has been reached, and we do not find any suggested systems attractive, we have developed our own! It does, however, share features of some of the other systems.

We extend the $m{:}l$ notation in the plane to become $m{:}n{:}l$, where m is the number of radial oscillations, when viewed from the rotation axis (as for two-dimensions) and n the number of vertical oscillations before the orbit closes after l rotations about the centre.[12] Unfortunately, this nomenclature needs to be supplemented to indicate whether the orbit is symmetric or anti-symmetric about the (x, z) plane, *i.e.* the plane through the bar centre normal to its major axis. When there is a need to distinguish these we add a subscript; thus, $m{:}n_\mathrm{s}{:}l$ and $m{:}n_\mathrm{a}{:}l$ refer to the symmetric and anti-symmetric families respectively. We illustrate this nomenclature with the orbits discussed in this section.

Our system, like most others, is too rigid to describe transition regions between families. A glance at Figure 12 shows that distinctly named families frequently join smoothly into a single orbit sequence in two-dimensions; any notation system based upon orbital shapes will also ascribe different names to parts of a sequence in three-dimensions. The gradual change in the properties of orbits over the transition region is not allowed for in notation systems which require an abrupt shift to a new designation at some arbitrary point along a sequence. We regard this weakness as more than outweighed by the advantage of a notation which clearly indicates the shape of the orbit away from transition regions.

5.2.3. Periodic orbit families. Pfenniger (1984a) investigated orbits in the combined potential of a rotating, tri-axial Ferrers bar with axes in the ratio 1:4:10, and a thickened Kuz'min disc (Miyamoto and Nagai 1975). He made the bar rotate about the short axis at a rate which placed co-rotation at the end of the long axis. First he examined the periodic orbits in the equatorial plane and found that the main x_1 family had something like the usual form. As his model was insufficiently centrally condensed to contain ILRs when axially symmetrized, it could not support the perpendicular families x_2 and x_3 of periodic orbits in the plane.

The x_1 family was vertically stable throughout most of the inner part of the bar, but was vertically unstable over several short stretches at higher energies. These instability strips lay between pairs of bifurcations from which new periodic orbit families with non-zero vertical excursions branched off. The first pair of bifurcations gave rise to families of orbits which retained an oval appearance from above, while developing small wrinkles when viewed from the side (Figure 14 top). These were symmetric and anti-symmetric 2:4:1 families. As both formed short sequences in the characteristic diagram and soon rejoined the main x_1 family, they were probably of little importance. At higher energies, the next two vertical families to appear were 4:4:1 orbits (again symmetric and anti-symmetric, Figure 14 middle) having much more extensive characteristic curves. They had the distinctive shape of the 4:1 orbits in the

---

[12] This differs from the superficially similar notation used by Schwarzschild, which counts oscillations parallel to the coordinate axes. His notation is well suited to non-rotating bars.
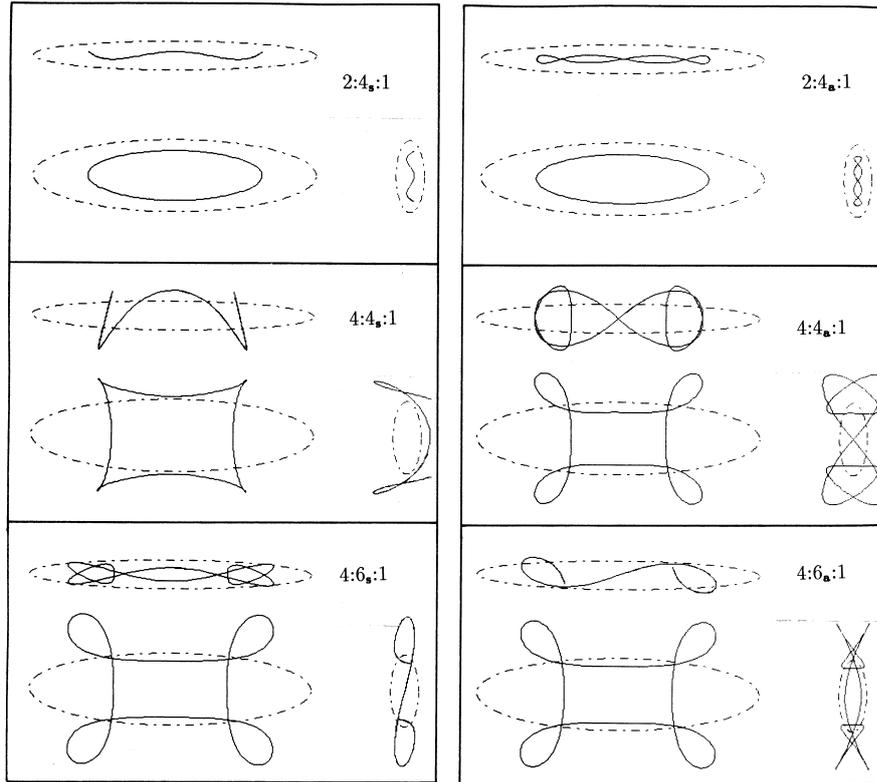
Figure 14.   Six three-dimensional periodic orbits found by Pfenniger (1984a); the three on the left are symmetric and those on the right are their anti-symmetric counterparts. We have re-labelled these orbits using our notation.

plane as well as a 4:1 oscillation normal to the plane. A third pair of bifurcations led to the 4:6:1 orbit families (Figure 14 bottom), which Pfenniger again viewed as less important. He found that all three anti-symmetric families were generally unstable over most of their length, but the symmetric sequences were stable over long regions.

Only the 4:4:1 families remained when he reduced the bar mass substantially. It seems likely that the low central density of his model prevented him from finding any m:2:1 families.

Pfenniger also tested the effect of changing the axial ratios of the bar. He found that both the horizontal and vertical stability of the x_1 family of orbits decreased as the bar became thinner in the plane of the disc; when the axis ratio in the plane exceeded $\sim 5-7$ most of the x_1 sequence became unstable. Increasing the bar thickness perpendicular to the plane (as far as making it prolate) also improved both the vertical and horizontal stability, probably because the non-axisymmetric component of the potential weakens as the bar is made thicker.

Most subsequent studies have been concerned with slowly rotating tri-axial ellipsoids, though some of the results are relevant to barred galaxies. In particular, directly rotating 2:2:1 resonant families seem to be most relevant to galactic bars. The 2:2$_\mathrm{s}$:1 orbits are commonly known as "bananas", and the Geneva group uses the deplorable term "anti-bananas" to describe the 2:2$_\mathrm{a}$:1 orbits![13] Both these families bifurcate from the main x_1 family in most mod-

---

[13]   It should be noted that these orbits in a rapidly rotating bar differ from those also termed anti-bananas in non-rotating bars (Miralda-Escudé and Schwarzschild 1989) which pass through the exact centre of the bar.

els (Mulder and Hooimeyer 1984, Cleary 1989) but they can also be found as bifurcations from x_2 when the bar rotates sufficiently slowly (Udry 1991). The family in the plane seems always to be vertically unstable between the two bifurcation points, which are generally quite close together. Most authors find that the symmetric family is stable and the anti-symmetric unstable from their bifurcation points, but that stability is exchanged between them at a higher energy. Mulder and Hooimeyer (1984) found an additional intermediate family connecting the two at the energy where stability was exchanged, but Udry (1991) could not, unless the potential was perturbed.

Udry also maps out the limiting bar axis ratios for which the 2:2:1 families can be found in a model having a tri-axial modified Hubble density profile. He finds that the short axis should not be more than 30% to 40% of the long axis, with only a slight variation over the entire range possible for the intermediate axis. He also notes that these values are hardly affected by rotation, although he did not investigate very rapidly rotating models. The addition of a small Plummer sphere at the centre of the mass model further confined the existence of these families to much flatter bars, however.

5.3. Structure of a three-dimensional N-body model

Pfenniger & Friedli (1991) have carried out a detailed study of the orbital structure of one of their three-dimensional N-body simulations. As the bar in their model thickened in the z-direction quite markedly during its first few tumbling periods (see §10.1), they chose two different moments for their study: one soon after the bar formed as a thin structure, and the second much later when evolution seemed to have ceased. They first searched for periodic orbits in the frozen potentials at the two instants, both in the raw potential of the model and when they imposed reflection symmetry about the three principal planes. The pattern speed of the bar dropped by some 20% and the approximate axis ratios of the bar shape rose from $\sim 1 : 0.42 : 0.33$ to $\sim 1 : 0.51 : 0.40$ between the two moments analysed.

In the symmetrized cases, they found that the planar x_1 family was stable, both horizontally and vertically, from the centre almost to the 3:1 bifurcation, except for a short vertical instability strip. The perpendicular families in the plane (x_2 and x_3) were absent from their model, but only marginally so. The bifurcations at either end of the short vertical instability strip in the main x_1 family lead to the symmetric and anti-symmetric 2:2:1 families, illustrated in Figure 15. As usual, the anti-symmetric family was unstable and the symmetric family stable near the plane, but they exchanged stability at a higher energy. The vertical extent of the stable part of the symmetric family had decreased quite markedly, and the bifurcation points moved out along the bar, by the later time.

There were no simple periodic orbits which remained precisely in the plane in the raw (un-symmetrized) potential of the N-body model, because the potential was not exactly symmetric in z at either time. Nevertheless, they could trace families generally resembling those in the symmetrized model, but with two important differences: first, the vertical bifurcations, which were of the pitchfork type in the symmetrized model, became resonant gaps in the raw potential, and second, the $2:2_a:1$ families became much more stable while the $2:2_s:1$ families lost still more of their stability. These stability differences were particularly marked at the later time.

Pfenniger and Friedli noted that the majority of particles in the bar seemed to follow quasi-periodic orbits trapped about the x_1 and the 2:2:1 families. Very few orbits were retrograde or belonged to any of the other families they found from their periodic orbit analysis. For energies approaching the Lagrange point, they found larger and larger fractions of irregular orbits.
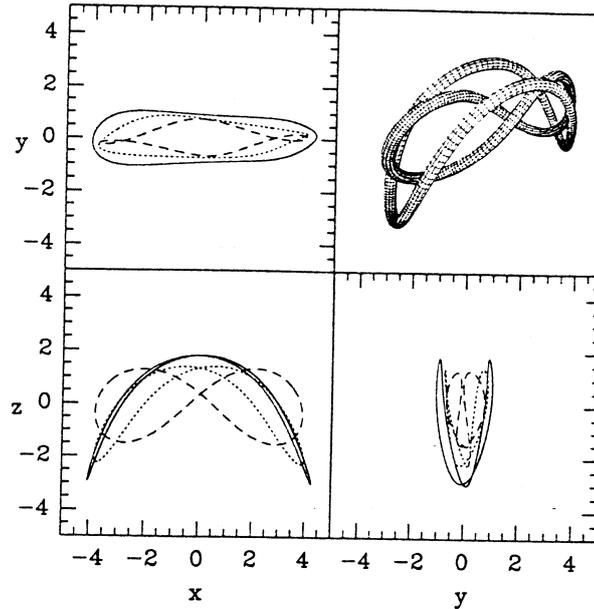
Figure 15. Three orthogonal projections and a "tube view" showing the three-dimensional shapes of both the symmetric and anti-symmetric 2:2:1 orbits. The symmetric orbit is drawn as a continuous line and the anti-symmetric is dashed; the dotted lines show an intermediate case! [Reproduced from Pfenniger and Friedli (1991).]

Given the stability properties of the 2:2:1 families, it seems likely that stars in the box-shaped final model are trapped about the $2:2_a:1$ family; a conclusion supported by the preliminary orbit analysis of his own models performed by Raha (private communication). These anti-symmetric orbits were first reported by Miller and Smith (1979) who found them in large numbers in their slowly rotating ellipsoidal model.

Pfenniger and Friedli note that their model also supported vertical bifurcations along the retrograde x_4 family, which gave rise to 2:1:1 orbits, also known as anomalous retrograde orbits. Their study of the orbital make-up of the bar makes it clear that these are of little importance in fast bars, though they have been of major interest for slowly rotating tri-axial systems (Heisler *et al.* 1982, Magnenat 1982a, Mulder and Hooimeyer 1984, Martinet and Pfenniger 1987, Martinet and de Zeeuw 1988, Cleary 1989, Martinet and Udry 1990, *etc.*).

5.4. Stochasticity in three-dimensions

The most important difference between two and three degrees of freedom is that the phenomenon of *Arnol'd diffusion* appears. Regular orbits form boundaries which irregular orbits cannot cross; for test particles in two-dimensions these invariant tori divide phase space into separate volumes so that an irregular orbit can be semi-trapped "inside" an invariant curve. The extra degree of freedom in three-dimensions means the chaotic regions are no longer isolated from each other by the invariant surfaces, which have too few dimensions, and are thought to be connected into a single network known as the Arnol'd web.

Self-consistent models containing a significant fraction of chaotic orbits would be difficult to construct, since any chaotic orbit fills a volume bounded only by its energy surface which is always more nearly spherical than the density distribution giving rise to the potential. Models containing some stochastic orbits are therefore likely to be only quasi-stationary. Since bars

have existed for some 50 orbital periods only, the fact that some stochastic orbits will cause them to evolve on a longer timescale may not be of great concern, as the essentially stationary three-dimensional models of Pfenniger and Friedli (1991) show.

Most orbits in non-rotating three-dimensional ellipsoids are of the box or short- and long-axis tube types (Schwarzschild 1979, Binney and Tremaine 1987), which are regular orbits trapped about the simplest periodic orbit families. However, the introduction of even slow rotation appears to change the orbital structure drastically – many orbits which were regular in stationary bars become stochastic. There seem to be a number of additional ways, apart from slow rotation, to foment stochasticity, but only rapid rotation is known to reduce it (§4.7).

Martinet and Pfenniger (1987) investigated the effect of a mass concentration in the galaxy core, and showed that for even a small mass, the z-motion close to the centre was quickly destabilized. Hasan and Norman (1990) confirmed that a central mass concentration is extremely effective at causing orbits close to the mass to become chaotic, particularly once the central condensation contains more than 5% of the total mass.

Udry and Pfenniger (1988) found that stochasticity rises when the bar is strengthened, *e.g.* by making it narrower or squaring off its ends, and again when the central concentration was raised. They also examined the effects of graininess in the potential; a very reasonable degree of granularity destabilized yet more regular orbits.

Though many questions remain unanswered, collectively, these results suggest that weak, rapidly-rotating, bar models should have the fewest chaotic orbits, and strong bars which end well before co-rotation would have the most.

6. Gas and dust

Although a small fraction of the total mass, at least in early type galaxies, the gas component is of considerable interest to the dynamicist mainly because it is an excellent tracer material. We have much more detailed knowledge of the flow patterns of gas in galaxies than we do of the stars because the Doppler shifts of the emission lines from excited gas are easier to measure than for the broader, weaker absorption lines seen in the composite spectra of a stellar population. Comparison between the observed flow pattern and the calculated gas behaviour in a number of realistic potentials can be used as a means to estimate such uncertain quantities as the pattern speed and mass-to-light ratio of the bar.

The dust lanes, which are dark narrow features along spiral arms and bars where the gas and dust density may be several times higher than normal, also demand an explanation. The widely accepted view that these delineate shocks in the inter-stellar gas seems to have been first proposed by Prendergast (unpublished c1962).

Finally, the specific angular momentum of gas elements changes with time, causing significant radial flows of material. These are important for evolution of the metal content of the galaxy and can cause a build-up of gaseous material in rings where the flow stops.

Almost all the theoretical work and simulations have neglected motion in the third dimension. This approximation may still be adequate, notwithstanding the existence of transient bending instabilities (§10.1) and vertical instability strips within the bar since dissipation must ensure that the gas clouds remain in a thin layer. However, the work of Pfenniger and Norman (1990) may indicate that the radial flow of gas is accelerated as the material passes through vertically unstable regions.

6.1. Observations of gas in barred galaxies

Most data come from optical or 21cm HI observations and much less is known of the distribution and kinematics of the possibly dominant molecular gas component. This is because molecular hydrogen must be traced indirectly through mm-wave emission of CO and other species; the resolution of single dish antennae is low and only small portions of galaxies can be mapped with the current mm interferometers; for a recent review of available CO data see Combes (1992).

6.1.1. Gas distribution.   The distribution of neutral hydrogen within each galaxy shows considerable variation. Neutral hydrogen appears to be deficient within the bar in a number of galaxies: *e.g.* NGC 1365 (Ondrechen and van der Hulst 1989) and NGC 3992 (Gottesman *et al.* 1984). On the other hand, counter-examples with significant HI in the bar are NGC 5383 (Sancisi *et al.* 1979), NGC 3359 (Ball 1986), NGC 4731 (Gottesman *et al.* 1984), NGC 1073 (England *et al.* 1990) and NGC 1097 (Ondrechen *et al.* 1989). The CO is sometimes distributed in a ring around the bar (*e.g.* Planesas *et al.* 1991) and sometimes concentrated towards the nucleus (*e.g.* Sandqvist *et al.* 1988).

Early type barred galaxies contain little gas, in common with their unbarred counterparts (*e.g.* Eder *et al.* 1991). Moreover, van Driel *et al.* (1988), who had two strongly barred galaxies (NGC 1291 and NGC 5101) in their sample having sufficient HI to be mapped, found that in both cases the gas was concentrated in an outer ring.

6.1.2. Kinematics.   The position-velocity maps of gas in a barred galaxy indicate that the flow pattern is more complicated than the simple circular streaming (sometimes) seen in an approximately axisymmetric galaxy. In general, systematic variations in the observed velocity field produce characteristic $\mathcal{S}$-shaped velocity contours and non-zero velocities on the minor axis, which are indicative of radial streaming. However, these features of the velocity field are seen only in those galaxies for which the viewing geometry is favourable, as emphasized by Pence and Blackman (1984b). The general morphology of the pattern is consistent with the gas following elliptical streamlines within the bar, but high resolution data sometimes show very abrupt changes in the observed velocity across a dust lane.

Optical and radio observations of the same galaxy are generally complementary. Although the HI gas is quite widely distributed, data from the high resolution aperture synthesis arrays has to be smoothed to a large beam (to improve the signal to noise) which blurs the maps, particularly near the centre where the velocity gradients are steep. Higher spatial resolution optical measurements of excited gas in the bright inner parts can overcome this inadequacy to some extent, especially from Fabry-Perot interferograms (*e.g.* Buta 1986b, Schommer *et al.* 1988, Duval *et al.* 1991), but strong optical emission tends to be very patchy, and is rarely found near the bar minor axis. mm data on molecular gas is also helpful in localized regions (*e.g.* Handa *et al.* 1990, Lord and Kenney 1991).

An excellent example is NGC 5383, one of the best studied galaxies; the Westerbork data of Sancisi *et al.* (1979) taken together with the optical slit data from Peterson *et al.* (1978), later supplemented by Duval and Athanassoula (1983), provided the sole challenge to theoretical models for many years. Fortunately, HI data from the Very Large Array (VLA) has become available in recent years, and the number of barred galaxies with well determined velocity fields is rising, albeit slowly. We mention individual papers in §6.7.

In the majority of galaxies, the gas rotates in the same sense as the stars. However, exceptions have been found: NGC 2217 (Bettoni *et al.* 1990) and NGC 4546 (Bettoni *et al.*

1991), in which the gas in the plane can be seen to rotate in a sense counter to that of the stars. This most surprising aspect strongly suggests an external origin for the gas in these two early type galaxies and such cases are believed to be rare.

6.1.3. Dust lanes. Dust lanes occur more commonly in types SBb and later. Those along the bar are offset from the major axis towards the leading side (assuming the spiral to be trailing). Athanassoula (1984) distinguished two types: straight, lying at an angle to the bar as in NGC 1300, or curved as in NGC 6782 and NGC 1433. Sometimes predominantly straight lanes curve around the centre to form a circum-nuclear ring. Dust can also be distributed in arcs and patches across the bar: NGC 1365 (Figure 1) is a good example.

6.1.4. Evidence for shocks. Direct observations of steep velocity gradients across dust lanes, which would be the most compelling reason to believe these are shocks, have been hard to obtain. The two best examples are for NGC 6221 (Pence and Blackman 1984a) and for NGC 1365 (Lindblad and Jörsäter 1987).

Evidence for gas compression also comes from the distribution of molecular gas, through CO emission, which appears to be concentrated in dust lanes (*e.g.* Handa *et al.* 1990, but see also Lord and Kenney 1991). Less direct evidence comes from the non-thermal radio continuum emission which is frequently strongly peaked along the dust lanes (*e.g.* Ondrechen 1985, Hummel *et al.* 1987a, Tilanus 1990) – the enhanced emission is consistent with gas compression, but could also have other causes.

6.1.5. Star formation and other activity. It has been noted frequently (*e.g.* Tubbs 1982, and references therein) that the distribution of young stars and HII regions is not uniform in barred galaxies. Stars appear to be forming prolifically near the centres (Hawarden *et al.* 1986, Sandqvist *et al.* 1988, Hummel *et al.* 1990) and at the ends of the bar, but not at intermediate points along the bar. This situation in some galaxies is so extreme as to have been interpreted as a star forming burst either in the nucleus or at the ends of the bar, *e.g.* NGC 4321 (Arsenault *et al.* 1988, Arsenault 1989). Dense concentrations of molecular gas are also sometimes found near the centres of barred galaxies (*e.g.* Gerin *et al.* 1988). It has also been noted by several authors (*e.g.* Simkin *et al.* 1980, Arsenault 1989) that active galactic nuclei are somewhat more likely to occur in galaxies having bars, than in those without.

6.2. Modelling the ISM

When speaking of shocks *etc.* in a gas flow, it is customary to think of a continuous fluid having a well defined sound speed. Unfortunately, the ISM (inter-stellar medium) is not that simple, which prompted Prendergast (1962) to muse that "it is unclear what to assume for the equation of state".

It might seem natural to assume that the inter-stellar gas in the neighbourhood of the Sun, which is the best studied portion of the ISM, has properties typical of that throughout all galaxies. Here, the bulk of the gas mass is contained in cool, dense clouds which orbit ballistically, virtually unaffected by external pressure forces, except when in collision with another dense cloud. By contrast, the bulk of the volume is filled with high temperature gas at a much lower density, which is in rough pressure balance with the dense material – the so called hot phase. The balance between the components is regulated by star formation and supernovae; for more information, see reviews by Cox and Reynolds (1987) or Spitzer (1990).

Unfortunately, the star formation rate (and probably also the supernova rate, though no data are available) within bars seems to differ from that near the Sun, and the ISM in bars may have somewhat different properties.

This "variously damped and heated multi-phase stew" (Toomre 1977) is believed to experience shocks of some form or other in the intriguingly located dust lanes. We cannot realistically hope to understand the large-scale behaviour of the ISM if we include the intricate small-scale dynamics of each fluid element, and most calculations assume some gross physical properties for the medium. The pervasive hot phase is the only component which can reasonably be described as a smooth fluid on galactic scales, but both the sound speed and the Alfvén speed are likely to be well in excess of 100 km sec^{-1}, implying that there is little chance of it being shocked by a potential perturbation with relative motion a fraction of the orbital velocity.

One approach has been to treat the dense material as a collection of ballistic particles having a finite cross-section for collision (Miller *et al.* 1970, Schwarz 1979, Matsuda and Isaka 1980, Combes and Gerin 1985). There is some disagreement over whether to dissipate all or just some fraction of the energy in the collision, whether to merge the colliding particles and what to assume for the collision cross-section.

It is not unreasonable, however, to view the collection of cool clouds as a fluid with a sound speed of the order of the velocity dispersion of the clouds, which is typically $5 - 10$ km sec^{-1}. The conditions under which this might be valid were examined by Cowie (1980), who attempted to calculate an equation of state for the cloud ensemble. This vastly simplifying assumption has led to a rival group of papers which calculates the gas flow as a continuous fluid using conventional two-dimensional fluid dynamical codes. A number of different codes have been tried; van Albada *et al.* (1982) assessed the relative performance of many common techniques and a multi-grid method was later introduced by Mulder (1986). Some authors (*e.g.* Roberts *et al.* 1979), with an understandable desire for yet higher spatial resolution, advocate 1-D codes which neglect pressure forces normal to the flow lines.

Some techniques are of intermediate type, such as the *beam scheme* (Sanders and Prendergast 1974), which has proved very popular, and *smooth particle hydrodynamics* or SPH (Lucy 1977, Gingold and Monaghan 1977). Both codes combine aspects of the previous two distinct approaches. Hernquist and Katz (1989) describe a three-dimensional fluid-dynamical scheme which uses SPH with self-gravity.

As the "gas" in all three types of code obeys equations which are at best very crude approximations to the real dynamics of the ISM, a discussion of which is intrinsically "the best" misses the point. Several authors argue the virtue of low numerical viscosity in high quality fluid codes, without pausing to consider the extent to which the ISM differs from an inviscid gas with a simple equation of state. In fact, bulk viscosity may be the most important physical property distinguishing the gas from the stars (*e.g.* Sanders 1977). Numerical viscosity is, of course, undesirable because its properties and magnitude are set by the nature of the numerical code, grid cell size, collision cross-section *etc.*, whereas it would be preferable to employ a viscous coefficient related to the properties of the medium! In summary, it is very helpful to have tried a variety of codes having different numerical weaknesses, because we gain confidence in results which all can reproduce, and learn to be suspicious of those unique to one type of code.

6.3. Streamlines and periodic orbits

Because the velocity dispersion of the gas clouds is so much lower than their orbital speeds, the influence of "pressure" (collisions) on the trajectories will generally be small. When pressure is completely negligible, the gas streamlines must coincide with the periodic orbits in the system. However, gas streamlines differ from stellar orbits in one crucial respect: they cannot cross, *i.e.* the gas must have a unique stream velocity at each point in the flow. This very obvious fact implies that when periodic orbits cannot be neatly nested, pressure or viscous forces must always intervene to prevent gas streamlines from crossing.

Even when the perturbing potential is a weak, rotating oval distortion and orbits can be computed by linear theory, as in §4.2, periodic orbits are destined to intersect at resonances. Not only do the the eccentricities of the orbits increase as exact resonance is approached, but the major axes switch orientation across all three principal resonances, making the crossing of orbits from opposite sides of a resonance inevitable. Sanders and Huntley (1976), using the beam scheme, showed that the gas response between the inner and outer Lindblad resonances takes the form of a regular two-arm spiral pattern in the density distribution. They argued that the orientation of the streamlines slews gradually over a wide radial range and the locus of the density maximum marks the regions where "orbit crowding" is greatest.

Each spiral arm winds through, at most, 90° per resonance crossed. As Sanders and Huntley's first model had a power-law rotation curve, only one ILR was present. In models having two ILRs, the orientation must change again through 90° at the inner ILR; note however, that we should expect a leading spiral arc at this resonance, because the dynamical properties of the orbits inside the inner ILR revert to those between the outer ILR and co-rotation. In a subsequent paper, Huntley *et al.* (1978) showed that the result in their case is a density response which leads the major axis of the potential by a maximum of about 45°.

Where a weak bar potential rotates fast enough for no ILRs to be present, orbit crossings might be avoidable everywhere inside co-rotation. The flow may then remain aligned with the bar all the way from the centre to co-rotation (*e.g.* Schwarz 1981), changing abruptly at co-rotation to trailing spiral arcs extending to the OLR.

It should be noted that all the results mentioned in this sub-section were obtained from a mild oval distortion of the potential having a large radial extent.

6.4. Strong bars

Streamlines still try to follow periodic orbits even in strongly non-axisymmetric potentials, though it becomes increasingly difficult to find circumstances in which the orbits can remain nested; not only can adjacent orbits cross, but a periodic orbit can also cross itself (*e.g.* Figure 11). Because this greatly complicates the relationship between periodic orbits and streamlines, we find the alternative picture described by Prendergast (1983), paraphrased here, easier to grasp.

As there is a formal analogy between compressible gas dynamics and shallow-water theory (*e.g.* Landau and Lifshitz 1987, §108), we can think of the gas flow within a bar as a layer of shallow water circulating in a rotating non-axisymmetric vessel having the shape of the effective potential (*e.g.* Figure 10); for a rapidly rotating bar, this has the shape of a non-circular volcano crater (see §4.3.2). As the crater rim defines co-rotation, the water within the crater flows in the same sense as the bar. It flows along the sides of the crater, but has too much momentum to be deflected round the end and back along the far side by the comparatively weak potential
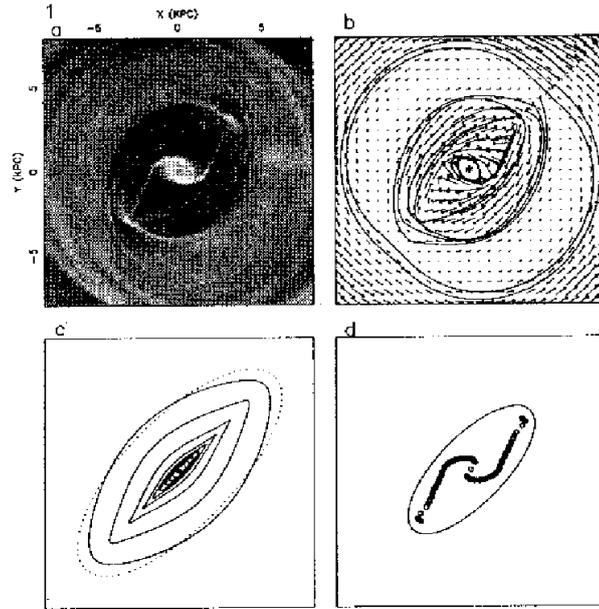
Figure 16. The gas flow pattern in one of Athanassoula's (1992b) simulations in which the inhomogeneous bar is positioned across the diagonal of each frame. (a) shows a grey scale representation of the gas density distribution (highest densities are white), (b) shows the velocity vectors and a few streamlines in the restframe of the bar, (c) shows some periodic orbits from the x_1 family (on an expanded scale) and (d) shows the loci of density maxima and the outline of the bar on the same scale as in (a) and (b).

gradients. Instead it rushes on past the major axis of the potential and on up the sides of the vessel, finally turning back when the flow stalls. The hydraulic jump which must form where fresh material encounters the stalled flow is the analogue of a shock in gas dynamics.

This analogy provides an intuitive explanation for the location of shocks on the leading edge of the bar, something which is not so easily understood from the discussion in terms of periodic orbits presented by van Albada and Sanders (1983). As their main conclusion is that the periodic orbits must loop back on themselves, a condition implicit in Prendergast's description, the two arguments are equivalent.

Strong offset shocks of this type were first revealed in the fluid dynamical simulations by Sørensen *et al.* (1976) and have been reproduced many times (Roberts *et al.* 1979, Sanders and Tubbs 1980, Schempp 1982, Hunter *et al.* 1988, *etc.*). Figure 16 shows such a result from the high quality simulations by Athanassoula (1992b). As expected, she finds that shocks develop only when the x_1 family of orbits possess loops, or are at least very sharply curved.

Athanassoula also concludes that the range of possible pattern speeds which gives rise to straight shocks is such that the major axis Lagrange points should lie between 1.1 and 1.3 times the bar semi-major axis, for a Ferrers bar model. If this result proves to be more general, and if the straight dust lanes are indeed the loci of shocks, then it supplies the tightest available constraint on the pattern speeds of bars in galaxies.

An additional result from her study is that the shocks are offset along the bar only when the potential supports a moderately extensive x_2 (perpendicular) family of orbits. If the mass distribution is insufficiently centrally concentrated, then the shocks lie close to the bar major axis.

6.5. Driven spiral arms?

The spirals that Sanders and Huntley (1976) and Schwarz (1981) were able to produce extended out to, and even a little beyond, the OLR. However, many authors have reported that they are unable to reproduce such extensive spiral responses in passive gas to forcing by an ellipsoidal bar model instead of an oval distortion to the potential. This is because the quadrupole field of a realistic bar, which ends near co-rotation, falls off too rapidly at larger radii to induce a spiral response in the gas (Figure 9). In order to maintain a spiral response well beyond the bar, Roberts *et al.* (1979) made the rather *ad hoc* assumption that the bar near the centre goes over to a trailing spiral perturbation beyond co-rotation, the whole pattern rotating at the same rate. Hunter *et al.* (1988) added a co-rotating oval distortion for similar reasons.

Spirals are more likely to be independent patterns, as in normal galaxies, and probably have a different pattern speed (Sellwood and Sparke 1988). Such a suggestion would seem to imply a random distribution of phase differences between the bar and the start of the arms which, it is generally felt, conflicts with the observed situation. Sellwood and Sparke point out that this is not a valid objection, for two reasons: Firstly, a phase difference can, in fact, be seen in a number of barred galaxies – even where a two arm "grand design" spiral pattern dominates (*e.g.* NGC 5383, Figure 2). Secondly, contour plots of the non-axisymmetric density in their model show that the spiral arms appear to the eye to be joined to ends of the bar for most of the beat period.

A review of the problems and ideas of spiral arm generation in disc galaxies would take us too far from the subject of barred galaxies.

The most convincing evidence for two separate pattern speeds in a galaxy is that for NGC 1365 (Figure 1). Ironically, the impressive grand design spiral arms of this galaxy have frequently been cited as a clear example of bar forcing, yet the kinematic data, presented in §6.7, strongly support two separate co-rotation radii for the bar and spiral patterns. Weaker evidence can also be found for other galaxies.

6.6. Angular momentum changes

Whenever gas is distributed asymmetrically about the major axis of the potential, it will experience a net torque which causes a secular change in its angular momentum. Where the density maximum leads the bar, the gas will systematically lose angular momentum, and conversely a trailing offset will cause it to gain. (The angular momentum is removed from, or given up to, the stellar population creating the non-axisymmetric potential.)

This process was emphasized by Schwarz (1981), who found that "gas" particles between co-rotation and the OLR were swept out to the OLR in a remarkably short time. The swept-up material quickly formed a ring, which was slightly elongated either parallel to the bar if the initial gas distribution extended to radii beyond the OLR, or perpendicular to it if the distribution was not so extensive. He obtained this result in an isochrone background potential using a bar pattern speed sufficiently high to have no ILRs, but in his thesis Schwarz (1979) also reports inner ring formation in a different model having an ILR.

Schwarz finds that the high rate at which gas is swept up into rings depends only weakly upon his numerical parameters: the collision box size, coefficient of restitution, *etc.* Since the torque responsible for these radial flows is proportional to the density contrast in the arms, as well as the phase lag (or lead) and strength of the non-axisymmetric potential, any realistic density contrast in the spiral or bar must give a similar flow rate. Schwarz's flow rates are

probably too high, however, because the bar-like potential perturbation he used, which peaks at co-rotation, is unrealistically strong in the outer parts.

Simkin *et al.* (1980) proposed a causal link between the inflow of gas within co-rotation and the existence of an active nucleus, which they suggest occurs somewhat more frequently in barred galaxies. This suggestion has been endorsed by Noguchi (1988), Barnes and Hernquist (1991) and others. While gas inflow along the bar is expected to raise the gas density in the central few hundred parsecs, its angular momentum must be further reduced by many more orders of magnitude before the material could be used to fuel a central engine.

6.7. Comparison with observations

NGC 5383 (Figure 2) is probably the most extensively studied and modelled barred galaxy. Sanders and Tubbs (1980) made a systematic attempt to model the gas flow pattern measured by Peterson *et al.* (1978) and Sancisi *et al.* (1979). By varying the bar mass, axis ratio, pattern speed and other parameters they were able to find a model which broadly succeeded in reproducing the qualitative features of the observed flow pattern, though discrepancies in detail remained. An altogether more comprehensive attempt to model this galaxy was made by Duval and Athanassoula (1983), who used the distribution of surface brightness to constrain the bar density distribution and added more high resolution optical observations to map the flow pattern within the bar in more detail. They ran simulations to determine the flow pattern when co-rotation was close to the bar end and experimented mainly with a range of mass-to-light ratios for the bar; again their best model resembled the observed flow pattern within the bar, though still not impressively so. It is possible that their low resolution beam scheme code precluded a better fit.

Pence and Blackman (1984b) found that the velocity field of NGC 7496 closely resembled that of NGC 5383.

Following this initial success, a number of attempts have been made to model other galaxies, notably by the Florida group. One galaxy in their sample, NGC 1073 (England *et al.* 1990), is too nearly face on for the kinematic data to constrain a model. In both the other two, NGC 3992 (Hunter *et al.* 1988) and NGC 1300 (England 1989), they encountered considerable difficulties in modelling the outer spiral. When a pure bar model failed to produce a sufficiently strong density contrast in the outer spiral arms, they added a global oval distortion, but that seemed to produce too open a spiral pattern. It seems likely, therefore, that the spiral arms in these galaxies do not result from forcing by the bar, but are independent dynamical structures of the type described in §6.5.

NGC 1365 (Figure 1) has also been observed extensively, though no good model for the whole galaxy has yet been published. Teuben *et al.* (1986) find quite convincing evidence for gas streamlines oriented perpendicularly to the bar near the very centre. They identify the location where this is observed with the x_2 family of periodic orbits, giving them a rough indication of the pattern speed; the value obtained in this manner places co-rotation close to the end of the bar – a reassuring circumstance, which is also corroborated by the presence of the offset dust lanes along the strong bar (see §6.4). However, Ondrechen and van der Hulst (1989) note that the inward direction of the gas flow on the projected minor axis provides an unambiguous indication that the spiral arms at this point are still inside co-rotation. These two conclusions can be reconciled only by accepting that the bar and spirals are two separate patterns, with the bar rotating much faster than the spirals.

Separate pattern speeds for the bar and spiral may occur in many galaxies. Co-rotation for the spiral pattern in NGC 1097 appears to lie beyond the bar (Ondrechen *et al.* 1989); Chevalier and Furenlid (1978) had difficulty in assigning a pattern speed for NGC 7723; the dust lanes in NGC 1365 (Figure 1) and NGC 1300 (Sandage 1961) cross the spiral (another, much weaker indication of co-rotation) well beyond the end of the bar. The co-rotation resonance for the two tightly wrapped spiral arms which make up the pseudo inner ring of NGC 6300 appears to lie inside the point where they cross minor axis (Buta 1987), yet this is close to the bar end; this may be an example where the spirals rotate more rapidly than the bar – the misalignment between the spirals and the bar also supports the idea of separate patterns.

The conclusions from all these studies are:

  i Most radio observations need to be supplemented by high resolution optical data before modelling of the observed flow pattern provides useful constraints on the properties of the bar.

  ii The gas flow *within the bar* can be modelled fairly successfully when the bar pattern speed is about that required to place co-rotation just beyond the end of the bar.

  iii Shocks along the bar also develop under the same conditions for the bar pattern speed, but are offset only if the x_2 family is present.

  iv The outer spiral arms usually cannot be modelled without assuming some additional non-axisymmetric component to the potential.

  v Not one of the well studied cases provides evidence that the spiral patterns are driven by the bar, while there is frequently a suggestion that the spiral arms have a lower pattern speed than does the bar.

7. Rings and lenses

Many galaxies, both barred and unbarred, exhibit rings which are believed to lie in the disc plane. These are thought to have an entirely different origin and properties from the much rarer polar rings, so named because they lie in a plane almost perpendicular to that of the disc. We do not discuss polar rings in this review (see *e.g.* Whitmore *et al.* 1990).

Unlike the spiral patterns in barred galaxies just discussed, there is considerable evidence that many rings share the same pattern speed with the bar, and therefore seem very likely to be driven responses to forcing by the bar.

7.1. Observed properties of rings

Statistical properties of some 1200 ringed galaxies selected from the southern sky survey are presented by Buta (1986a); these appear to be quite representative of the complete catalogue (Buta 1991), which will contain about twice this number. Three major ring types are distinguished by the radii, relative to the bar major axis, at which they occur.

7.1.1. Outer rings. Outer rings are the largest, relative to the host galaxy, having a diameter some 2.2 ± 0.4 times the bar major axis (Kormendy 1979). A good example is NGC 2217 in Figure 2 and others include NGC 1291, NGC 2859 (de Vaucouleurs 1975) and NGC 3945 (Kormendy 1981). The frequency of outer rings is difficult to estimate because they could be missed on all but the deepest plates; early estimates (de Vaucouleurs 1975, Kormendy 1979) suggested they occur in only $4-5\%$ of all galaxies, but Buta's survey may well indicate a higher fraction (Buta, private communication).

The ring is centred on the nuclear bulge and is thought to lie in the disc plane. Statistical arguments indicate that outer rings have intrinsic axis ratios in the range 0.7 to 1.0 (Athanassoula *et al.* 1982, Schwarz 1984b, Buta 1986a). Buta notes that although the longer axis is usually perpendicular to the bar, there is a significant sub-population for which the ring is parallel to the bar.

True outer rings are not always easily distinguished from *pseudo outer rings*, which occur when the outer spiral arms almost close.

7.1.2. Inner rings.   Inner rings are somewhat smaller, and generally have a diameter similar to the bar major axis – good examples are NGC 1433 and NGC 2523 in Figure 2 – but are sometimes noticeably larger, *e.g.* NGC 936 (also in Figure 2). They are more common than outer rings, but are found mainly in later types; Kormendy (1979) reports that 76% of SBab-SBc galaxies have inner rings, while few early-type galaxies have them.

Inner rings in barred galaxies are generally more elliptical than outer rings, having an axis ratio in the range 0.6 – 0.95 (Buta 1986a) and are elongated parallel to the bar (Schwarz 1984b) with few exceptions.[14] Buta (1988) finds some evidence for non-circular motion in the rings of a few nearby galaxies, thereby confirming their intrinsic non-circular shape. Buta (1991) notes that some are more rectangular or even hexagonal; the best example of hexagonal isophotes is for the weakly barred galaxy NGC 7020 (Buta 1990b).

In galaxies having both types of ring, the ratio of the outer to inner ring major axis diameters is on average 2.21 ± 0.02 with a long tail to higher values (Buta 1986a).

Both inner and outer rings tend to be bluer than the surrounding disc and many have HII regions, as do spiral arms (Buta 1988, Buta and Crocker 1991).

7.1.3. Nuclear rings.   A third type of ring has so far been found in relatively few systems, *e.g.* NGC 1512 (Jörsäter 1979), NGC 1365 (Teuben *et al.* 1986), NGC 1097 (Hummel *et al.* 1987b, Gerin *et al.* 1988), NGC 4321 (Arsenault *et al.* 1988), NGC 5728 (Schommer *et al.* 1988) and NGC 4314 (Garcia-Barreto *et al.* 1991a). They are usually very small, radius a few hundred parsecs, nearly round, and not aligned with the bar (Buta 1986a). An exceptionally large nuclear ring is seen in ESO 565-11 (Buta and Crocker 1991). As they are hard to find, because of their small size, their apparent rarity could again simply be a selection effect. In some cases, co-incident radio and optical emission from discrete sources lying in the ring is found, together with significant quantities of molecular gas and dust (*e.g.* Sandqvist *et al.* 1988). Hawarden *et al.* (1986) also note an excess of 25μm emission from barred galaxies, which they interpret as being due to enhanced star formation in a nuclear ring. However, Garcia-Barreto *et al.* (1991b) point out that similar phenomena can also occur without a detectable ring.

Several galaxies contain short *nuclear bars* within the nuclear ring. We discussed such features in §2.4.

7.2. Lenses and oval distortions

While inner rings are rare in early type galaxies, some $\sim 54\%$ of SB0-SBa galaxies (Kormendy 1981) manifest a flattened ellipsoidal structure known as a lens. Clear examples are NGC 5101

---

[14] Exceptions are NGC 4319, which is a tidally interacting system, and NGC 6300 in which two tightly wrapped arms make a pseudo-inner ring (Buta 1987).

(Sandage 1961) and NGC 3945 and NGC 4596 (Sandage and Brucato 1979). This feature is similar in size to the inner rings discussed above; Kormendy (1979) notes that the bar usually fills the lens in one (frequently the longest) dimension. The axial ratio in the disc plane is typically $\sim 0.9 \pm 0.05$, *i.e.* they are slightly rounder than inner rings.

Comparatively few late-type galaxies (SBb to SBm types) are classified as having a lens, but many have a so-called *oval disc* or *distortion*. Kormendy suggests that lenses and oval discs are distinct phenomena, on the grounds that the kinematic properties appear to be different: the rotation curves of oval discs are flat (*e.g.* NGC 4736, Kormendy 1979), whereas the rotation curve of a lens seems to rise with radius (Kormendy 1981). Clearly more data are required to establish his case.

7.3. Formation of rings

By far the most popular theory is that rings form from radial flows of gas driven by the bar. The gas dynamical simulations by Schwarz (1979) showed that material gathers in rings where the radial flow, caused by the spiral response to the bar, ends at a major resonance of the pattern. In this picture, the outer rings lie at the OLR for the bar while the inner rings occur either at co-rotation or at the 4:1 resonance. The nuclear rings are thought to lie at the ILR for the bar (*e.g.* Combes and Gerin 1985, Buta 1986b, Schommer *et al.* 1988), and the inner bar may be populated by stars on the perpendicular orbit family x_2 (*e.g.* Teuben *et al.* 1986).

There are two pieces of evidence in favour of this interpretation. Firstly, making plausible assumptions about the shapes of rotation curves, Athanassoula *et al.* (1982) concluded that radii were consistent with the hypothesis that the outer rings lay at the OLR while the inner were located at the 4:1 resonance. Secondly, and more convincingly, the ring orientations fit extremely well with the results from the simulations and suggest that rings trace the major periodic orbits. In particular, Schwarz (1979, 1981) found two orientations for the outer ring, depending upon the extent of the original gas disc; both cases seem to occur abundantly in nature, and there are even a few galaxies which seem to possess both simultaneously (Buta 1986a, 1991).

However, the theory does not offer convincing reasons for the existence of rings in unbarred galaxies – less common, but by no means rare (Buta 1991) – and the absence of rings in other barred galaxies. The first might be explained by arguing that the bars are unseen in the optical (§1) or that they have dissolved after first forming a ring (§10.3). The second may indicate a finite lifetime for these features.

The theory loses more of its appeal if, as we be have argued, spiral patterns in barred galaxies rotate at a rate different from the bar. The spirals themselves may also drive gas radially, but the radii of rings formed by the spirals cannot be expected to correlate with the resonances of the bar.[15] A way to salvage the theory, is to suppose that outer rings are formed at the same time as the bar. The bar formation process causes a substantial re-arrangement of angular momentum in the disc, and frequently forms a transient ring in the stellar component near the OLR for the bar (§9.2, a weak example is shown in Figure 17). (This is a much more efficient way to accumulate material at the OLR than through slow forcing by the weak quadrupole field of a steady bar.) The lifetime of the gaseous ring, which must be formed at the same time as the stellar ring, is likely to be much greater because the random motions,

---

[15] Unless the pattern speeds are related in some special way (*e.g.* Sellwood 1991)

which cause the stellar ring to dissolve, can be dissipated in the gas. The comparatively small fraction of outer rings observed may indicate that these are still rather short lived features, and therefore that the bar may have formed recently in galaxies where they are seen.

The theory that bar-driven radial flows form rings may account for the outer and nuclear rings, but it is less clear that it can account for inner rings. It has been suggested (*e.g.* Schwarz 1984a) that inner rings contain material trapped about the stable Lagrange points on the bar minor axis, or on higher resonant orbit families. This last suggestion is an attractive one to account for the rectangular, or even hexagonal, shapes of some inner rings (Buta 1990a, b).

Buta (1988) and Buta and Crocker (1991) have started to acquire more data on a few good candidates, but detailed photometric and optical and radio kinematic data are required for several more cases in order to provide a serious test of the bar driven ring theory.

7.4. Formation of lenses

At present there is no good theoretical interpretation of lenses and oval distortions. A number of rather speculative ideas have been discussed in the literature, none of which we find entirely convincing. Kormendy (1979) speculated that a lens is formed by the dissolution of a bar; since current ideas suggest that bars formed from instabilities in the disc, this hypothesis does not seem to account for the substantially higher surface brightness of the lens. Bosma (1983) proposed that the lens is an inner disc formed earlier than the faint outer disc and Athanassoula (1983) suggested that a lens results from a bar-instability in a high velocity dispersion disc. The latter idea suffers from the same flaw as does Kormendy's, and requires a cool population of stars to be also present to form the narrow bar. Teuben and Sanders (1985) weigh in with a similar suggestion that the lens is made up of chaotic orbits while Buta (1990a) suggests that lenses are no more than aging inner rings.

8. Asymmetries

Unfortunately, many barred galaxies are still more complicated, in that they depart strongly from the perfect bi-symmetry which has been implicit in all our theoretical discussion so far. Mild asymmetries are seen in virtually all spiral galaxies, but gross asymmetries occur much more frequently in late type galaxies. They are not confined to barred galaxies, as emphasized by Baldwin *et al.* (1980).

8.1. Observed properties

In some cases, the disc and spiral pattern is simply much more extensive on one side of the galaxy. An example of this type is NGC 4027 (de Vaucouleurs *et al.* 1968), in which the velocity field of the emission line gas remains centred on the bar (Pence *et al.* 1988) even though the bar is far from the centre of the outer isophotes. Other examples, for which there is no kinematic data available, are NGC 4618 and NGC 4625 (Odewahn 1991).

Another type of asymmetry is for the velocity field to be noticeably asymmetric while the light distribution is only mildly so. Examples are NGC 2525, which has a 50 km s^{-1} asymmetry between ends of bar (Blackman and Pence 1982), NGC 3359 (Duval and Monnet 1985), NGC 55 (Hummel *et al.* 1986) and NGC 7741 (Duval *et al.* 1991). Bettoni and Galletta (1988) noted a slight displacement in the centre of symmetry of the velocity pattern for 6 out of the 15 galaxies in their sample.

In other cases, the bar is displaced from both the optical and kinematic centre. Two of the most extreme examples are the LMC where the rotation centre is nowhere near the bar (de Vaucouleurs and Freeman 1972) and NGC 1313 (Figure 2) in which the rotation centre is at one end of the bar (Marcelin and Athanassoula 1982).

8.2. Models

There have been very few attempts to model such asymmetries. Marcelin and Athanassoula (1982) built a mass model based on photometric measurements of the galaxy NGC 1313, and solved for the gas flow assuming a uniform rotation of the eccentric mass distribution about the rotation centre. They obtained quite a good match between their heuristic model and the observed velocity field, but declined to speculate as to why the mass distribution was so asymmetric or how it could remain so. Colin and Athanassoula (1989) followed up this study with a similar treatment of other offset bar geometries.

There are no really convincing theories for the origin or persistence of these asymmetries. It is probably significant that these late type galaxies have almost solid body rotation curves, so it would take a very large number of orbital periods for asymmetric structures to be torn apart by the shear. The rate at which asymmetric patterns are sheared can be further slowed if they are kinematic density waves and not material features (Baldwin *et al.* 1980).

It seems likely that they originate through interactions with other galaxies or accretion of dwarf companions, but there is also a possibility that they arise from $m = 1$ type instabilities. No detailed work appears to have been done to develop either hypothesis. A further possibility is that they are primordial, and that such galaxies are simply dynamically very young.

9. Origin of bars

The first N-body simulations of collisionless stellar discs (Miller and Prendergast 1968, Hockney and Hohl 1969) revealed that it is easy to construct a rotationally supported stellar disc which is globally unstable and forms a large-amplitude bar on a dynamical timescale. Figure 17 shows a recent high quality simulation illustrating this behaviour. While this instability offers a natural explanation for the existence of bars in some galaxies, it has proved surprisingly difficult to construct stable models for unbarred galaxies. The problem of the origin of bars in galaxies was therefore quickly superseded by that of how a fraction of disc galaxies could have avoided such an instability.

Though this last question is of only peripheral interest to a review of barred galaxies, it is hard to overstate its importance for disc galaxy dynamics. The bar instability has therefore been repeatedly re-examined from a number of directions, which have all tended to confirm that rotationally supported discs suffer from vigorous, global, bi-symmetric instabilities. It would take us too far from the subject of this review to discuss the bar instability in great depth, and we confine ourselves to a description of two aspects: the formulation of a global stability analysis for discs as an eigenvalue problem and the mechanism for the instability.

9.1. Global analysis

A full stability analysis which leads to an eigenvalue problem for normal modes of an axisymmetric stellar disc was first formulated by Shu (1970) and by Kalnajs (1971). Though much can be formally deduced from this approach (Kalnajs 1971, 1977), it has proved very difficult
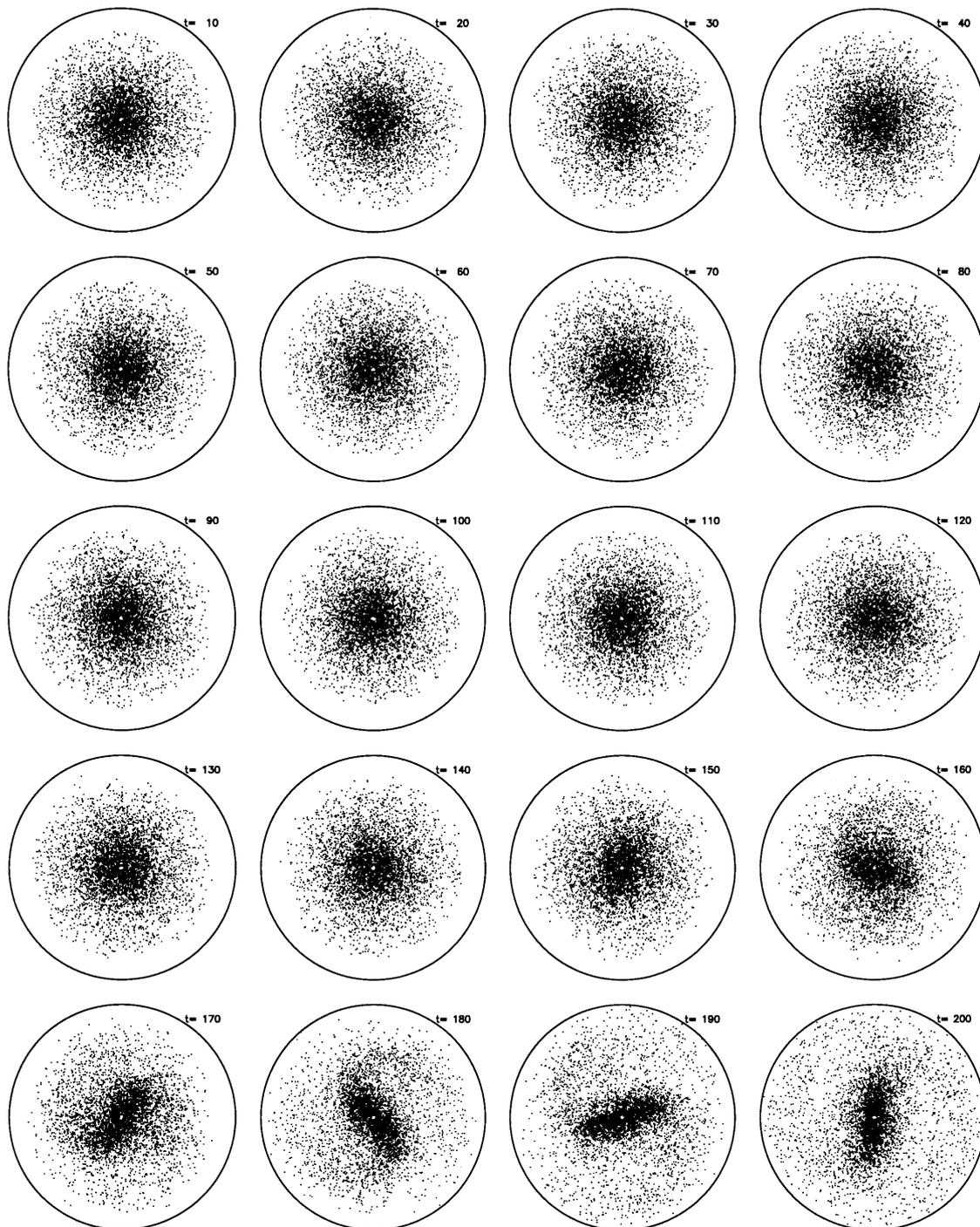
Figure 17. The formation of a bar through dynamical instability in a largely rotationally supported disc. The model is a completely self-gravitating, two-dimensional isochrone/6 model, whose dominant unstable mode was calculated by Kalnajs (1978). 100K particles are employed, but only 5K are shown in each frame, the times are marked in units of $\sqrt{a^3/GM}$ and the circle is drawn at a radius of 6.18a, where a is the isochrone scale length and M is the mass of the untruncated disc. The linear growth of the mode can be detected by Fourier analysis before time 150, and the estimated growth rate is some 16% below the predicted value. The discrepancy is probably caused by the gravity softening (scale = 0.05a) which was introduced in the simulation.

to find eigenvalues in practice. We describe Kalnajs's method and its practical difficulties of implementation here not only because it gives a vivid illustration of the analytical problems encountered in galactic dynamics, but also because it reveals the power and limitations of action-angle variables. The limited results that have emerged from this work are, however, of immense value as they provide predictions against which we can test the N-body results. Moreover, the dominant linear modes found are almost always those which seem likely to form bars.

9.1.1. Formulation of the eigenvalue problem. Kalnajs works in action-angle variables, introduced in §4.2.3. As these are canonically conjugate coordinates, he is able describe the dynamics using the elegant formulae of classical Hamiltonian mechanics (*e.g.* Goldstein 1980). In particular, the collisionless Boltzmann equation (1) can be written very compactly in Poisson bracket form

$$\frac{\partial F}{\partial t} + [F, H] = 0, \tag{30}$$

where F is the distribution function and H is the Hamiltonian.

In order to calculate small departures from equilibrium, we divide the Hamiltonian into a sum of the unperturbed axisymmetric part H_0 plus a small perturbing potential, h. Similarly, we divide the distribution function: $F = F_0 + f$. Substituting into (31), expanding the Poisson bracket, making use of the equations of unperturbed motion

$$\dot{J}_i = -\frac{\partial H_0}{\partial w_i} \equiv 0 \qquad \text{and} \qquad \dot{w}_i = \frac{\partial H_0}{\partial J_i} = \Omega_i, \tag{31}$$

and neglecting $[f, h]$ as being second order, we obtain

$$\frac{\partial f}{\partial t} + \boldsymbol{\Omega} \cdot \frac{\partial f}{\partial \boldsymbol{w}} = \frac{\partial F_0}{\partial \boldsymbol{J}} \cdot \frac{\partial h}{\partial \boldsymbol{w}} \tag{32}$$

to first order. We have adopted vector notation for the quantities $\boldsymbol{w} = (w_{\rm r}, w_{\rm a})$, $\boldsymbol{J} = (J_{\rm r}, J_{\rm a})$ and $\boldsymbol{\Omega} = (\Omega_{\rm r}, \Omega_{\rm a})$.

Since all unperturbed orbits are quasi-periodic, we can expand the perturbation potential, h, as a Fourier series in the angle variables:

$$h(\boldsymbol{J}, \boldsymbol{w}, t) = \frac{1}{(2\pi)^2} \sum_{\boldsymbol{m}} h_{\boldsymbol{m}}(\boldsymbol{J}, t) e^{i\boldsymbol{m} \cdot \boldsymbol{w}}. \tag{33}$$

where $\boldsymbol{m} = (l, m)$. The coefficients are given by

$$h_{\boldsymbol{m}}(\boldsymbol{J}, t) = \int_0^{2\pi} \int_0^{2\pi} h(\boldsymbol{J}, \boldsymbol{w}, t) e^{-i\boldsymbol{m} \cdot \boldsymbol{w}} d^2 \boldsymbol{w}, \tag{34}$$

We also transform f in the same way. Introducing these decompositions into (33), we see it must be satisfied by each Fourier component separately, thereby converting the PDE (33) into a set of first order ODEs:

$$\frac{\partial f_{\boldsymbol{m}}}{\partial t} + i\boldsymbol{m} \cdot \boldsymbol{\Omega} f_{\boldsymbol{m}} = h_{\boldsymbol{m}} i\boldsymbol{m} \cdot \frac{\partial F_0}{\partial \boldsymbol{J}}, \tag{35}$$

which has the solution

$$f_{\boldsymbol{m}}(\boldsymbol{J}, t) = i\boldsymbol{m} \cdot \frac{\partial F_0}{\partial \boldsymbol{J}} e^{-i\boldsymbol{m} \cdot \boldsymbol{\Omega} t} \int_{-\infty}^{t} h_{\boldsymbol{m}}(\boldsymbol{J}, t) e^{i\boldsymbol{m} \cdot \boldsymbol{\Omega} t'} dt'. \tag{36}$$

Assuming $|f(\boldsymbol{J}, \boldsymbol{w}, t)|$ does not grow any faster than $e^{\alpha t}$, (α real and > 0), we may write as a Laplace transform

$$f(\boldsymbol{J}, \boldsymbol{w}, t) = \frac{1}{2\pi} \int_{-\infty+i\alpha}^{\infty+i\alpha} \tilde{f}(\boldsymbol{J}, \boldsymbol{w}, \omega) e^{-i\omega t} d\omega. \tag{37}$$

With this substitution into (37), we can evaluate the t' integral to obtain

$$\tilde{f}_{\boldsymbol{m}}(\boldsymbol{J}, \omega) = \frac{\tilde{h}_{\boldsymbol{m}}(\boldsymbol{J}, \omega)}{\boldsymbol{m} \cdot \boldsymbol{\Omega} - \omega} \boldsymbol{m} \cdot \frac{\partial F_0}{\partial \boldsymbol{J}}. \tag{38}$$

This is an equation for one Fourier component of the perturbation to the DF caused by a single Fourier component of a disturbance potential having frequency ω. Notice that the denominator passes through zero for purely real ω and certain values of $\boldsymbol{\Omega}(\boldsymbol{J})$; these are the familiar resonances where linear theory breaks down for steady waves, as we saw in §4.2. However, this problem does not arise for growing or decaying disturbance (complex ω).

The total response is the sum of these components

$$\tilde{f}(\boldsymbol{J}, \boldsymbol{w}, \omega) = \frac{1}{(2\pi)^2} \sum_{\boldsymbol{m}} \tilde{f}_{\boldsymbol{m}}(\boldsymbol{J}, \omega) e^{i\boldsymbol{m}\cdot\boldsymbol{w}} = \frac{1}{(2\pi)^2} \sum_{\boldsymbol{m}} \frac{\tilde{h}_{\boldsymbol{m}}(\boldsymbol{J}, \omega)}{\boldsymbol{m} \cdot \boldsymbol{\Omega} - \omega} e^{i\boldsymbol{m}\cdot\boldsymbol{w}} \boldsymbol{m} \cdot \frac{\partial F_0}{\partial \boldsymbol{J}}. \tag{39}$$

We obtain an eigenvalue equation for the normal mode frequencies, ω, by requiring that the perturbation potential arises from the disturbance density; *i.e.*

$$\nabla^2 \tilde{h}(\boldsymbol{J}, \boldsymbol{w}, \omega) = 4\pi G \tilde{\Sigma}_p \delta_z = 4\pi G \delta_z \int \int \tilde{f}(\boldsymbol{J}, \boldsymbol{w}, \omega) d^2\boldsymbol{v}. \tag{40}$$

Two practical difficulties are posed by this eigenvalue problem. Firstly, the Fourier components of the disturbance potential, $\tilde{h}_{\boldsymbol{m}}(\boldsymbol{J}, \omega)$ are coupled by Poisson's equation. Because of the rotational invariance of the Laplacian operator, the different angular harmonics of the potential can be treated separately (for infinitesimal perturbations), but the entire set of l components for a given m remain coupled. We therefore have to solve for eigenvalues of an infinite set of coupled equations.

Secondly, it may seem that the use of action-angle variables aggravates the difficulty of finding solutions to (41), since we have to evaluate the perturbed surface density, $\tilde{\Sigma}_p$, by integration over the velocities. The transformation needed to express $\tilde{f}(\boldsymbol{J}, \boldsymbol{w}, t)$ in $(\boldsymbol{x}, \boldsymbol{v})$ coordinates cannot be written in closed form, except for a few special potentials. Were we to eschew these variables, and approximate the orbits as Lindblad epicycles, we would avoid this problem, but we would still be faced with the difficulty of calculating the disturbance potential through Poisson's equation. Since the solution of Poisson's equation for an arbitrary mass distribution in a disc cannot be written down directly, the eigenvalue problem is not much easier in $(\boldsymbol{x}, \boldsymbol{v})$ coordinates!

Kalnajs (1977) proceeds by introducing a bi-orthonormal set of basis functions; the surface densities $\{\Sigma_i\}$ and corresponding potentials $\{h_i\}$ are related through Poisson's equation and normalized such that

$$-\frac{1}{2\pi G} \int h_i^* \Sigma_j d^2\boldsymbol{r} = \begin{cases} 1 & \text{if } i = j, \\ 0 & \text{otherwise.} \end{cases} \tag{41}$$

He then writes the (unknown) density perturbation, $\tilde{\Sigma}_p$, as a sum over the set

$$\tilde{\Sigma}_p = \sum_{j=0}^{\infty} a_j \Sigma_j \qquad \text{where} \qquad a_j = -\frac{1}{2\pi G} \int h_j^* \tilde{\Sigma}_p d^2\boldsymbol{r}. \tag{42}$$

The self-consistency requirement for modes is now that both $\tilde{\Sigma}_p$ and the perturbed potential, $\tilde{h}$, have the same expansion in the chosen basis which enables him to avoid calculating the perturbed density altogether. With this trick, he is able to rewrite the mode equation (41) in matrix form

$$\sum_{j=0}^{\infty} \mathcal{M}_{ij}(\omega) a_j = a_i, \tag{43}$$

where the matrix coefficients are

$$\mathcal{M}_{ij}(\omega) = -\frac{1}{8\pi^3} \sum_{\boldsymbol{m}} \int \int F(\boldsymbol{J}) \, \boldsymbol{m} \cdot \frac{\partial}{\partial \boldsymbol{J}} \left[\frac{(\tilde{h}_i)_{\boldsymbol{m}}^* (\tilde{h}_j)_{\boldsymbol{m}}}{\boldsymbol{m} \cdot \boldsymbol{\Omega} - \omega} \right] d^2 \boldsymbol{J}; \tag{44}$$

they are more readily evaluated after integration by parts. The overall technique involves a laborious calculation of all the coefficients $(\tilde{h}_i)_{\boldsymbol{m}}$ (which fortunately are independent of ω) and a non-linear search for the eigenvalue, ω; results have so far been obtained for three disc models (Kalnajs 1978, Zang 1976, Hunter 1992).[16]

A number of short-cuts have been devised to simplify the method, such as using cold discs with softened gravity (Erickson 1974, Toomre 1981), gaseous approximations (Bardeen 1975, Aoki *et al.* 1979, Pannatoni 1983, Lin and Bertin 1985) and moment methods (Hunter 1970, 1979).

9.2. Bar-forming modes

The dominant modes found in many of these analyses have very high growth rates and an open bi-symmetric spiral form. In several cases the equilibrium model has also been studied in high quality N-body simulations which reveal a dominant mode with a shape and eigenfrequency in close agreement with the analytic prediction (Zang and Hohl 1978, Sellwood 1983, Sellwood and Athanassoula 1986). A further example of such a comparison has been made in the simulation shown in Figure 17; as usual, the linear instability leads to a large-amplitude bar. The possibility that N-body simulations somehow exaggerate the saturation amplitude, and hence the significance of the instability, was eliminated by Inagaki *et al.* (1984), who compared an N-body simulation with a direct integration of the collisionless Boltzmann equation for the same problem. The bars which form appear to be robust structures that survive for as long as the simulations are continued (see §10 for caveats).

It seems likely that bars in real galaxies were created in this way, since many of their observed properties are similar to those of bars in the simulations (*e.g.* Sparke and Sellwood 1987), yet the majority of galaxies do not possess a *strong* bar (Figure 3). To account for this, we must understand how most galaxies could have either avoided this instability or subsequently regained axial symmetry. We discuss several ways in which the instability might be averted in §9.5, but we cannot claim to have a completely satisfactory theory for the formation of bars in some galaxies unless we can also account for the fraction of galaxies that contain strong bars.

---

[16] The method has also been successfully used for spherical stellar systems (Polyachenko and Shukhman 1981, Saha 1991, Weinberg 1991).

9.3. Properties of the resulting bars

The type of behaviour illustrated in Figure 17 is typical of almost every two-dimensional simulation for which the underlying model is unstable to a global bi-symmetric distortion. As the instability runs its course, the transient features in the surrounding disc fade quickly and the only non-axisymmetric feature to survive is the steadily tumbling bar.

Many authors (*e.g.* Sellwood 1981, Combes and Sanders 1981, *etc.*) have observed that the bar ends at, or usually just inside, co-rotation (or more correctly the Lagrange point – see §4.3.2). Thus, as the linear global mode saturates, its spiral shape straightens within co-rotation while the trailing arms outside co-rotation become more tightly wrapped and fade. Also the pattern speed of the bar *immediately as it forms* is generally close to that of the original global mode, in most cases slightly lower but sometimes higher (*e.g.* Figure 8 of Sellwood 1983). The figure rotation rate may quickly start to change as the model evolves further (see §10.3).

The rule that the initial bar nearly fills its co-rotation circle appears to be widely held and no counter examples have been claimed. Sellwood (1981) also found that the bar length appeared to be related to the shape of the rotation curve, but his models were all of a particular type and different results are obtained from other models (Efstathiou *et al.* 1982, Sellwood 1989).

The axis ratio of the bar largely depends upon the degree of random motion in the original disc: generally speaking, the cooler the initial disc the narrower the resulting bar (Athanassoula and Sellwood 1986).[17] The most extreme axial ratios to survive for at least a few tumbling periods are in the range 4 – 5:1.

Sparke and Sellwood (1987) give a comprehensive description of one of these N-body bars. They emphasize that the bar is much more nearly rectangular than elliptical and matches the observed profiles remarkably well (§2.1). The stars within the bars in these simulations exhibit a systematic streaming pattern, which again bears some resemblance to the observed velocity field (§2.5.1).

9.4. Mechanism for the mode

The impressive agreement between the results from global analysis and the behaviour in N-body simulations leaves little room for doubt that rotationally supported, self-gravitating discs have a strong desire to form a bar. Yet these results do not explain why this instability should be so insistent, nor do they reveal the mechanism for the mode or give any indication as to how it could be controlled. Ideas to answer these questions have emerged from local theory, however.

Toomre (1981) proposed that the bar-forming mode was driven by positive feedback to an amplifier. The inner part of a galaxy acts as a resonant cavity which may be understood as follows:

  (i) the group velocity of trailing spiral waves is inwards while that of leading waves is outwards,
 (ii) trailing spiral waves that can reach the centre are reflected as leading waves,
(iii) a second reflection occurs at co-rotation where a leading wave rebounds as an amplified trailing disturbance.

---

[17] A possible exception occurs for catastrophically unstable cold discs (*e.g.* Hohl 1975), but as these discs are unstable on all scales down to the smallest that can be resolved, one can argue that the local instabilities have caused so much heating that this is not a real exception to the rule.

Standing waves can occur at only those frequencies for which the phase of the wave closes, which implies a discrete spectrum. Super-reflection off the co-rotation resonance causes the standing wave to grow, however, making the mode unstable. The super-reflection, which Toomre (1981) aptly named "swing amplification", was first discussed by Goldreich and Lynden-Bell (1965) and by Julian and Toomre (1966). It has been further developed by Drury (1980) and invoked by Bertin (1983) and Lin and Bertin (1985). Wave action at co-rotation is conserved through a third, transmitted wave which carries away angular momentum to the outer galaxy.

9.5. *Controlling the bar instability*

The mechanism for the bar instability just outlined indicates three distinct strategies for controlling it. These are:

(i) Raising the velocity dispersion to inhibit collective effects. This option is unattractive as it would also inhibit spiral waves, though it might be possible to construct a model galaxy which could sustain spirals in the outer disc and inhibit the bar instability by having an unresponsive region near the centre of the disc only.

(ii) Immersing the galaxy in a massive halo, as favoured by Ostriker and Peebles (1973). The additional central attraction increases the stabilizing contribution from rotational forces while keeping the destabilizing gravitational forces from the density perturbations unchanged. There are two reasons why this method seems unattractive for galaxies: firstly, the halo must dominate the rotation curve even in the centre (Kalnajs 1987), whereas evidence suggests that halos dominate only the very outer rotation curve (van Albada and Sancisi 1986), and secondly, galaxies stabilized in this way would exhibit multi-armed spiral patterns (Sellwood and Carlberg 1984), whereas the more common visual impression is of a dominant bi-symmetric pattern.

(iii) Interrupting the feed-back cycle, as favoured by Toomre (1981). The feed-back loop will be broken if in-going waves are prevented from reaching the centre. This should occur if the wave encounters an ILR, which damps the oscillation through wave-particle interactions. ILRs are likely to arise in galaxies having high circular velocities close to the rotation centre. Lin (1975) was probably the first to conjecture that a dense central bulge might be effective in preventing the bar instability.

9.6. *Meta-stability and tidal triggering*

The simulations reported by Sellwood (1989) were designed to test this last stabilizing mechanism. He found that almost fully self-gravitating discs could indeed be *linearly* stable when the centre was made sufficiently hard; *i.e.* he found that no bar formed when initial perturbations are kept to small amplitudes. When the same model was subjected to a larger amplitude disturbance, however, it formed a bar with properties very similar to those in other linearly unstable models!

The reason the outcome depends upon the amplitude of the initial disturbance is that the Lindblad resonance can damp only weak perturbations; particles become trapped in the valleys of a large-amplitude wave – *i.e.* the resonance saturates. Sellwood found that waves arising from noise fluctuations in the random distribution of 2×10^4 particles were of large enough amplitude to alter the linear behaviour!

Another method of inducing a bar in a meta-stable galaxy model is by tidal triggering, which was explored by Noguchi (1987) and by Gerin *et al.* (1990). This work has been criticised

on the grounds that it is not fully self-consistent (Hernquist 1989), and Noguchi's choice of $Q = 1$ for the initial discs means that his simulations probably over-estimate the efficiency of bar formation. Notwithstanding these criticisms, this idea may offer an explanation for the possible over-abundance of barred galaxies amongst binary pairs and small groups of galaxies (Elmegreen *et al.* 1990).

9.7. An alternative theory of bar formation

While this section has focused on the idea that bars are formed quickly as a result of some large-scale collective oscillation of the disc stars, we should note that an entirely different viewpoint was proposed by Lynden-Bell (1979).

In a brief, but elegant paper, Lynden-Bell suggested that bars may grow slowly through the gradual alignment of eccentric orbits. He pointed out that a bar-like perturbing potential would exert a torque on an elongated orbit close to inner Lindblad resonance. He then showed that the torque would cause the major axis of the orbit to oscillate about an axis orthogonal to the density perturbation in outer parts of galaxies, but near the centre, in regions where double ILRs are possible, the orbit would tend to align with the perturbation.

In the aligning region, orbits having very similar frequencies would tend to group together at first, creating a bi-symmetric density perturbation which would then exert sufficiently strong tangential forces to trap orbits whose frequencies differ somewhat from that of the bar. A large perturbation can gradually be assembled in this manner over many dynamical times. Significantly, the pattern speed of the bar would also decline as the orbits become more eccentric, enabling yet lower frequency orbits to be caught by the potential. The excess angular momentum which needs to be shed from the barring region would be carried away by spiral arms. Such a bar would not extend as far as its co-rotation point.

Although Lynden-Bell was originally motivated to understand the weak bar-like features which developed in the bar-stable simulations of James and Sellwood (1978), he proposed that the mechanism describes the general evolution of most galaxies. Given the ease with which bars are formed by fast collective instabilities, it is unclear whether this mechanism plays any rôle in the formation of the strong bars we see in galaxies today. However, the alternative view of interacting orbits presented in his paper does provide considerable insight into the structure of a bar.

This mechanism gives rise to the linear bi-symmetric modes of a radially hot, non-rotating disc calculated by Polyachenko (1989). In the appendix of their paper, Athanssoula and Sellwood (1986) described a few vigorous bi-symmetric modes in their simulations of hot disc models which, however, saturated at a very low amplitude. If these modes were indeed of the type suggested by Polyachenko. based on Lynden-Bell's mechanism, the instability is probably unrelated to the formation of strong bars.

10. Evolution of the bar

Many authors have described the bar as the "end point" of the simulation. Sparke and Sellwood (1987) presented convincing evidence that a two-dimensional stellar bar is indeed a steady, robust feature when all particles except those in the bar are frozen and therefore prevented from interacting with it. They knew at the time that the bar evolves through interactions with other responsive components, but were unaware that an isolated bar can suffer a further instability when motion into the third dimension is permitted.
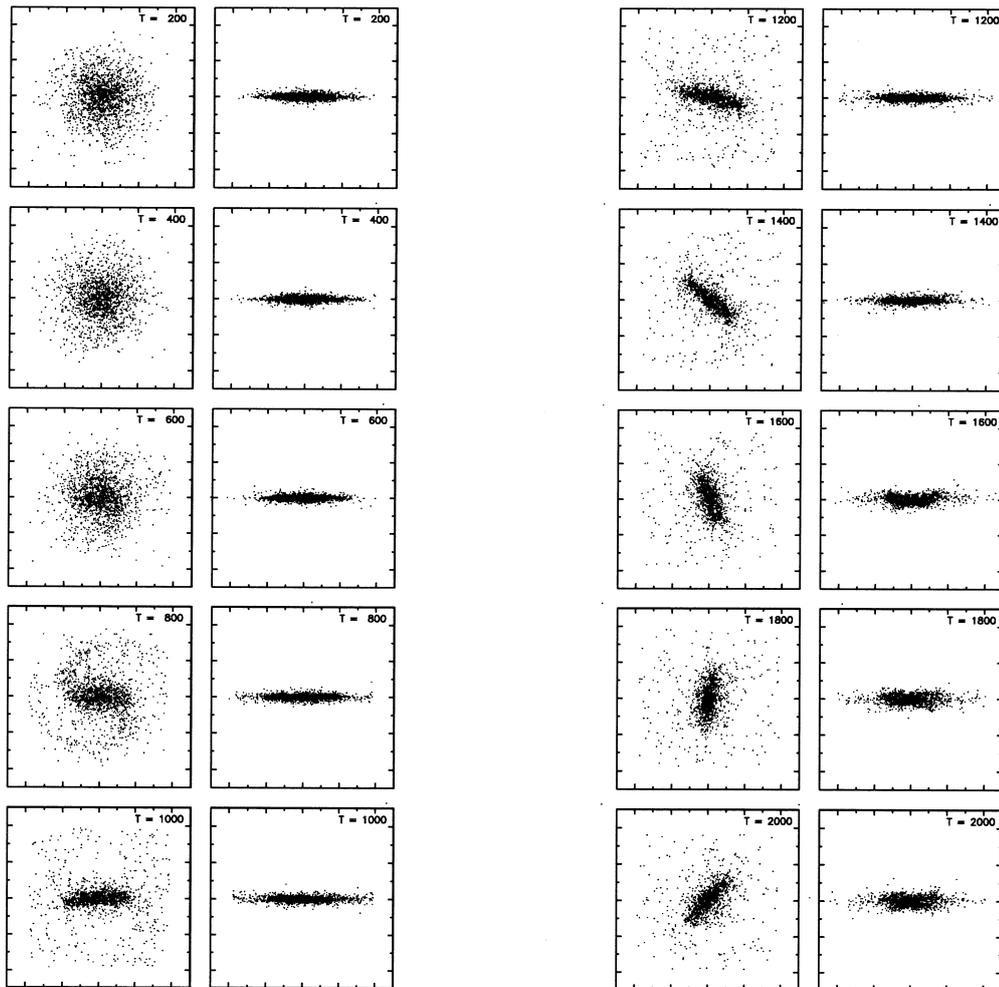
Figure 18. Pole and side views of bar formation and subsequent buckling in the fully three-dimensional thicker disc experiment reported by Raha *et al.* (1991). The side views are always shown from a position perpendicular to the bar major axis. Only 2K of the 90K disc particles are shown in each plot, and none of the 60K spheroid particles is shown. The bar rotation period is a little less than 200 time units.

10.1. Buckling instability

The "fire hose" (buckling or corrugation) instability for a stellar disc was considered by Toomre (1966), Kulsrud *et al.* (1971), Fridman and Polyachenko (1984) and Araki (1985) in an idealized, non-rotating, infinite sheet model. Subsequent papers have all confirmed Toomre's original conclusion that buckling modes develop in this simple model only when the sheet is thin, or more exactly, when the velocity dispersion in the z-direction is less than about one third (Araki quotes 0.29) that of the velocity dispersions in the plane. As the value observed in the solar neighbourhood is approximately 0.5 (*e.g.* Woolley 1965), all these authors concluded that buckling modes are unlikely to be of importance in disc galaxies.

However, the formation of a bar within the disc changes this conclusion. Not only does a bar typically make the orbits more eccentric in the plane, but the direction of their principal axes are also aligned; *i.e.* the majority of stars in the bar move up and down the bar in highly eccentric orbits (§4.9). The creation of organized streaming motion along the major axis of the

bar occurs without affecting the "pressure" normal to the plane, and compromises the stability to buckling modes (Raha *et al.* 1991).

Figure 18 shows the development of a bar in a disc which then buckles out of the plane; the model illustrated is one of the two cases presented by Raha *et al.*. The viewing direction for the edge-on frames is from a point always on the bar intermediate axis. The bend develops soon after the bar has formed and becomes quite pronounced by time 1600, after which the bar regains symmetry about the plane but is somewhat thicker than before and has a distinctive peanut shape when viewed from the side. The instability also weakens the bar amplitude in the plane (only slightly in this case), and could perhaps destroy it entirely when very violent (Raha *et al.* 1991).

A similar outcome was originally reported by Combes and Sanders (1981) and later confirmed and strengthened in simulations of much higher quality (Combes *et al.* 1990). However, these authors propose that the bar thickens because of the narrow instability strip associated with the vertical Lindblad resonances within the bar. Pfenniger and Friedli (1991) attempt to develop this alternative mechanism, which has to be reconciled with their empirical results that collective effects and a z-asymmetry in the potential are essential.

While there is no doubt that a narrow strip of vertically unstable orbits exists in their N-body bar models, it seems unlikely that the comparatively small fraction of orbits affected (at any one time) could lead to the exponentially growing, uniform bend, of the type shown in Figure 18. On the other hand, Pfenniger and Friedli (1991) and Raha (1992) show quite convincingly that the final peanut shape of the bar is caused by a large number of orbits trapped about the stable $2:2_a:1$ periodic orbit family (§5.2.3); thus the structure of bar after the instability has saturated, though not the linear instability itself, is determined by the periodic orbits (§5.3).

Moreover, the existence of the fire-hose instability in thin non-rotating bars was predicted by Fridman and Polyachenko (1984). The N-body simulations of Merritt and Hernquist (1991) confirmed that highly prolate models suffer from buckling modes, which clearly cannot be caused by unstable orbits in their Stäckel initial models. It therefore seems most likely that the buckling modes in both these and the rapidly rotating bars are of the fire-hose type.

10.2. Peanut growth

The final bar in Figure 18 resembles a peanut shape when viewed from the side. A similar shape appeared in every bar which formed in the many experiments reported by Combes *et al.* (1990), although it is not certain that the formation mechanism was the same.

Their results seem to indicate that any strong bar which forms in a galaxy must quickly become much thicker than the disc, a conclusion at variance with those observers who argue that bars seem to be thin (*e.g.* Kormendy 1982). The simulators have, of course, seized upon box-peanut shaped bulges sometimes observed (§2.3.3) and argued that they are the thickened bars. Two further pieces of indirect evidence add credence to this speculation: firstly, it is believed (on admittedly very slender evidence) that the rotation rate of the stars in a box-peanut shaped bulge is independent of distance from the plane, a property which is not found for normal bulges (Kormendy and Illingworth 1982). Secondly, the fraction of box-peanut shaped bulges in nearly edge-on galaxies is some 20% (*e.g.* Shaw 1987) which is not very different from the expected fraction of strongly barred galaxies, when allowance is made for those systems in which the randomly oriented major axis of the bar must lie close to our line of sight.

Unfortunately, there are two drawbacks to this simple association: Athanassoula (private communication) points out that most, though not all, box-peanut bulges are much less extensive, relative to the host galaxy's size, than are strong bars. Moreover, Shaw (private communication) raises the further concern that the 30% of strong bars expected in edge-on galaxies, have apparently *not* all developed a recognisable peanut shape. A further observational test of this hypothesis might be to determine whether the luminosity functions of bars and box/peanut bulges are similar, though dust obscuration might make this difficult. Before this last question acquires the status of a major puzzle, however, it seems necessary for the simulators to verify that the bars continue to thicken in a much wider range of mass distributions than have so far been tested, especially those having a more realistic bulge with a high central density.

10.3. Continuing interactions with the disc

Sellwood (1981) emphasized that when the initial bar in his simulations was short compared with the total extent of the disc, it continued to exchange angular momentum with the outer disc through further spiral activity. As always, the trailing spirals remove angular momentum from particles at their inner end; Sellwood found that this enabled more stars to be trapped into the bar, which increased its length and also lowered its pattern speed. In the most extensive disc he studied, this process continued through a number of spiral episodes while the bar increased in length by more than 50%. Interestingly, the changes in both bar length and pattern speed conspired to keep co-rotation just beyond the end of the bar.

Combes and Sanders (1981), on the other hand, reported that bars tend to weaken in the long term. There are at least two physical reasons for their different finding: firstly, their models started with much less extensive discs, precluding the type of secondary bar growth Sellwood observed; secondly, theirs were three-dimensional models in which the bar thickened normal to the plane, which caused the strength in the plane to decline (see §10.1). No three-dimensional models with an extensive outer disc have so far been run to settle the question of which effect wins.

10.4. Interations with spheroidal components

The large majority of simulations to date have employed fixed additional contributions to the radial force to represent the effects of spheroidally distributed matter, such as the bulge and halo. This computational expedient excludes the possibility of interactions between the disc population and a responsive bulge/halo component. In a direct check on the validity of this approximation, Sellwood (1980) found it adequate while the disc remained nearly axisymmetric. Once a strong bar had formed, however, the (initially non-rotating) bulge/halo population of particles began to gain angular momentum from the disc at a prodigious rate. Thus the coupling between the disc and spheroidal populations of particles in *barred* galaxies ought not to be ignored.

The interaction process can be described as a kind of dynamical friction (Tremaine and Weinberg 1984a) between the rotating massive object, the bar, and a background sea of collisionless particles. Weinberg (1985) calculated that angular momentum should be exchanged between the bar and a non-rotating spheroid at a rate consistent with Sellwood's observed value. Unfortunately, Sellwood's experiment did not continue for very many bar tumbling periods and did not reveal the long term consequences for both the bar and the halo population of a very protracted period of interaction. We therefore still do not know whether the bar pattern speed

will be reduced (or even raised), whether its amplitude will be increased or diminished or how the spheroid will appear once a substantial exchange of angular momentum has occurred.

The only truly long term experiment to examine this issue has been conducted by Little and Carlberg (1991), but for computational economy they again used a two-dimensional model. Their "flat halo" was an entirely pressure supported population of particles co-planar with the rotationally supported disc in which the bar formed. They found that the bar was indeed slowed by the angular momentum loss to the "halo", but a more realistic experiment is clearly warranted.

The predicted efficiency of angular momentum transfer is embarassingly high, sufficient to arrest a rigid bar in a few rotations, yet a number of lines of evidence suggest that bars in galaxies rotate rapidly. We are not, however, forced to an unattractive conclusion that bars must either be very young or they have stopped rotating; there are other ways to avoid this dilemma. The most plausible seems to us that Weinberg over-estimates the efficiency of exchange by assuming a non-rotating spheroid. The luminous bulges of galaxies generally rotate sufficiently rapidly for their flattening to be consistent with a rotating isotropic model (*e.g.* Kormendy and Illingworth 1982). In the few cases that have been measured, bulge streaming velocities are typically 40% of those at the corresponding distance in the disc and the angular momentum vector lies in the same direction as that of the disc. This degree of rotation will alter the angular momentum exchanges with a bar, and may make them less efficient. It is not clear whether the observed angular momentum has been acquired from the disc component already, or whether it was primordial. Weinberg himself also notes that the bar is simultaneously spun up by interactions with the outer disc, and speculates that it could act as a catalyst transferring angular momentum from the disc to the spheroid while not changing its own angular momentum content by much. Finally, the bar is not a rigid body and probably has a much lower moment of inertia (possibly even negative) than that assumed by Weinberg. These issues can be addressed only by high quality, long term experiments.

10.5. Destruction of bars

Even three-dimensional bars seem to be long-lived; Pfenniger and Friedli (1991) report that their bar models cease to evolve after the thickening phase, and survive essentially unchanged as long as the calculation is run. Thus although the buckling instability (§10.1) dented the common perception that bars are rugged structures, it does not seem to have invalidated it.

It is therefore interesting to ask whether a galaxy, having once acquired a bar, could ever rid itself of it. A few ideas for achieving this have been mooted.

The most recent (Raha *et al.* 1991) is that the buckling instability could be so violent that the bar is destroyed. Raha *et al.* seemed to find that the buckling instability was more violent when the bar formed in a thinner disc, though in both their cases the bar was merely weakened, not completely destroyed. If ever the buckling instability could be violent enough to destroy the bar, therefore, the bar would have to have formed in an extremely thin, and probably very young, disc.

Another suggestion is that bars could be destroyed during an interaction with a companion galaxy. It has generally been felt that an interaction violent enough to destroy the bar would also destroy the disk, but Pfenniger's (1991) report of a simulation in which a dwarf was accreted by a barred galaxy seems to show that the bar can be destroyed, and the companion disrupted, without doing very much damage to the disc.

A further suggestion has been made by Norman and his co-workers (Pfenniger and Norman 1990, Hasan and Norman 1990) that the growth of a comparatively light, but dense, object at the centre can destroy the bar. They argue that the growth of central mass changes the major orbit families which support the bar, and thereby threaten its survival. Friedli *et al.* (1991) present preliminary results which seem to indicate that a bar can drive sufficient gas towards the galactic centre to have this effect – *i.e.* that bars in gas rich galaxies may self-destruct.

11. Conclusions

It should be clear that we are still far from a complete understanding of the basic structure of barred galaxies, but progress has been rapid in recent years – especially where orbit studies have been connected to observational or simulated results. There are a few aspects where the observed facts seem to fit reasonably well with theoretical ideas.

On the bright side, it seems very likely that strong bars are formed by the dynamical instability discussed in §9. Bars formed in the N-body experiments end near co-rotation and have mass distributions and kinematic properties which seem to correspond with those observed, though more detailed comparisons would be desirable. Moreover, such bar models appear to have the right strength, and to rotate sufficiently rapidly to shock gas in places resembling the dust lane patterns in some barred galaxies. The flow patterns described in §6 are understood in terms of orbit theory and fit the observed kinematics for entirely plausible model parameters. We also think we understand the origins of rings (§7) sufficiently well to be able to interpret them as signatures of major resonances with the bar pattern.

These successes add up to a compelling, but indirect, case for a bar pattern speed in galaxies which places the major axis Lagrange point just beyond the bar's end. Such a value is consistent with the more direct observational estimates of pattern speed (§2.6) which unfortunately are subject to large uncertainties.

Current observational work is beginning to provide more quantitative data on the light distributions and kinematics of barred galaxies. In particular, the kind of comparison with theoretical models made by Kent and Glaudell (1989) for NGC 936 should be extended to several other galaxies in case the structure of that galaxy is special in any way. Moreover, the theory of ring formation is in dire need of more detailed observational comparisons; we need good kinematic maps of many more such galaxies to confirm that the rings do indeed lie at the resonances for the bar.

Yet our understanding of the dynamical structure of bars is still far from complete. The vast literature on orbits in bar-like potentials has led to a few major conclusions relevant to the structure of barred galaxies: the most important is that the majority of stars within the bar probably follow eccentric orbits which are trapped, or semi-trapped, about the main family of orbits aligned with the bar (the x_1 family). Apart from this, knowledge of the main orbit families has improved our understanding of gas flows and indicates that it would be hopeless to try to construct a self-consistent bar having a mean rotational streaming in a sense counter to the pattern rotation. It is progress, of a kind, to learn that a simple generalization of the two-dimensional orbital structure does not provide a complete description of three-dimensional bars. Only one set of approximately self-consistent two-dimensional numerical solutions has been found (Pfenniger 1984b) and the prospects for analytic models in the near future are bleak. Next to this, our fragmentary understanding of the evolution of barred galaxies, and almost total blanks on the origins of lenses and the pronounced asymmetries in some galaxies, seem of secondary concern.

Probably the most pressing need on the theoretical side is for a more sustained attack on the orbital structure of three-dimensional bars, preferably through studies of rapidly rotating three-dimensional objects having density distributions resembling those seen in galaxies. It should be possible to address the evolutionary issues as more powerful computers enable the quality of N-body simulations to rise.

Other fundamental questions also need to be pursued. The prime candidate is what determines the $\sim 30\%$ fraction of galaxies seen to have strong bars. Since the bar instability seems able to create strong bars in nearly all disc galaxies, how can we account for the current moderate fraction? The ideas for controlling the bar instability (§9.5) and those for destroying bars (§10.5) do not explain either why some $\sim 70\%$ of galaxies manage to avoid a bar instability, or why the bar was subsequently weakened or destroyed in that fraction of galaxies. Are the weak bars in galaxies of intermediate type (SAB) formed through the partial dissolution of strong bars, or is some totally different mechanism required?

The bar instability we discuss in §9 assumed an initially unstable equilibrium disc without specifying how that could have been created. A discussion of the formation of disc galaxies is well beyond the scope of this review, but it does seem likely that the bar instability would be profoundly affected by the manner in which galactic discs form. Sellwood and Carlberg (1984), in a few preliminary experiments mimicking gradual disc formation, found that the velocity dispersion of the stars rose sufficiently rapidly to inhibit the formation of a strong bar as the disc mass built up. Further experiments of this kind, especially including gas dynamics seem warranted.

Another issue is whether it is sensible to separate a barred galaxy into distinct dynamical components. Most theoretical and observational work has proceeded on the assumption that the bar and the bulge are distinct, but we have seen in §10 that there may be no dynamical basis for considering them as separable. Moreover, as it seems likely that the bar formed from the disc, we may confuse ourselves by trying to understand these also as unrelated components.

Although we have a lot more to do before we can claim to understand the structure of these objects, we should be encouraged that progress over the last few years has been rapid, especially since the knowledge which enabled us to formulate many of these questions has only recently been acquired. The many new telescopes and observational techniques, particularly operating in the infra-red, are likely to advance the subject at its currently intense rate.

References

Adamson A J, Adams D J and Warwick R S 1987 *Mon. Not. R. Astron. Soc.* **224** 367
Aoki S, Noguchi M and Iye M 1979 *Publs. Astron. Soc. Japan* **31** 737
Araki S 1985 *PhD thesis* MIT
Arsenault R 1989 *Astron. Astrophys.* **217** 66
Arsenault R, Boulesteix J, Georgelin Y and Roy J-R 1988 *Astron. Astrophys.* **200** 29
Athanassoula E 1983 *Internal Kinematics and Dynamics of Galaxies* IAU Symposium **100** ed E Athanassoula
    (Dordrecht: Reidel) p 243
—— 1984 *Phys. Reports* **114** 320

—— 1990 *Galactic Models* Annals of the New York Academy of Sciences **596** ed J R Buchler, S T Gottesman and J H Hunter (New York: NY Academy of Sciences) p 181

—— 1992a *Astron. Astrophys.* in press

—— 1992b *Astron. Astrophys.* in press

Athanassoula E, Bienaymé O, Martinet L and Pfenniger D 1983 *Astron. Astrophys.* **127** 349

Athanassoula E, Bosma A, Crézé M and Schwarz M P 1982 *Astron. Astrophys.* **107** 101

Athanassoula E, Bosma A and Papaioannou S 1987 *Astron. Astrophys.* **179** 23

Athanassoula E and Martinet L 1980 *Astron. Astrophys.* **87** L10

Athanassoula E, Morin S, Wozniak H, Puy D, Pierce M J, Lombard J and Bosma A 1990 *Mon. Not. R. Astron. Soc.* **245** 130

Athanassoula E and Sellwood J A 1986 *Mon. Not. R. Astron. Soc.* **221** 213

Athanassoula E and Wozniak H 1992 Preprint

Baker N H, Moore D W and Speigel E A 1971 *Quart. J Mech. and Applied Math.* **24** 419

Baldwin J E, Lynden-Bell D and Sancisi R 1980 *Mon. Not. R. Astron. Soc.* **193** 313

Ball R 1986 *Astrophys. J.* **307** 453

Ball R, Sargent A I, Scoville N Z, Lo K Y and Scott S L 1985 *Astrophys. J. Lett.* **298** L21

Bardeen J M 1975 *Dynamics of Stellar Systems* IAU Symposium **69** ed A Hayli (Dordrecht: Reidel) p 297

Barnes J E and Hernquist L E 1991 *Astrophys. J. Lett.* **370** L65

Baumgart C W and Peterson C J 1986 *Publs. Astron. Soc. Pacific* **98** 56

Berry M V 1978 *Topics in Non-Linear Dynamics – A Tribute to Sir Edward Bullard* AIP Conference series **46** ed S Jorna (New York: AIP) p 16

Bertin G 1983 *Internal Kinematics and Dynamics of Galaxies* IAU Symposium **100** ed E Athanassoula (Dordrecht: Reidel) p 119

Bettoni D 1989 *Astron. J.* **97** 79

Bettoni D, Fasano G and Galletta G 1990 *Astron. J.* **99** 1789

Bettoni D and Galletta G 1988 *ESO Messenger* **54** 51

Bettoni D, Galletta G and Osterloo T 1991 *Mon. Not. R. Astron. Soc.* **248** 544

Bettoni D, Galletta G and Vallenari A 1988 *Astron. Astrophys.* **197** 69

Binney J 1981 *Mon. Not. R. Astron. Soc.* **196** 455

Binney J, Gerhard O E and Hut P 1985 *Mon. Not. R. Astron. Soc.* **215** 59

Binney J and Lacey C 1988 *Mon. Not. R. Astron. Soc.* **230** 597

Binney J and Spergel D 1982 *Astrophys. J.* **252** 308

—— 1984 *Mon. Not. R. Astron. Soc.* **206** 159

Binney J and Tremaine S 1987 *Galactic Dynamics* (Princeton: Princeton University Press)

Blackman C P 1983 *Mon. Not. R. Astron. Soc.* **202** 379

Blackman C P and Pence W D 1982 *Mon. Not. R. Astron. Soc.* **198** 517

Block D L and Wainscoat R J 1991 *Nature* **353** 48

Bosma A 1983 *Internal Kinematics and Dynamics of Galaxies* IAU Symposium **100** ed E Athanassoula (Dordrecht: Reidel) p 253

—— 1992 *Morphology and Physical Classification of Galaxies* ed G Longo, M Capaccioli and G Busarello (Dordrecht: Kluwer) p 207

Bottema R 1990 *Astron. Astrophys.* **233** 372

Broucke R A 1969 *Am. Inst. Aeron. Astronautics J.* **7** 1003

Burstein D 1979 *Astrophys. J. Suppl.* **41** 435

Buta R 1986a *Astrophys. J. Suppl.* **61** 609

—— 1986b *Astrophys. J. Suppl.* **61** 631

—— 1987 *Astrophys. J. Suppl.* **64** 383

—— 1988 *Astrophys. J. Suppl.* **66** 233

—— 1990a *Galactic Models* Annals of the New York Academy of Sciences **596** ed J R Buchler, S T Gottesman and J H Hunter (New York: NY Academy of Sciences) p 58

—— 1990b *Astrophys. J.* **356** 87

—— 1991 *Dynamics of Galaxies and their Molecular Cloud Distributions* IAU Symposium **146** ed F Combes and F Casoli (Dordrecht: Kluwer) p 251

Buta R and Crocker D A 1991 *Astron. J.* **102** 1715

Canzian B, Mundy L G and Scoville N Z 1988 *Astrophys. J.* **333** 157

Casertano S and van Albada T S 1990 *Baryonic Dark Matter* ed D Lynden-Bell and G Gilmore (Dordrecht: Kluwer) p 159

Chandrasekhar S 1941 *Astrophys. J.* **94** 511

Chevalier R A and Furenlid I 1978 *Astrophys. J.* **225** 67

Chirikov B V 1979 *Phys. Reports* **52** 265

Cleary P W 1989 *Astrophys. J.* **337** 108

Colin J and Athanassoula E 1989 *Astron. Astrophys.* **214** 99

Combes F 1992 *Physics of Galaxies: Nature or Nurture?* ed C Balkowski (to appear)

Combes F, Debbasch F, Friedli D and Pfenniger D 1990 *Astron. Astrophys.* **233** 82

Combes F and Gerin M 1985 *Astron. Astrophys.* **150** 327

Combes F and Sanders R H 1981 *Astron. Astrophys.* **96** 164

Contopoulos G 1978 *Astron. Astrophys.* **64** 323

—— 1980 *Astron. Astrophys.* **81** 198

—— 1983a *Physica D* **8** 142

—— 1983b *Astron. Astrophys.* **117** 89

—— 1988 *Astron. Astrophys.* **201** 44

Contopoulos G and Barbanis B 1989 *Astron. Astrophys.* **222** 329

Contopoulos G and Grosbøl P 1989 *Astron. Astrophys. Review* **1** 261

Contopoulos G and Magnenat P 1985 *Celestial Mechanics* **37** 387

Contopoulos G and Mertzanides C 1977 *Astron. Astrophys.* **61** 477

Contopoulos G and Papayannopoulos Th 1980 *Astron. Astrophys.* **92** 33

Contopoulos G and Vandervoort P O 1992 *Astrophys. J.* **389** 118

Cowie L L 1980 *Astrophys. J.* **236** 868

Cox D P and Reynolds R J 1987 *Ann. Rev. Astron. and Astrophys.* **25** 303

Crane P C 1975 *Astrophys. J.* **197** 317

Davidson R C, Chan H-W, Chen C and Lund S 1991 *Rev. Mod. Phys.* **63** 341

de Souza R E and dos Anjos S 1987 *Astron. Astrophys. Suppl.* **70** 465

de Vaucouleurs G 1974 *Formation and Dynamics of Galaxies* IAU Symposium **58** ed J R Shakeshaft (Dordrecht: Reidel) p 335

—— 1975 *Astrophys. J. Suppl.* **29** 193

de Vaucouleurs G, de Vaucouleurs A and Corwin H G 1976 *Second Reference Catalogue of Bright Galaxies* (Austin: University of Texas Press) (RC2)

de Vaucouleurs G, de Vaucouleurs A and Freeman K C 1968 *Mon. Not. R. Astron. Soc.* **139** 425

de Vaucouleurs G and Freeman K C 1972 *Vistas Astron.* **14** 163

de Zeeuw T 1985 *Mon. Not. R. Astron. Soc.* **216** 273 and 599

de Zeeuw T and Franx M 1991 *Ann. Rev. Astron. and Astrophys.* **29** 239

de Zeeuw T, Peletier R and Franx M 1986 *Mon. Not. R. Astron. Soc.* **221** 1001

Disney M, Davies J and Phillipps S 1989 *Mon. Not. R. Astron. Soc.* **239** 939

Dragt A J and Finn J M 1976 *J. Geophys. Res.* **81** 2327

Drury L O'C 1980 *Mon. Not. R. Astron. Soc.* **193** 337

Duval M F and Athanassoula E 1983 *Astron. Astrophys.* **121** 297

Duval M F and Monnet G 1985 *Astron. Astrophys. Suppl.* **61** 141

Duval M F, Monnet G, Boulesteix J, Georgelin Y, Le Coarer E and Marcelin M 1991 *Astron. Astrophys.* **241** 375

Eddington A S 1915 *Mon. Not. R. Astron. Soc.* **76** 37

Eder J, Giovanelli R and Haynes M P 1991 *Astron. J.* **102** 572

Efstathiou G, Lake G and Negroponte J 1982 *Mon. Not. R. Astron. Soc.* **199** 1069

Elmegreen B G and Elmegreen D M 1985 *Astrophys. J.* **288** 438

Elmegreen D M, Elmegreen B G and Bellin A D 1990 *Astrophys. J.* **364** 415

England M N 1989 *Astrophys. J.* **344** 669

England M N, Gottesman S T and Hunter J H 1990 *Astrophys. J.* **348** 456

Erickson S A 1974 *PhD thesis* MIT

Ferrers N M 1877 *Quart. J Pure Appl. Math.* **14** 1

Freeman K C 1966 *Mon. Not. R. Astron. Soc.* **134** 15

Fridman A M and Polyachenko V L 1984 *Physics of Gravitating Systems* (New York: Springer-Verlag)

Friedli D, Benz W and Martinet L 1991 *Dynamics of Disc Galaxies* ed B Sundelius (Gothenburg: Göteborgs University) p 181

Garcia-Barreto J A, Downes D, Combes F, Gerin M, Magri C, Carrasco L and Cruz-Gonzalez I 1991a *Astron. Astrophys.* **244** 257

Garcia-Barreto J A, Downes D, Combes F, Carrasco L, Gerin M and Cruz-Gonzalez I 1991b *Astron. Astrophys.* **252** 19

Gerhard O E and Vietri M 1986 *Mon. Not. R. Astron. Soc.* **223** 377

Gerin M, Combes F and Athanassoula E 1990 *Astron. Astrophys.* **230** 37

Gerin M, Nakai N and Combes F 1988 *Astron. Astrophys.* **203** 44

Gingold R A and Monaghan J J 1977 *Mon. Not. R. Astron. Soc.* **181** 375

Goldreich P and Lynden-Bell D 1965 *Mon. Not. R. Astron. Soc.* **130** 125

Goldreich P and Tremaine S 1982 *Ann. Rev. Astron. and Astrophys.* **20** 249

Goldstein H 1980 *Classical Mechanics* 2nd edition (Addison-Wesley)

Gottesman S T, Ball R, Hunter J H and Huntley J M 1984 *Astrophys. J.* **286** 471

Hackwell J A and Schweizer F 1983 *Astrophys. J.* **265** 643

Hadjidemetriou J D 1975 *Celestial Mechanics* **12** 255

Handa T, Nakai N, Sofue Y, Hayashi M and Fujimoto M 1990 *Publs. Astron. Soc. Japan* **42** 1

Hasan H and Norman C 1990 *Astrophys. J.* **361** 69

Hawarden T G, Mountain C M, Leggett S K and Puxley P J 1986 *Mon. Not. R. Astron. Soc. Short Communication* **221** 41p

Heisler J, Merritt D and Schwarzschild M 1982 *Astrophys. J.* **258** 490

Hénon M 1976 *Celestial Mechanics* **13** 267

Hénon M 1983 *Chaotic Behaviour of Deterministic Systems* Les Houches Session XXXVI ed G Iooss, R H G Helleman and R Stora (Amsterdam: North-Holland) p 55

Hénon M and Heiles C 1964 *Astron. J.* **69** 73

Hernquist L 1989 *Nature* **340** 687

Hernquist L and Barnes J E 1990 *Astrophys. J.* **349** 562

Hernquist L and Katz N 1989 *Astrophys. J. Suppl.* **70** 419

Hietarinta J 1987 *Phys. Reports* **147** 87

Hill G W 1878 *Am. J. Math.* **1** 5

Hockney R W and Brownrigg D R K 1974 *Mon. Not. R. Astron. Soc.* **167** 351

Hockney R W and Hohl F 1969 *Astron. J.* **74** 1102

Hohl F 1975 *Dynamics of Stellar Systems* IAU Symposium **69** ed A Hayli (Dordrecht: Reidel) p 349

—— 1978 *Astron. J.* **83** 768

Hubble E 1926 *Astrophys. J.* **64** 321

Huizinga J E and van Albada T S 1992 *Mon. Not. R. Astron. Soc.* **254** 677

Hummel E, Dettmar R J and Wielebinski R 1986 *Astron. Astrophys.* **166** 97

Hummel E, Jörsäter S, Lindblad P O and Sandqvist A 1987a *Astron. Astrophys.* **172** 51

Hummel E, van der Hulst J M and Keel W C 1987b *Astron. Astrophys.* **172** 32

Hummel E, van der Hulst J M, Kennicutt R C and Keel W C 1990 *Astron. Astrophys.* **236** 333

Hunter C 1970 *Studies in Applied Math* **49** 59

—— 1979 *Astrophys. J.* **227** 73

—— 1992 *Astrophysical Disks* ed S F Dermott, J H Hunter and R E Wilson (New York Academy of Sciences) (to appear)

Hunter C and de Zeeuw P T 1992 *Astrophys. J.* **389** 79

Hunter C, de Zeeuw P T, Park Ch and Schwarzschild M 1990 *Astrophys. J.* **363** 367

Hunter J H, Ball R, Huntley J M, England M N and Gottesman S T 1988 *Astrophys. J.* **324** 721

Huntley J M, Sanders R H and Roberts W W 1978 *Astrophys. J.* **221** 521

Inagaki S Nishida M T and Sellwood J A 1984 *Mon. Not. R. Astron. Soc.* **210** 589

Ishizuki S, Kawabe R, Ishiguro M, Okamura S K, Morita K-I, Chikada Y and Kasuga T 1990 *Nature* **344** 224

James R A and Sellwood J A 1978 *Mon. Not. R. Astron. Soc.* **182** 331

Jarvis B J 1986 *Astron. J.* **91** 65

Jarvis B J, Dubath P, Martinet L and Bacon R 1988 *Astron. Astrophys. Suppl.* **74** 513

Jörsäter S 1979 *Photometry, Kinematics and Dynamics of Galaxies* ed D S Evans (Austin: University of Texas Press) p 197

Julian W H and Toomre A 1966 *Astrophys. J.* **146** 810

Kalnajs A J 1965 *PhD thesis* Harvard

—— 1971 *Astrophys. J.* **166** 275

—— 1977 *Astrophys. J.* **212** 637

—— 1978 *Structure and Properties of Nearby Galaxies* IAU Symposium **77** ed E M Berkhuisjen and R Wielebinski (Dordrecht: Reidel) p 113

—— 1987 *Dark Matter in the Universe* IAU Symposium **117** ed J Kormendy and G R Knapp (Dordrecht: Reidel) p 289

Kenney J D P 1991 *Dynamics of Disc Galaxies* ed B Sundelius (Gothenburg: Göteborgs University) p 171

Kent S M 1987 *Astron. J.* **93** 1062

—— 1990 *Astron. J.* **100** 377

Kent S M and Glaudell G 1989 *Astron. J.* **98** 1588

Kormendy J 1979 *Astrophys. J.* **227** 714

—— 1981 *The Structure and Evolution of Normal Galaxies* Eds Fall SM and Lynden-Bell D (Cambridge: Cambridge University Press)

—— 1982 *Morphology and Dynamics of Galaxies* 12th Advanced Course of the Swiss Society of Astronomy and Astrophysics at Saas Fee Eds Martinet L and Mayor M (Sauverny: Geneva Observatory)

—— 1983 *Astrophys. J.* **275** 529

Kormendy J and Illingworth G 1982 *Astrophys. J.* **256** 460

Kulsrud R M, Mark J W-K and Caruso A 1971 *Astrophys. Sp. Sci.* **14** 52

Kuz'min G G 1956 *Astr. Zh.* **33** 27

Landau L D and Lifshitz E M 1987 *Fluid Mechanics* 2nd edition (Oxford: Pergamon)

Liapunov A M 1907 Reprinted 1947 in *Ann. Math Studies* **17** (Princeton)

Lichtenberg A J and Lieberman M A 1983 *Regular and Stochastic Motion* Applied Math Sciences **38** (New York: Springer-Verlag)

Lin C C 1975 *Structure and Evolution of Galaxies* ed G Setti (Dordrecht: Reidel) p 119

Lin C C and Bertin G 1985 *The Milky Way Galaxy* IAU Symposium **106** ed H van Woerden, R J Allen and W B Burton (Dordrecht: Reidel) p 513

Lindblad B 1927 *Mon. Not. R. Astron. Soc.* **87** 553

Lindblad P O and Jörsäter S 1987 *Evolution of Galaxies* Proceedings of the 10th IAU Regional Astronomy Meeting vol 4 ed J Palouš *Publ. Astr. Inst. Czech. Acad. Sci.* **69** 289

Little B and Carlberg 1991 *Mon. Not. R. Astron. Soc.* **250** 161

Long K 1992 Preprint

Lord S D and Kenney J D P 1991 *Astrophys. J.* **381** 130

Louis P D and Gerhard O E 1988 *Mon. Not. R. Astron. Soc.* **233** 337

Lucy L B 1977 *Astron. J.* **82** 1013

Lynden-Bell D 1962a *Mon. Not. R. Astron. Soc.* **124** 1

—— 1962b *Mon. Not. R. Astron. Soc.* **124** 95

—— 1979 *Mon. Not. R. Astron. Soc.* **187** 101

McGill C and Binney J 1990 *Mon. Not. R. Astron. Soc.* **244** 634

MacKay R S, Meiss J D and Percival I C 1984 *Physica D* **13** 55

Magnenat P 1982a *Astron. Astrophys.* **108** 89

—— 1982b *Celestial Mechanics* **28** 319

Marcelin M and Athanassoula E 1982 *Astron. Astrophys.* **105** 76

Martinet L 1984 *Astron. Astrophys.* **132** 381

Martinet L and Pfenniger D 1987 *Astron. Astrophys.* **173** 81

Martinet L and Udry S 1990 *Astron. Astrophys.* **235** 69

Martinet L and de Zeeuw T 1988 *Astron. Astrophys.* **206** 269

Mathews J and Walker R L 1970 *Mathematical Methods of Physics* 2nd edition (Menlo Park: Benjamin/ Cummings)

Matsuda T and Isaka H 1980 *Prog. Theor. Phys.* **64** 1265

Merritt D and Hernquist L 1991 *Astrophys. J.* **376** 439

Merritt D and Stiavelli M 1990 *Astrophys. J.* **358** 399

Miller R H and Prendergast K H 1968 *Astrophys. J.* **151** 699

Miller R H, Prendergast K H and Quirk W J 1970 *Astrophys. J.* **161** 903

Miller R H and Smith B F 1979 *Astrophys. J.* **227** 785

Miralda-Escudé J and Schwarzschild M 1989 *Astrophys. J.* **339** 752

Miyamoto M and Nagai R 1975 *Publs. Astron. Soc. Japan* **27** 533

Moser J 1973 *Stable and Random Motions in Dynamical Systems* Annals of Math Studies **77** (Princeton: Princeton University Press)

Mulder W A 1986 *Astron. Astrophys.* **156** 354

Mulder W A and Hooimeyer J R A 1984 *Astron. Astrophys.* **134** 158

Newton A J and Binney J 1984 *Mon. Not. R. Astron. Soc.* **210** 711

Nilson P 1973 *Uppsala General Catalogue of Galaxies* (= Acta Upsaliensis Ser V: A Vol I)

Noguchi M 1987 *Mon. Not. R. Astron. Soc.* **228** 635

Noguchi M 1988 *Astron. Astrophys.* **203** 259

Odewahn S C 1991 *Astron. J.* **101** 829

Ohta K, Hamabe M and Wakamatsu K-I 1990 *Astrophys. J.* **357** 71

Okamura S 1978 *Publs. Astron. Soc. Japan* **30** 91

Ondrechen M P 1985 *Astron. J.* **90** 1474

Ondrechen M P and van der Hulst J M 1989 *Astrophys. J.* **342** 29

Ondrechen M P, van der Hulst J M and Hummel E 1989 *Astrophys. J.* **342** 39

Ostriker J P and Peebles P J E 1973 *Astrophys. J.* **186** 467

Pannatoni R F 1983 *Geophys. Astrophys. Fluid Dynamics* **24** 165

Papayannopoulos Th 1979 *Astron. Astrophys.* **77** 75

Papayannopoulos T and Petrou M 1983 *Astron. Astrophys.* **119** 21

Pence W D and Blackman C P 1984a *Mon. Not. R. Astron. Soc.* **207** 9

—— 1984b *Mon. Not. R. Astron. Soc.* **210** 547

Pence W D, Taylor K, Freeman K C, de Vaucourlers G and Atherton P 1988 *Astrophys. J.* **326** 564

Percival I C 1979 *Nonlinear Dynamics and the Beam-Beam Interaction* AIP Conference series **57** ed M Month and J C Herrera (New York: AIP) p 302

Peterson C J, Rubin V C, Ford W K and Thonnard N 1978 *Astrophys. J.* **219** 31

Petrou M and Papayannopoulos T 1986 *Mon. Not. R. Astron. Soc.* **219** 157

Pfenniger D 1984a *Astron. Astrophys.* **134** 373

—— 1984b *Astron. Astrophys.* **141** 171

—— 1990 *Astron. Astrophys.* **230** 55

—— 1991 *Dynamics of Disc Galaxies* ed B Sundelius (Gothenburg: Göteborgs University) p 191

Pfenniger D and Friedli D 1991 *Astron. Astrophys.* **252** 75

Pfenniger D and Norman C 1990 *Astrophys. J.* **363** 391

Pierce M J 1986 *Astron. J.* **92** 285

Planesas P, Scoville N and Myers S T 1991 *Astrophys. J.* **369** 364

Poincaré 1892 *Les Methods Nouvelles de la Mechanique Celeste* (Paris: Gauthier-Villars)

Polyachenko V L 1989 *Soviet Astr. Letters* **15** 385

Polyachenko V L and Shukhman I G 1981 *Soviet Astr.* **25**, 533

Prendergast K H 1962 *Interstellar Matter in Galaxies* ed L Woltjer (Benjamin) p 217

Prendergast K H 1983 *Internal Kinematics and Dynamics of Galaxies* IAU Symposium **100** ed E Athanassoula (Dordrecht: Reidel) p 215

Raha N 1992 *PhD thesis* University of Manchester

Raha N, Sellwood J A, James R A and Kahn F D 1991 *Nature* **352** 411

Ratcliff S J, Chang K M and Schwarzschild M 1984 *Astrophys. J.* **279** 610

Richstone D O 1987 *Structure and Dynamics of Elliptical Galaxies* IAU Symposium **127** ed T de Zeeuw (Dordrecht: Reidel) p 261

Roberts W W, Huntley J M and van Albada G D 1979 *Astrophys. J.* **233** 67

Saha P 1991 *Mon. Not. R. Astron. Soc.* **248** 494

Sancisi R, Allen R J and Sullivan W T 1979 *Astron. Astrophys.* **78** 217

Sandage A 1961 *Hubble Atlas of Galaxies* Publication 618 (Washington: Carnegie Institute of Washington)

Sandage A and Brucato R 1979 *Astron. J.* **84** 472

Sandage A and Tammann G A 1981 *A Revised Shapley-Ames Catalogue of Bright Galaxies* Publication 635 (Washington: Carnegie Institute of Washington) (RSA)

Sanders R H 1977 *Astrophys. J.* **217** 916

Sanders R H and Huntley J M 1976 *Astrophys. J.* **209** 53

Sanders R H and Prendergast K H 1974 *Astrophys. J.* **188** 489

Sanders R H and Tubbs A D 1980 *Astrophys. J.* **235** 803

Sandqvist Aa, Elfhag T and Jörsäter S 1988 *Astron. Astrophys.* **201** 223

Schempp W V 1982 *Astrophys. J.* **258** 96

Schommer R A, Caldwell N, Wilson A S, Baldwin J A, Phillips M M, Williams T B and Turtle A J 1988 *Astrophys. J.* **324** 154

Schwarz M P 1979 *PhD thesis* Australian National University

—— 1981 *Astrophys. J.* **247** 77

—— 1984a *Mon. Not. R. Astron. Soc.* **209** 93

—— 1984b *Astron. Astrophys.* **133** 222

Schwarzschild M 1979 *Astrophys. J.* **232** 236

Scoville N Z, Matthews K, Carico D P and Sanders D B 1988 *Astrophys. J. Lett.* **327** L61

Sellwood J A 1980 *Astron. Astrophys.* **89** 296

—— 1981 *Astron. Astrophys.* **99** 362

—— 1983 *J. Comp. Phys.* **50** 337

—— 1987 *Ann. Rev. Astron. and Astrophys.* **25** 151

—— 1989 *Mon. Not. R. Astron. Soc.* **238** 115

—— 1991 *Dynamics of Disk Galaxies* ed B Sundelius (Gothenburg: Göteborgs University) p 123

Sellwood J A and Athanassoula E 1986 *Mon. Not. R. Astron. Soc.* **221** 195 (with a Corrigendum in **229** 707)

Sellwood J A and Carlberg R G 1984 *Astrophys. J.* **282** 61

Sellwood J A and Sparke L S 1988 *Mon. Not. R. Astron. Soc. Short Communication* **231** 25p

Shaw M A 1987 *Mon. Not. R. Astron. Soc.* **229** 691

Shaw M A, Combes F, Axon D and Wright G 1992 *Astron. Astrophys.* submitted

Shu F H 1970 *Astrophys. J.* **160** 89

Simkin S M, Su H J and Schwarz M P 1980 *Astrophys. J.* **237** 404

Sørensen S-A, Matsuda T and Fujimoto M 1976 *Astrophys. Sp. Sci.* **43** 491

Sparke L S 1990 *Dynamics and Interactions of Galaxies* ed R Wielen (Berlin: Springer-Verlag) p 338

Sparke L S and Sellwood J A 1987 *Mon. Not. R. Astron. Soc.* **225** 653

Spitzer L 1990 *Ann. Rev. Astron. and Astrophys.* **28** 71

Statler T S 1987 *Astrophys. J.* **321** 113

Stäckel P 1890 *Math. Ann.* **35** 91

Teuben P J 1987 *Mon. Not. R. Astron. Soc.* **227** 815

Teuben P J and Sanders R H 1985 *Mon. Not. R. Astron. Soc.* **212** 257

Teuben P J, Sanders R H, Atherton P D and van Albada G D 1986 *Mon. Not. R. Astron. Soc.* **221** 1

Thronson H A, Hereld M, Majewski S, Greenhouse M, Johnson P, Spillar E, Woodward C E, Harper D A and Rauscher B J 1989 *Astrophys. J.* **343** 158

Tilanus R 1990 *PhD thesis* Groningen University

Toomre A 1966 *Geophysical Fluid Dynamics* notes on the 1966 Summer Study Program at the Woods Hole Oceanographic Institution, ref no 66-46 p 111

—— 1977 *Ann. Rev. Astron. and Astrophys.* **15** 437

—— 1981 *Structure and Evolution of Normal Galaxies* ed S M Fall and D Lynden-Bell (Cambridge: Cambridge University Press) p 111

Tremaine S 1989 *Dynamics of Astrophysical Discs* ed J A Sellwood (Cambridge: Cambridge University Press) p 231

Tremaine S and Weinberg M D 1984a *Mon. Not. R. Astron. Soc.* **209** 729

—— 1984b *Astrophys. J. Lett.* **282** L5

Tsikoudi V 1980 *Astrophys. J. Suppl.* **43** 365 (see also *Astrophys. J.* **234** 842)

Tubbs A D 1982 *Astrophys. J.* **255** 458

Udry S 1991 *Astron. Astrophys.* **245** 99

Udry S and Pfenniger D 1988 *Astron. Astrophys.* **198** 135

Valentijn E A 1990 *Nature* **346** 153

van Albada G D, van Leer B and Roberts W W 1982 *Astron. Astrophys.* **108** 76

van Albada T S 1986 *Use of Supercomputers in Stellar Dynamics* ed S McMillan and P Hut (New York: Springer-Verlag)

van Albada T S and Sancisi R 1986 *Phil. Trans. R. Soc. London A* **320** 447

van Albada T S and Sanders R H 1983 *Mon. Not. R. Astron. Soc.* **201** 303

Vandervoort P O 1979 *Astrophys. J.* **232** 91

——- 1980 *Astrophys. J.* **240** 478

—— 1991 *Astrophys. J.* **377** 49

van Driel W, Rots A H and van Woerden H 1988 *Astron. Astrophys.* **204** 39

Wakamatsu K-I and Hamabe M 1984 *Astrophys. J. Suppl.* **56** 283

Weinberg M D 1985 *Mon. Not. R. Astron. Soc.* **213** 451

—— 1991 *Astrophys. J.* **368** 66

Whitmore B C, Lucas R A, McElroy D B, Steiman-Cameron T Y, Sackett P D and Olling R P 1990 *Astron. J.* **100** 1489

Woolley R 1965 *Galactic Structure* ed A Blaauw and M Schmidt (Chicago: University of Chicago Press) p 85

Wozniak H and Athanassoula E 1992 *Astron. Astrophys.* (in press)

Wozniak H and Pierce M J 1991 *Astron. Astrophys. Suppl.* **88** 325

Zang T A 1976 *PhD thesis* MIT

Zang T A and Hohl F 1978 *Astrophys. J.* **226** 521